AN ABSTRACT OF THE DISSERTATION OF

Kevin J. Buffington for the degree of Doctor of Philosophy in Wildlife Science presented on March 7, 2017.

Title: Improving Projections of Tidal Marsh Persistence under Climate Change with Remote Sensing and Site-Specific Data

Abstract approved: _____

Bruce D. Dugger

Tidal marshes are dynamic ecosystems that are threatened by climate change and sea-level rise. To characterize baseline condition and historic climate sensitivities, and improve projections into the future, new methods are required that integrate data from the field and remote sensing platforms. Marsh elevation response models can be calibrated with site-specific data to determine the vulnerability of a marsh to sea-level rise and help guide management decisions. Elevation models are sensitive to initial elevation, the rate of accretion, and aboveground biomass. The overarching goal of this dissertation was to develop techniques to improve these important model inputs and evaluate the range of spatial and temporal variation.

Light detection and ranging (lidar) is an invaluable tool for collecting elevation data, however dense vegetation prevents the accurate measurement of the tidal marsh surface. In Chapter 2, I describe the development of a technique to calibrate lidar digital elevation models with survey elevation data using readily available multispectral aerial imagery from the National Agricultural Inventory Program (NAIP). Using survey elevation data across 17 Pacific Coast tidal marshes, I demonstrated the utility of the

Lidar Elevation Adjustment with NDVI (LEAN) technique to account for the positive bias in lidar due to vegetation. LEAN reduced error from an average of 23.1 cm to 7.2 cm root mean squared error and removed the positive bias caused by vegetation. This increase in accuracy will facilitate more accurate assessments of current and future vulnerability to sea-level rise.

The phenology of aboveground biomass in tidal marsh plants in relation to climate variation has not been explored in the Pacific Northwest (PNW). In Chapter 3 I explain how I leveraged the Landsat archive and cloud computing capabilities to assess how Tasseled Cap Greenness (TCG, a proxy for aboveground biomass) in three PNW tidal marshes has responded to recent variation in climate to characterize sensitivity to climate change. Through analysis of over 3700 Landsat images obtained from 1984-2015, I found increased annual precipitation resulted in a higher peak TCG, while warmer May temperatures resulted in an earlier day of peak TCG. These results also demonstrate how time-series analysis of remote sensing data can be used to examine the sensitivity of tidal marsh plants to climate variability and directional change.

The range of variation in tidal marsh accretion rates has not been characterized across the PNW. For Chapter 4, I collected and analyzed twenty-two soil cores from eight estuaries to estimate historic accretion rates with radioisotope dating techniques and evaluated the amount and source of variation across estuaries. I found that tidal marshes across the PNW had accretion rates greater than the current rate of sea-level rise, ranging from 2.3 – 7.3 mm yr^{-1}. Using a watershed-scale analysis, I found that long-term average annual fluvial discharge was the top predictor of tidal marsh accretion rates. Additionally,

I found that calibrating the Wetland Accretion Rate Model for Ecosystem Resilience (WARMER) with accretion rate data from nearby estuaries can result in uncertainties of up to 41% (50 cm) after 100 years. Finally, in Chapter 5, I demonstrate that a range of 62 cm of error is possible in WARMER models after a 100 year simulation when both uncorrected lidar and non-local accretion rates are used, fundamentally changing the interpretation of the results. Altogether, this dissertation illustrates the importance of collecting site-specific wetland vegetation and elevation data and demonstrates how lidar and multispectral remote sensing data can be leveraged to improve our understanding of how climate variability and change impacts coastal ecosystems.

Improving Projections of Tidal Marsh Persistence under Climate Change with Remote Sensing and Site-Specific Data

by
Kevin J. Buffington

A DISSERTATION

Submitted to

Oregon State University

in partial fulfillment of
the requirements for the
degree of

Doctor of Philosophy

Presented March 7, 2017
Commencement June 2017

Doctor of Philosophy dissertation of Kevin J. Buffington presented on March 7, 2017

APPROVED:

_____

Major Professor, representing Wildlife Science

_____

Head of the Department of Fisheries and Wildlife

_____

Dean of the Graduate School

I understand that my dissertation will become part of the permanent collection of Oregon State University libraries. My signature below authorizes release of my dissertation to any reader upon request.

_____

Kevin J. Buffington, Author

ACKNOWLEDGMENTS

The success of any graduate student depends in no small part on the support of their mentors. I want to thank my former mentors, especially Paula Kleintjes-Neff, Chris Floyd, and Rosemary Smith, for their valuable guidance early in my scientific development. I was fortunate to have Bruce Dugger as my PhD advisor and am grateful for his support and encouragement to follow my research interests, even if that meant messing around with mud and plants rather than birds. I also want to thank my USGS mentors, Karen Thorne and John Takekawa, for supporting my transition back to school and having the vision of a coast-wide research program. Thanks as well to Chris Janousek for invaluable conversations, and to my PhD committee for their advice and guidance throughout my dissertation project.

I had the assistance of many research technicians throughout my project, but I want to specifically thank Karl Schmidt, Kyle Miller, Mee-ya Monnin, and Brandon Drucker for their work in the field and lab. Chase Freeman, Ari Goodman, and Kat Powelson were especially helpful in managing the trove of USGS datasets so they were readily available for analysis.

Funding support was provided by U.S. Geological Survey, Western Ecological Research Center, National Climate Change and Wildlife Science Center, the National Oceanic and Atmospheric Administration EESLR program, Northwest Climate Science Center (NWCSC), Southwest Climate Science Center, U.S. Fish & Wildlife Service North Pacific and California Landscape Conservation Cooperatives, and Oregon State

University. I especially want to acknowledge the NWCSC fellowship and thank them for their generous support throughout my project.

Finally, a huge thanks to my family and friends for their support and the necessary distractions throughout my grad school experience. I'm forever grateful for the support, advice and, brainstorming sessions that JV has provided throughout my dissertation. Thank you!

CONTRIBUTION OF AUTHORS

Dr. Bruce D. Dugger supported the development of and provided editing support for all chapters.

Dr. Karen M. Thorne facilitated access to the underlying datasets in chapters 2-4 and provided editorial support

Dr. John Y. Takekawa developed the coast-wide research program and provided editorial support for Chapter 2.

TABLE OF CONTENTS

TABLE OF CONTENTS (Continued)

Page

LIST OF FIGURES

LIST OF FIGURES (Continued)

LIST OF TABLES

LIST OF TABLES (Continued)

Improving Projections of Tidal Marsh Persistence under Climate Change with Remote Sensing and Site-Specific Data

CHAPTER 1

GENERAL INTRODUCTION

Kevin J. Buffington

Contemporary climate change, driven by the anthropogenic addition of greenhouse gases, will reshape coastal estuaries through changes in sea level, salinity, and storm frequency and severity (IPCC 2007, NRC 2012). Dense human populations along the coasts already impact these ecosystems through urbanization, habitat fragmentation, altered hydrology, pollution, and the introduction of invasive species (Thorne et al. 2012, Williams 2013), compounding the impacts of climate change. Global projections of sea-level rise (SLR) to 2100, are highly variable (10-180 cm; Rahmstorf 2007, Vermeer and Rahmstorf 2009, Grinsted et al. 2010, Church et al. 2013)**,** largely due to uncertainty in future greenhouse gas emissions and melting rates in the polar regions. Despite the uncertainty surrounding the magnitude of sea-level rise through 2100, there is no doubt in the direction. At the beginning of the 20th century, global sea levels rose at a rate of 1.7 mm/yr that has increased in the last two decades to 3.1 mm/yr (Williams 2013).

On the Pacific Coast of the United States, sea levels are projected to increase by 10-166 cm by 2100 (NRC 2012), but with substantial variation due to regional factors. Local tectonic movement can offset or exacerbate relative sea-level rise. For example, tectonic rebound from the last ice age is projected to partially mitigate SLR in Oregon and Washington (NRC 2012). Other local factors, such as subterranean fluid extraction (i.e. water and oil) can cause local subsidence, increasing the rate of relative SLR (Bawden et al. 2001).

Within coastal estuaries, salt marshes are vulnerable to climate change. Ecological vulnerability is defined by both the exposure and sensitivity of an ecosystem or habitat to

shifts in climate (Glick et al. 2011). Sea-level rise and increasing storminess will both impact salt marshes, but on different time scales (Thorne et al. 2013). Sea level is not projected to increase at near exponential rates until the second half of this century, however, marshes are already experiencing the synergistic effects of sea-level rise and storms (e.g., Hurricane Katrina; Morton and Barras 2011**)**. Storm surges caused by wind forcing and the inverse barometer effect increases inundation depth and duration, which can increase sediment deposition (Thorne et al. 2013). Wind-induced waves can mobilize sediment from adjacent mudflats and result in increased deposition (Fagherazzi et al. 2013), but can also increase erosion at the marsh scarp. In fluvial-dominant estuaries, freshwater runoff during storms can carry large sediment loads; for example in the Tijuana Estuary, marsh sediment deposition rates were 8-9 cm/yr during the 1997-98 El Nino Southern Oscillation (ENSO; Ward et al. 2003).

Salt marshes may also be sensitive to changes in temperature and precipitation associated with climate change. Increasing temperature can boost biomass production in some salt marsh plants (Charles and Dukes 2009), while increasing precipitation may reduce salt stress or increase waterlogging stress, depending on the ambient conditions (Noe and Zedler 2000). The phenology of salt marshes are also likely to shift as the climate changes, leading to the potential of trophic mismatches (Walther et al. 2002, Cleland et al. 2007). Assessing the biomass and phenology response to climate variation is important for a holistic understanding of climate change impacts to salt marsh ecosystems.

The changes due to sea-level rise, climate change, and increasing storminess threaten the sustainability of intertidal systems (Day et al. 2008). Historically, salt

marshes have kept pace with changes in sea level through a variety of feedback mechanisms, including the inverse relationship between elevation and inundation (sedimentation) and the relationship between autochthonous productivity and inundation (Morris et al. 2002, Day et al. 2008, Janousek et al. 2016). However, the rapid rise in projected sea level casts doubt on the capacity of salt marshes to persist into the future. A comparison of several marsh elevation models found the combination of low suspended sediment concentrations and small tidal range increases the risk of marsh drowning (Kirwan et al. 2010). Continued development of dynamic, elevation response models calibrated with site-specific data can assist land managers in planning for the uncertainty of climate change.

Three parameters are particularly critical for accurate models of marsh elevation responding to sea-level rise: baseline elevation, sedimentation rates, and organic production. High quality elevation data are necessary to accurately predict the timing of habitat changes, which is of particular concern for resource managers. Marsh accretion models are sensitive to initial elevation (Swanson et al. 2015) and high quality DEMs improve marsh inventories and habitat distribution estimates necessary for characterizing risk for species of concern. Second, site-specific data on sedimentation rates are required. Substantial variation in sediment accumulation rates across estuaries can be linked to terrestrial land use patterns (Wright and Schoellhamer 2004) and freshwater flow (Weston 2014), and needs to be accurately estimated for local projections of marsh elevation. Finally, the plant community contributes to vertical elevation by facilitating sediment deposition and through direct deposition of organic matter to marsh soils (Leonard and Luther 1995, Morris et al. 2002**)**.

Remote sensing data offers invaluable spatial information for monitoring and modeling coastal ecosystems and can improve our projections of climate change impacts. Airborne light detection and ranging (lidar) is a common tool used to generate digital elevation models (DEMs) and is becoming more readily available to coastal managers and scientists. Detectors mounted underneath small aircraft record the timing of laser pulse reflections off the ground to determine elevation. However, the inability of the laser pulse to penetrate the dense vegetation canopy of most tidal marshes limits the accuracy of lidar-derived DEMs (Rosso et al. 2005, Montané and Torres 2006, Sadro et al. 2007, Schmid et al. 2011, Hladik and Alber 2012). Correcting vertical errors in lidar is then necessary for accurate predictions of flooding risk, marsh elevation change under sea-level rise, or any application where inundation is of primary concern. In chapter 2, I assessed the error of lidar with GPS elevation field survey data across 17 marshes on the Pacific Coast of the United States and developed a novel method for correcting the bias in lidar-derived DEMs using fine resolution aerial imagery.

Landsat satellite imagery offers another crucial remote sensing dataset for continuous monitoring of ecosystem change in wetlands. Imagery dating back to the 1980s can be used to compare wetland extent and relative stress (Klemas 2001). Transformations of the spectral bands create vegetation indices that correlate with photosynthetic activity and when calibrated with ground data can be used to map aboveground biomass (Klemas 2013). With a revisit period of 16 days, calibrated Landsat scenes can be used to track changes in aboveground biomass over the course of a year and through time (Mo et al. 2015). Time-series remote sensing datasets are especially valuable for tracking responses to abiotic factors that are being altered as the climate

shifts (e.g., O'Donnell and Schalles 2016). In chapter 3, I calibrated Landsat data with biomass clip-plots and assessed how marsh biomass and phenology have responded to ENSO-driven variation in temperature, precipitation and sea level since 1984.

While remote sensing datasets aide our ability to monitor and measure salt marshes, site-specific data is also required to parameterize models that project elevation changes in to the future. Previous sea-level rise modeling assessments of Pacific Northwest salt marshes (e.g., Glick et al. 2007) have used an average rate of accretion for the region based on data from Thom (1992), which is the only available study with results for accretion in the region. Estuaries across the PNW are heterogeneously exposed to sea level rise and storms and have a range of land use histories that may make the regional mean an overly simplistic approximation of marsh accretion rates. For chapter 4, I collected and analyzed 22 soil cores across eight PNW salt marshes and correlated the variation in accretion rates with watershed-scale factors. I also demonstrated the amount of uncertainty that can be incurred by using a regional mean instead of site-specific data in marsh elevation models. Finally, in Chapter 5 I calculate how much uncertainty is possible when both uncorrected lidar and non-local accretion rates are used in marsh elevation models, and identify several next steps for tidal marsh climate change research.

LITERATURE CITED

Bawden, G. W., W. Thatcher, R. S. Stein, K. W. Hudnut, and G. Peltzer. 2001. Tectonic contraction across Los Angeles after removal of groundwater pumping effects. Nature 412:812–5.

Charles, H., and J. S. Dukes. 2009. Effects of warming and altered precipitation on plant and nutrient dynamics of a New England salt marsh. Ecological Applications 19:1758–1773.

Church J. A., D. Monselesan, J. M. Gregory and B. Marzeion. 2013. Evaluating the ability of process based models to project sea-level change. Environ. Res. Lett. 8 014051 8pp.

Cleland, E. E., I. Chuine, A. Menzel, H. A. Mooney, and M. D. Schwartz. 2007. Shifting plant phenology in response to global change. Trends in Ecology and Evolution 22:357–365.

Day, J. W., R. R. Christian, D. M. Boesch, A. Yáñez-Arancibia, J. Morris, R. R. Twilley, L. Naylor, L. Schaffner, and C. Stevenson. 2008. Consequences of climate change on the ecogeomorphology of coastal wetlands. Estuaries and Coasts 31:477–491.

Fagherazzi, S., P. L. Wiberg, S. Temmerman, E. Struyf, Y. Zhao, and P. a Raymond. 2013. Fluxes of water, sediments, and biogeochemical compounds in salt marshes. Ecological Processes 2:3.

Glick, P., Clough, J., and Nunley, B. 2007. Sea-level Rise and Coastal Habitats in the Pacific Northwest: An Analysis for Puget Sound, Southwestern Washington, and Northwestern Oregon, National Wildlife Federation, Seattle, Washington, 94 pp.

Glick, P., B.A. Stein, and N.A. Edelson, editors. 2011. Scanning the Conservation Horizon: A Guide to Climate Change Vulnerability Assessment. National Wildlife Federation, Washington, D.C.

Grinsted, A., J. C. Moore, and S. Jevrejeva. 2010. Reconstructing sea level from paleo and projected temperatures 200 to 2100 AD. Climate Dynamics 34:461–472.

Hladik, C., and M. Alber. 2012. Accuracy assessment and correction of a LIDAR-derived salt marsh digital elevation model. Remote Sensing of Environment 121:224–235.

Janousek, C., K. Buffington, K. Thorne, G. Guntenspergen, J. Takekawa, and B. Dugger. 2016. Potential effects of sea-level rise on plant productivity: species-specific responses in northeast Pacific tidal marshes. Marine Ecology Progress Series 548:111–125.

Kirwan, M. L., G. R. Guntenspergen, A. D'Alpaos, J. T. Morris, S. M. Mudd, and S. Temmerman. 2010. Limits on the adaptability of coastal marshes to rising sea level. Geophysical Research Letters 37:1–5.

Klemas, V. 2013. Remote Sensing of Coastal Wetland Biomass: An Overview. Journal of Coastal Research 29:1016–1028.

Klemas, V. V. 2001. Remote sensing of landscape-level coastal environmental indicators. Environmental Management 27:47–57.

Leonard, L. A., and M. E. Luther. 1995. Flow hydrodynamics in tidal marsh canopies.

Limnology and Oceanography 40:1474–1484.

Mo, Y., B. Momen, and M. S. Kearney. 2015. Quantifying moderate resolution remote sensing phenology of Louisiana coastal marshes. Ecological Modelling 312:191–199.

Montané, J. M., and R. Torres. 2006. Accuracy Assessment of Lidar Saltmarsh Topographic Data Using RTK GPS. Photogrammetric Engineering & Remote Sensing:961–967.

Morris, J. T., P. V. Sundareshwar, C. T. Nietch, B. Kjerfve, and D. R. Cahoon. 2002. Responses of coastal wetlands to rising sea level. Ecology 83:2869–2877.

Morton, R. A., and J. A. Barras. 2011. Hurricane Impacts on Coastal Wetlands: A Half-Century Record of Storm-Generated Features from Southern Louisiana. Journal of Coastal Research 275:27–43.

National Research Council. 2012. Sea-Level Rise for the Coasts of California, Oregon, and Washington: Past, Present, and Future.

Noe, G. B., and J. B. Zedler. 2000. Differential effects of four abiotic factors on the germination of salt marsh annuals. American Journal of Botany 87:1679–1692.

O'Donnell, J. P. R., and J. F. Schalles. 2016. Examination of abiotic drivers and their influence on Spartina alterniflora biomass over a twenty-eight year period using Landsat 5 TM satellite imagery of the Central Georgia Coast. Remote Sensing 8:477.

Rahmstorf, S. 2007. Projecting Future Sea-Level Rise. Science 315:368–370.

Rosso, P. H., S. L. Ustin, and A. Hastings. 2005. Mapping marshland vegetation of San Francisco Bay, California, using hyperspectral data. International Journal of Remote Sensing 26:5169–5191.

Sadro, S., M. Gastil-Buhl, and J. Melack. 2007. Characterizing patterns of plant distribution in a southern California salt marsh using remotely sensed topographic and hyperspectral data and local tidal fluctuations. Remote Sensing of Environment 110:226–239.

Schmid, K. A., B. C. Hadley, and N. Wijekoon. 2011. Vertical Accuracy and Use of Topographic LIDAR Data in Coastal Marshes. Journal of Coastal Research 275:116–132.

Swanson, K. M., J. Z. Drexler, C. Fuller, and D. H. Schoellhamer. 2015. Modeling tidal freshwater marsh sustainability in the Sacramento-San Juaquin Delta under a broad suite of potential future scenarios. San Francisco Estuary and Watershed Science 13:217–220.

Thorne, K. M., K. J. Buffington, K. M. Swanson, and J. Y. Takekawa. 2013. Storm Surges and Climate Change Implications for Tidal Marshes: Insight from the San Francisco Bay Estuary, California, USA. The International Journal of Climate

Change: Impacts and Responses 4:169–190.

Thorne, K. M., J. Y. Takekawa, and D. L. Elliott-Fisk. 2012. Ecological Effects of Climate Change on Salt Marsh Wildlife: A Case Study from a Highly Urbanized Estuary. Journal of Coastal Research 285:1477–1487.

Vermeer, M., and S. Rahmstorf. 2009. Global sea level linked to global temperature. Proceedings of the National Academy of Sciences of the United States of America 106:21527–21532.

Walther, G.-R., E. Post, P. Convey, A. Menzel, C. Parmesan, T. J. C. Beebee, J.-M. Fromentin, O. Hoegh-Guldberg, and F. Bairlein. 2002. Ecological responses to recent climate change. Nature 416:389–395.

Ward, K. M., J. C. Callaway, and J. B. Zedler. 2003. Episodic colonization of an intertidal mudflat by native cordgrass (Spartina foliosa) at Tijuana Estuary. Estuaries 26:116–130.

Weston, N. B. 2014. Declining Sediments and Rising Seas: An Unfortunate Convergence for Tidal Wetlands. Estuaries and Coasts 37:1–23.

Williams, S. J. 2013. Sea-Level Rise Implications for Coastal Regions. Journal of Coastal Research 29:184–196.

Wright, S. A., and D. H. Schoellhamer. 2004. Trends in the sediment yield of the Sacramento River, California, 1957 – 2001. San Francisco Estuary and Watershed Science 2:1–14.

Improving Projections of Tidal Marsh Persistence under Climate Change with Remote Sensing and Site-Specific Data

CHAPTER 2

STATISTICAL CORRECTION OF LIDAR-DERIVED DIGITAL ELEVATION MODELS WITH MULTISPECTRAL AIRBORNE IMAGERY IN TIDAL MARSHES

Kevin J. Buffington, Bruce D. Dugger, Karen M. Thorne, and John Y. Takekawa

Remote Sensing of Environment

Radarweg 29, 1043 NX Amsterdam, The Netherlands

186:616-625

ABSTRACT

Airborne light detection and ranging (lidar) is a valuable tool for collecting large amounts of elevation data across large areas; however, the limited ability to penetrate dense vegetation with lidar hinders its usefulness for measuring the tidal marsh surface. Methods to correct lidar elevation data are available, but a reliable method that requires limited field work and maintains spatial resolution is lacking. We present a novel method, the Lidar Elevation Adjustment with NDVI (LEAN), to correct lidar digital elevation models (DEMs) with vegetation indices from freely available multispectral airborne imagery (NAIP) and RTK-GPS surveys. Using 17 study sites along the Pacific coast of the U.S., we achieved an average root mean squared error (RMSE) of 0.072 m, with a 40-75% improvement in accuracy from the lidar bare earth DEM. Results from our method compared favorably with results from three other methods (minimum-bin gridding, mean error correction, and vegetation correction factors), and a power analysis applying our extensive RTK-GPS dataset showed that on average 118 points were necessary to calibrate a site-specific correction model for tidal marshes along the Pacific coast. By using freely available data and with minimal field surveys, we showed that lidar-derived DEMs can be adjusted for greater accuracy while maintaining high (1 m) resolution.

INTRODUCTION

The structure and function of tidal marshes are strongly driven by physical gradients including elevation and tidal range. Elevation, relative to mean sea level, is responsible for variation in abiotic features like accretion rates (Butzeck et al. 2014), soil characteristics (Cahoon and Reed 1995), pore water salinity, and oxygen availability (Hackney et al. 1996). Tidal marsh plants and animals have numerous adaptations for surviving these gradients in physical conditions (Pennings et al. 1992, Silvestri et al. 2005); however, the elevation range in which species can persist is often narrow (< 1 m). In addition, small changes in marsh elevation can lead to large increases in inundation time under normal tidal cycles. Consequently, accurate characterization of elevation is critical for understanding tidal marsh ecogeomorphology, and tidal marsh structure and function are especially sensitive to changes in relative elevation due to sea level rise (Kirwan and Temmerman 2009, Kolker et al. 2009).

Growing concern about the effects of climate change and sea-level rise on tidal marsh sustainability has increased interest in creating accurate digital elevation models (DEMs) of tidal marshes to better inform modeling and planning efforts. Airborne light detection and ranging (lidar) is a common tool used to generate DEMs and is becoming more readily available to coastal managers and scientists. High point return densities (1-10 points/m) and relative ease of data collection across large areas have made lidar a popular option for measuring bare earth elevation and vegetation height (Hodgson and Bresnahan 2004, Kane et al. 2010). In areas with low vegetative cover (e.g., open terrain or concrete), the vertical accuracy of airborne lidar is between 15-25 cm root mean squared error (RMSE, eq. 2; Hodgson and Bresnahan 2004, Mitasova et al. 2009), with

normally distributed errors (mean error approaching zero). However, the inability of the laser pulse to penetrate the dense vegetation canopy of most tidal marshes limits the accuracy of lidar-derived DEMs (Montané and Torres 2006, Rosso et al. 2005, Sadro et al. 2007, Schmid et al. 2011, Hladik and Alber 2012). For example, one study found that just 3% of lidar points were reflected off the marsh surface (Sadro et al. 2007), and another found that lidar elevation error in tidal marshes was greater than in adjacent upland habitats (Schmid et al. 2011), creating a positive bias in mean elevation of 10-40 cm (Sadro et al. 2007, Foxgrover et al. 2011, Hladik and Alber 2012). Even lidar collected during periods of seasonally low biomass in tidal marshes can exhibit significant (>20 cm) vertical errors (Schmid et al. 2011). Correcting vertical errors is necessary for accurate predictions of flooding risk, marsh elevation change under sea-level rise, or any application where inundation is of primary concern.

Several methods have been used to correct lidar error in tidal marshes, including vegetation correction factors (Hladik and Alber 2012), minimum-bin gridding (Schmid et al. 2011), an aboveground biomass model (Medieros et al. 2015), and statistical correction of full waveform lidar (Parrish et al. 2014); however, each of these methods have limitations that may hinder broad adoption. Vegetation correction factors require extensive vegetation surveys or expert knowledge of a marsh coupled with high accuracy GPS surveys to correlate lidar error with plant communities (Hladik and Alber 2012; overall RMSE = 0.1 m). Hyperspectral data can be useful in species and community classification in wetlands (Rosso et al. 2005, Sadro et al. 2007, Adam et al. 2010), but those data are not widely available and expensive to acquire. In addition, plant height and cover can vary substantially across elevation and salinity gradients, potentially requiring

multiple corrections for a single species or community. Minimum-bin gridding (MBG) uses the minimum lidar return value within a predefined grid pixel to set the value for the DEM. As pixel size increases lidar error generally decreases as more low values are included; however, horizontal resolution of the DEM decreases and because so few lidar returns hit the marsh platform, a positive bias remains (Schmid et al. 2011; RMSE = 0.17 m). Medieros et al. (2015) used a combination of remote sensing datasets (ASTER imagery and interferometric synthetic aperture radar, InSAR) in a Florida tidal marsh to model aboveground biomass density and then correct lidar error. They achieved a 38% reduction in RMSE at 5-m horizontal resolution (0.65 to 0.40 RMSE). In addition to Real-Time Kinematic (RTK) GPS surveys, the biomass model requires labor-intensive vegetation sampling that may require destructive sampling if allometric equations for biomass are not available. Relying on two statistical models, each with a measure of uncertainty, may also limit the accuracy of the adjusted DEM. Vertical correction of full waveform lidar using waveform features is promising (Parrish et al. 2014), however, broad collection of waveform lidar is still relatively rare and it requires extensive processing skills; we focus our analysis on DEMs derived from discrete return lidar.

Our objective was to develop a correction model for lidar-derived DEMs using readily available, high resolution (1 m), multispectral (red, green, blue, near-infrared) airborne imagery from the US Department of Agriculture (USDA) National Agriculture Inventory Program (NAIP). Derived products from the NAIP imagery, such as the Normalized Difference Vegetation Index (NDVI), correlate well with the spatial variation in vegetation biomass and structure (Gamon et al. 1995, Myneni et al. 1995, Filella et al. 2004, Pettorelli et al. 2005), and we tested the ability of NDVI to calibrate a statistical

model of lidar error when used in conjunction with baseline elevation datasets (e.g., RTK-GPS surveys). We developed a statistical model of lidar error for a gradient of study sites in 17 tidal marsh sites along the Pacific coast of the United States. We applied the models and compared them to RTK-GPS field data to assess DEM accuracy, and we compared the performance of our model against other commonly applied correction techniques. Finally, we determined the minimum density of RTK-GPS data points necessary to achieve a DEM with maximum accuracy and tested the sensitivity of the statistical model to use NAIP images from years different than when the lidar data were collected.

METHODS

Study Area

Our study included 17 tidal marsh sites located in eleven estuaries where both lidar data and NAIP imagery were available (Fig. 2.1, Table 2.1). Sites were chosen to be representative of historic marsh conditions and many were on U.S. Fish and Wildlife Service National Wildlife Refuges (NWRs). While each study site had unique ecological and geomorphic characteristics, for broad comparisons they were grouped into three regions. Pacific Northwest (PNW) sites included: Grays Harbor NWR (hereafter Grays Harbor); Tarlet Slough in Willapa Bay NWR (Willapa); Millport Slough in Siletz Bay NWR (Siletz); Bull Island within the South Slough National Estuarine Research Reserve in Coos Bay (Bull Island); and the Bandon marsh unit in Bandon NWR in the Coquille Estuary (Bandon). San Francisco Bay (SFB) sites included: Black John marsh (Black John) and Petaluma marsh (Petaluma) on the west shore of the Petaluma River at the

northwest corner of San Pablo Bay; Coon Island and Fagan along the Napa river; San Pablo NWR (San Pablo) along the north shore of San Pablo Bay; China Camp State Park along the south shore of San Pablo Bay (China Camp); and the Corte Madera Marsh Ecological Reserve (Corte Madera) on the west shore of Central San Francisco Bay. Southern California (SCA) sites included: Morro Bay State Park (Morro); Naval Air Station Point Mugu (Mugu); Seal Beach NWR (Seal Beach); Upper Newport Bay Nature Preserve (Newport); and Tijuana Slough NWR (Tijuana). Tidal range increases with latitude, ranging from 1.75 m at Tijuana in the south, to 2.79 m at Grays Harbor in the north (tidesandcurrents.noaa.gov).

Plant community composition and species richness varies substantially in marshes along the Pacific coast (Table 2.1). The PNW sites are comparatively species rich with a mix of salt, brackish, and fresh water sedges, grasses and rushes (Thorne et al. 2015). In SFB, the higher salinity sites (San Pablo, China Camp, Corte Madera, Black John and Petaluma) are dominated by *Salicornia pacifica* (mean height 20 cm), that creates dense mats at mid-high elevations, with *Schoenoplectus spp.* (mean height 86 cm) and *Spartina foliosa* and invasive *Spartina alterniflora* hybrids (mean height 91 cm) in lower elevations and along channels. The more brackish sites (Coon Island and Fagan) have higher species richness, with *Schoenoplectus spp.*, *Typha angustifolia* (mean height 108 cm), and *Potentilla anserina* (mean height 26 cm) also common (Takekawa et al. 2013). The SCA sites are characterized by high salinity and plants with a shorter growth forms including *Salicornia pacifica* (mean height 33 cm), *Batis maritima* (mean height 20 cm), and *Distichlis spicata* (mean height 14 cm; Thorne et al. 2016).

RTK-GPS surveys

We conducted elevation surveys using survey-grade GPS rovers (RTK GPS, 2-5 cm vertical accuracy, Leica Viva GS15 and Leica GX1230, Atlanta, GA, USA) and referenced the rovers to nearby National Geodetic Survey (NGS) benchmarks. Real-time corrections were provided by the Leica SmartNet station network in SFB, while in Oregon the Oregon Real-Time GNSS Network (ORGN) provided corrections. In SCA and Washington, we deployed a Leica GS10 base station with a radio link at a temporary benchmark that provided real-time corrections to the Leica Viva GS15 rover. We surveyed nearby NGS benchmarks for vertical control. We submitted the temporary benchmark locations to the NGS Online Positioning User Service that uses the precise ephemeris from the GPS satellite network to provide accurate (< 2 cm) temporary benchmark locations. We surveyed elevations at stations placed on gridded transects that ran perpendicular to the marsh-mudflat boundary. Transects were separated by 50 m and RTK sample stations were located every 25 m (SFB) or 12.5 m (PNW and SCA) on each transect for a density of 7-14 points per hectare. We used the geoid09 gravitational model to convert ellipsoid heights to North American Vertical Datum of 1988 (NAVD88) for the SFB and SCA sites, and used the geoid03 model for the PNW sites, matching the geoid models used in each lidar datasets. Across all sites the mean RMSE of the RTK–GPS surveys was 0.046 m.

For this study, we were interested in correcting the positive bias across the marsh platform, or mineral surface, and not in correcting possible bias in unvegetated marsh channels or mudflats. The RTK-GPS dataset used in this study were originally meant for developing DEMs through interpolation and included points that were near

topographically steep features (channels and scarps). We manually removed RTK-GPS points from the dataset that were within 2 pixels (m) of marsh channels or platform edge and likely subject to error due to pixel resolution (i.e., the lidar DEM pixel represented the side or bottom of a steep channel while the RTK-GPS point is on the marsh platform adjacent to the channel).

Airborne lidar data

We obtained lidar-derived DEMs from the NOAA Digital Coastal Data Access Viewer (https://coast.noaa.gov/dataviewer/; Table 2.2). We used the local UTM (zone 10 or 11) for the horizontal datum, and NAVD88 for the vertical datum. We selected mean grid averaging of all lidar returns at 1-m resolution. Our goal was to use 'as-received' lidar DEMs to eliminate any lidar processing from the workflow and to maximize the accessibility of the procedure. We determined lidar elevation at each RTK-GPS location with the 'extract' function in the 'raster' package in R (www.r-project.org).

Multispectral imagery

We obtained multispectral airborne imagery data for each site from the National Agriculture Imagery Program (NAIP, 1-m resolution; USDA Farm Service Agency). NAIP imagery is collected for each state on a rotating basis, roughly every two years and typically at the peak of the growing season. We preferentially chose imagery that was collected during the same year that lidar was flown to minimize potential error due to annual variation in plant productivity (Table 2.1). While the majority of our sites had imagery and lidar data collected in the same year, there were three exceptions. At two sites (Bandon, Bull Island) imagery was not available for 2008, so we used 2009 imagery

instead. At China Camp and Corte Madera part of the 2010 image for the marsh was taken at high tide resulting in an uneven image; we instead used 2012 imagery for China Camp and Corte Madera. To assess the quality of georeferencing of the NAIP imagery, we visually compared NAIP and lidar landscape features (channels, roads, buildings) at each site. We found the 2009 and 2010 NAIP images aligned with the lidar and made no adjustments. The 2011 and 2012 NAIP imagery, however, were misaligned with the lidar; in ArcGIS we shifted those NAIP datasets slightly (< 3 m) to align with the lidar datasets, using 1-2 points across the marsh as ground control.

The USDA releases full county, color-corrected mosaics of their NAIP imagery; however, the near-infrared band is removed and image compression reduces image fidelity. We instead used multiple unadjusted 4-band quarter quads at each study site for full coverage. We mosaicked together quarter quads in ENVI (v. 5, Exelis Inc, Boulder, CO, USA) using histogram matching of overlapping scenes to correct for differences in brightness across images. We then applied a dark object subtraction using the histogram of each band to correct for atmospheric interference (Chavez 1988). From the NAIP imagery, we calculated the Normalized Difference Vegetation Index (NDVI), as:

$$\mathrm{NDVI} = \frac{\mathrm{NIR}-\mathrm{R}}{\mathrm{NIR}+\mathrm{R}} \qquad \text{Eq. 1.}$$

where, *NIR* is the near-infrared band (750 nm, band 4), and *R* is the red band (650 nm, band 3). NDVI is a relative index that ranges from -1 to 1, with values above 0 generally considered to be vegetated. While not an issue at our study sites, NDVI can saturate at high values; in areas where this occurs we suggest using the Wide Dynamic Range Vegetation Index instead. NDVI is also sensitive to electromagnetic absorption from water, thus it is important to use imagery collected during low tides.

Accuracy Assessment

Following the accuracy assessment guidelines from Maune et al. (2007) and the National Standard for Spatial Data Accuracy (Federal Geographic Data Committee, 1998), we used root mean squared error (RMSE), Fundamental Vertical Accuracy (FVA), and the 95th Percentile Error (PE) as metrics of DEM accuracy (Flood, 2004). RMSE is calculated as:

$$\mathrm{RMSE} = \mathrm{sqrt}[\sum(z_{\mathrm{lidari}} - z_{\mathrm{RTKi}})^2/n] \qquad \text{Eq. 2}$$

where, z_{lidari} is the elevation of the lidar-derived DEM at *i*th RTK-GPS point, z_{RTKi} is the elevation of the *i*th RTK-GPS point, *n* is the number of RTK-GPS points, and *i* is an integer (1 - *n*). *RMSE* is a common statistic used to determine the difference between two datasets and can be interpreted as the standard deviation if errors are normally distributed (NDEP, 2004). If errors are not normally distributed, then interpretation of RMSE is simply the magnitude of error. FVA is the 95% confidence interval for RMS and is calculated by RMSE*1.96. PE is defined as the absolute value that is greater than 95% of dataset. RMSE and FVA are only appropriate if errors follow a normal distribution; otherwise PE should be used (Flood 2004). We calculated the skewness of error of the original and adjusted DEMs, and following Flood (2004), considered error distributions normal if skewness was within the range [-0.5, 0.5]. We also calculated mean error (ME) as a measure of bias in the original and adjusted lidar DEMs

$$\mathrm{ME} = \sum \frac{(\text{lidar elevation} - \text{RTKGPS elevation})}{n} \qquad \text{Eq. 3}$$

where, n is the number of RTK-GPS points.

Model development

We used a site-specific, multivariate approach to model the relationship between lidar error, determined by subtracting the lidar DEM from the RTK-GPS data, NAIP-derived vegetation indices, and lidar elevation. Specifically, the model was defined as:

$$E = l + v + v^2 + l*v + l*v^2 + v^2*v + l*v*v^2 \quad \text{Eq. 4}$$

where, E is the error (lidar elevation minus RTK-GPS elevation), l is the uncorrected lidar DEM elevation, and v is the NDVI. The model is fit to a training dataset using least-squares regression. We define this technique (Eq. 4) as the Lidar Elevation Adjustment with NDVI method (hereafter, the LEAN method).

To test the sensitivity of LEAN to particular RTK-GPS points, we ran a 100-fold cross-validation analysis, randomly withholding 30% of the dataset for testing in each iteration. We calculated the average model correction from the individual cross-validation runs and reported the standard deviation of percent improvement in RMSE compared with the original lidar-derived DEM. To develop the best possible LEAN model, we trained the final NAIP model using the entire RTK-GPS dataset for each site.

We produced an adjusted DEM by applying LEAN to the lidar DEM and NDVI from the NAIP image. This was accomplished by converting the raster values of the aligned lidar DEM and NDVI datasets to numeric vectors and using the ‘predict’ function in base R to generate predictions of lidar error. The predicted lidar error was then subtracted from the original lidar DEM to produce an adjusted DEM of the marsh platform. To restrict model corrections to areas above the elevation of the mudflat and

channels, we determined a site-specific marsh elevation height from inspection of the original lidar and NAIP imagery (Table 2.4). The final DEM was a mosaic of the LEAN-adjusted DEM above the marsh elevation height, and the original lidar DEM below the marsh elevation height. Our calibration RTK-GPS dataset did not include data from the channels (sides nor bottoms) or mudflats; we assumed any error in these areas were not due to dense vegetation and therefore LEAN was not appropriate for making adjustments to the DEM.

The timing of lidar acquisition is an important factor when considering effects of marsh vegetation on lidar returns. To assess the importance of concurrent (same year) lidar collection and NAIP imagery, we compared performance of models trained using NAIP images from different years than the lidar was flown at a subset of sites (Coon Island, Fagan, Mugu, Petaluma, Siletz, Tijuana). We analyzed the difference in RMSE between the correction models using a paired t-test (α=0.05).

Seasonal differences in vegetation height and density due to phenology are important in the context of vertical lidar error. To make our technique as broadly applicable as possible, we relied on readily available NAIP imagery that was collected in a different season than the lidar acquisition at several of our sites (Table 2.1). Our goal was not to directly infer aboveground biomass in our models, but rather to use the NAIP imagery as an indicator of spatial variability in vegetation height and density. Our approach assumes that the spatial variability detected in the NAIP imagery correlates with the variability in plant height and density when the lidar was flown (e.g., the location of dense vegetation in June is reasonably correlated with the location of dense vegetation in October). As we are relying on site-specific data to calibrate the correction

model, only the relative magnitude of the NDVI signal across marsh is important, rather than the absolute value, thereby reducing the effect of seasonal differences in lidar and NAIP collection in our model. Caution should be used in areas with substantial senescence of vegetation when there is seasonal mismatch between lidar and multispectral imagery acquisitions.

Comparison of LEAN to Alternative Models

We compared LEAN to three published methods for adjusting lidar derived DEMs; minimum-bin gridding (MBG), mean error correction (MEC), and vegetation correction (VC). We compared LEAN to MBG and MEC across all our sites. For MBG, we acquired 5-m resolution lidar DEMs from NOAA's Coastal Data Viewer using the minimum grid averaging option. We then estimated the RMSE and mean error between the RTK-GPS elevation and elevation of the 5-m DEM at each RTK-GPS location. For MEC, we subtracted the mean difference between the 1-m lidar DEM and the RTK-GPS elevation from the original DEM. We then calculated the RMSE and ME for the MEC DEM. As MEC only uses RTK-GPS data, the difference in performance between MEC and LEAN represent the benefit for including NDVI from NAIP imagery into a correction model. For the three correction models (LEAN, MBG, MEC), we randomly subset the RTK data into 70% training and 30% testing datasets and used a 100-fold cross-validation compare model performance. For two sites in SFB (China Camp and Coon Island), we also compared the RMSE of an existing VC DEM (Schile et al., 2014) with the RMSE from LEAN using our RTK data. The existing VC DEMs were created from the same SFB lidar dataset used in this study. We used paired t-tests (α=0.05) to

compare the RMSE from the alternative methods with LEAN, and one-way ANOVAs to compare initial and adjusted RMSE across regions.

Power Analysis

Finally, we conducted a power analysis to estimate the minimum number of RTK-GPS points necessary to create a LEAN model that was statistically equivalent to the cross-validated LEAN model. For each site we randomly stratified RTK-GPS points into four classes, above and below mean lidar elevation and mean NDVI value, selecting an increasing number of points per class and replicating the subset 1000 times. We then determined the number of RTK-GPS points that would calibrate a model with a RMSE within 1 cm of the mean cross-validated RMSE. We calculated the mean, standard deviation and median of the lowest number of points per site. We conducted all analyses and model development using R version 3.2.2 (http://cran.r-project.org) and ArcGIS (version 10.1, ESRI, Redlands, CA).

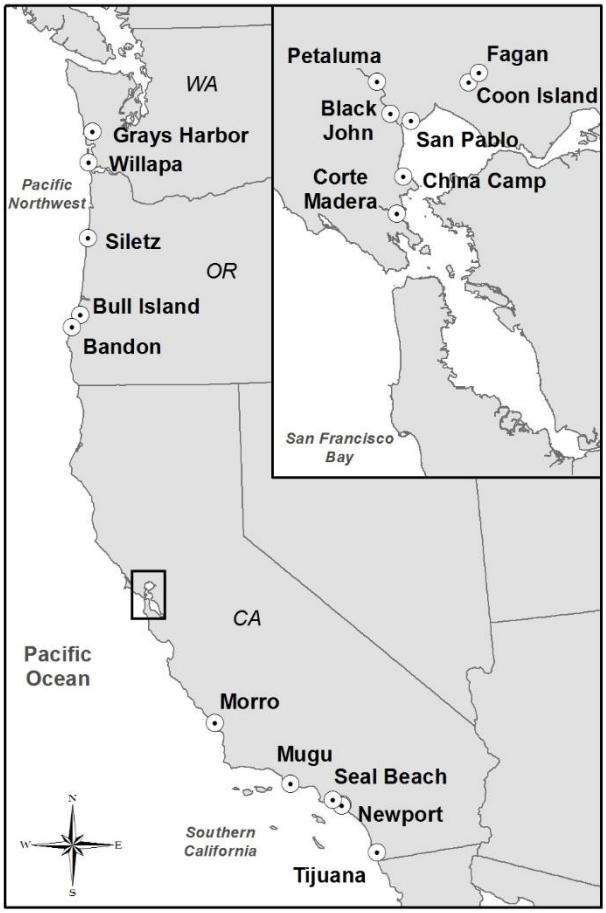

Figure 2.1. Location of 17 tidal marsh study sites along the Pacific coast of the United States. Study sites represented a range of dominant tidal marsh vegetation, climate, and tidal ranges to test the applicability of model corrections across different veg

Table 2.1. Characteristics of study sites used to correct lidar data for coastal tidal marshes using NAIP imagery. Area (ha), number of RTK-GPS points and year collected, lidar and NAIP acquisition months, and dominant vegetation. More specific acquisition dates could not be determined from available metadata at Bull Island and Bandon, and we could only determine a range of dates for San Francisco Bay. Species are listed if they were found in at least 25% of vegetation survey plots (Takekawa et al. 2013, Thorne et al. 2015, Thorne et al. 2016).

Site	Area	RTK-GPS	RTK Year	Lidar Acq.	NAIP Acq.	Dominant Vegetation
Pacific Northwest						
Grays H.	68	1166	2012	9/2009	9/2009	CarLyn, ArgSto, TriMar, PotAns
Willapa	27	420	2012	9/2009	9/2009	DisSpi, SalPac, TriMar, DesCep, CarLyn
Siletz	69	1113	2014	9/2009	6/2009	ArgSto, CarLyn, DisSpi, PotAns, JunBal
Bull Island	97	1166	2012	2008	6/2009	CarLyn, SalPac, DisSpi, DesCep
Bandon	97	1495	2012	2008	6/2009	SalPac, DisSpi, DesCep, CarLyn, AgrSto
San Francisco Bay						
Petaluma	81	623	2009	2-4/2010	6/2010	SalPac, SpaFol
Black John	31	203	2009	2-4/2010	6/2010	SalPac, SpaFol
San Pablo	147	374	2009	2-4/2010	6/2010	SalPac, SpaFol
Fagan	68	578	2010	2-4/2010	5/2010	SalPac, BolMar, PotAns
Coon Island	99	728	2009	2-4/2010	5/2010	SalPac, BolMar
China Camp	97	697	2009	2-4/2010	5/2012	SalPac, SpaFol
Corte Madera	45	399	2010	2-4/2010	5/2012	SalPac, SpaFol
Southern California						
Morro	154	2247	2013	10/2009	6/2009	SalPac, JauCar
Mugu	109	1465	2013	11/2009	6/2009	SalPac, FraSal
Seal Beach	266	3208	2011	9/2009	6/2009	SalPac FraSal, SpaFol
Newport	60	962	2012	9/2009	6/2009	SalPac, SpaFol, BatMar
Tijuana	62	896	2011	11/2009	6/2009	SalPac, JauCar, FraSal, DisSpi

Species codes are: CarLyn = *Carex lyngbyei*; ArgSto = *Agrostis stolonifera;* TriMar = *Triglochin maritima*; PotAns = *Potentilla anserine*; DisSpi = *Distichlis spicata*; DesCep = *Deschampsia cespitosa*; JunBal = *Juncus balticus*; SalPac = *Salicornia pacifica*; SpaFol = *Spartina foliosa*; JauCar = *Jaumea carnosa*; FraSal = *Frankenia salina*; BatMar = *Batis maritima*; BolMar = *Bolboschoenus maritimus*.

Table 2.2. Flight characteristics and accuracy of lidar data.

	San Francisco Bay	CA State Coastal Conservancy	DOGAMI
Contractor	Fugro EarthData	Fugro EarthData	Watershed Sciences
Sensor	Leica ALS60 MPiA	Leica ALS60 MPiA	Leica ALS50 Phase II
Points/m	1	1	8.60
RMSE (m, open terrain)	0.026	0.048	0.044
Geoid Model	Geoid09	Geoid09	Geoid03
Flightline overlap (%)	20	20	50
Altitude (m)	2000	1900	900
Field of View (degrees)	30	30	28
Pulse Rate (Hz)	121,300	121,300	105,000
Scan Rate (Hz)	41	41	52.2
Returns	Discrete	Discrete	Discrete
Abbreviation	SFB	SCA	PNW

RESULTS

RTK-GPS Surveys

After removing points outside the marsh platform, a total of 17,740 RTK-GPS points across all sites were included in model development and analysis. Sites had an average of 96.0% (SD = 7.7) of their RTK-GPS elevations lower than the lidar DEM, indicating that vegetation biased lidar returns across all our study sites. Even when accounting for 5 cm of RTK-GPS measurement error, sites had an average of 88.9% (SD = 15.5) points that were lower than the lidar DEM. Across all sites, ME for lidar was 0.208 m (SD = 0.109) and RMSE was 0.231 m (SD = 0.010; Table 2.3).

Lidar data

Lidar error varied across study regions and between sites within regions (Fig. 2.2). Grays Harbor and Willapa had higher initial lidar RMSE, while Bull Island,

Bandon, Mugu and Tijuana had lower initial RMSE. The higher point density of the PNW lidar dataset (8 pts/m vs. 1 pt/m) did not appear to have an effect on lidar error, as Willapa and Grays Harbor had the highest lidar error while Bull Island and Bandon had some of the lowest error. This likely is related to differences in the vegetation communities across the sites.

Initial RMSE across the PNW sites and the SFB sites were significantly greater than the initial RMSE across the SCA sites (PNW vs. SCA, $t = 2.39$, $df = 8$, $p = 0.044$; SFB vs. SCA, $t = 5.29$, $df = 10$, $p < 0.0001$). While the PNW sites had a larger range of initial RMSE, it was not significantly different than the SFB initial RMSE ($t = 0.78$, $df = 10$, $p = 0.45$). Mean initial RMSE across all site was 0.231 m (sd = 0.098).

DEM correction

The LEAN model reduced lidar bias by an average of 58.5% across all sites, ranging from 40-75% (Table 2.3). The mean RMSE after LEAN correction across all sites was 0.072 m (sd = 0.018). LEAN successfully eliminated the positive bias in lidar error (Fig. 2.3); ME across all sites was 0 (sd = 0.065). Mean percent improvement in RMSE using LEAN varied significantly across regions (ANOVA, $F_{2, 14} = 5.05$, $p = 0.022$).

Alternative Models

Mean RMSE across the sites calibrated with alternative year NDVI data was 0.059 m (SD=0.005), while the mean RMSE of models calibrated with the NDVI from the same year as the lidar was 0.065 m (SD=0.009). Correlation in NDVI between years ranged from moderate (0.52) to low (0.028) with a mean of 0.20. There was no

significant difference in RMSE between the alternative NDVI year models and the models with the original NDVI (paired t-test; $t = 1.50$, $df = 4$, $p = 0.103$).

The MGB, MEC, and VC lidar correction methods reduced the RMSE of the lidar data, but not as much as the LEAN method when compared to the RTK-GPS elevation points. Correcting the lidar DEM with the MEC reduced RMSE to an average of 0.096 m (CI = 0.188 m), which was significantly greater than the RMSE using LEAN (paired t-test, $t = 2.79$, $df = 16$, $p = 0.007$; Table 2.4). MBG at 5 m resolution increased mean RMSE across sites to 0.271 m, and ME was positively biased at 0.065 m. At a few sites (Newport, Tijuana), MBG reduced signed mean error to within ±5 cm of 0, however, the RMSE was > 0.2 m (Table 2.5). At China Camp, RMSE of the VC DEM was 0.12 m, compared to 0.051 m RMSE achieved using LEAN, while at Coon Island, RMSE of the VC DEM was 0.084 m compared to a RMSE of 0.070 m using LEAN.

Power Analysis

Across sites, an average of 118.3 (SD = 56.7) total RTK-GPS ground points, stratified by mean elevation and NDVI, resulted in a LEAN model RMSE that was within 1 cm of the mean cross-validated RMSE, while an average of 87 total RTK-GPS points resulted in models within 2 cm of the mean RMSE. Three sites (Corte Madera, China Camp, and Willapa) did not converge on the mean cross-validated RMSE and were excluded from the average. Grays Harbor needed the highest number of RTK-GPS points (236), while Black John required only 52 to build a robust LEAN model. The median number of RTK-GPS points needed was 104. Figures for each site are provided as supplemental information (Appendix A, S1-S3).

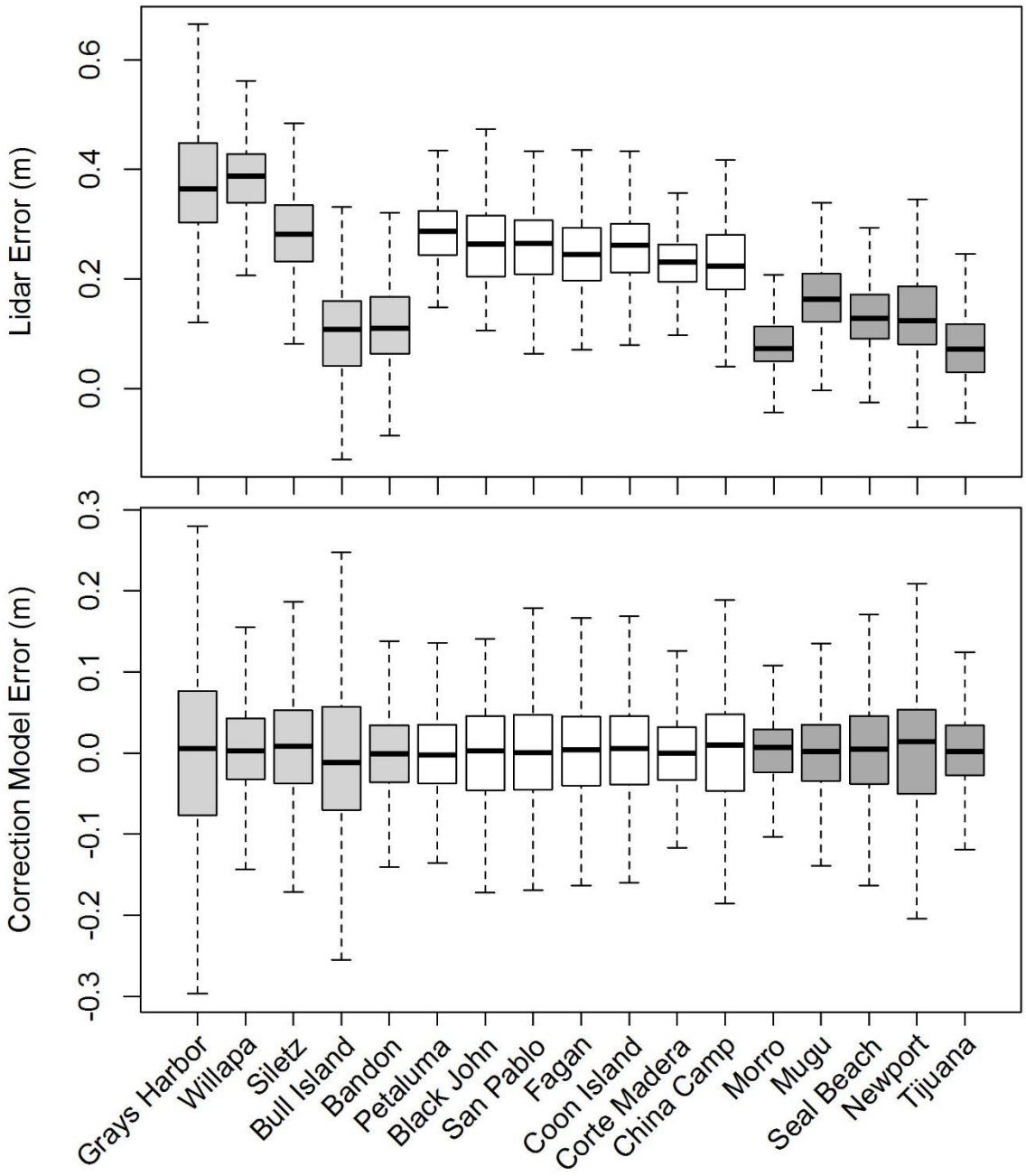

Figure 2.2. Boxplot of uncorrected lidar error (top) and errors from Lidar Elevation Adjustment using NDVI (LEAN) corrections (bottom) across study sites. Lidar error was calculated by subtracting RTK-GPS elevation from the lidar DEM. Box shading designates region.

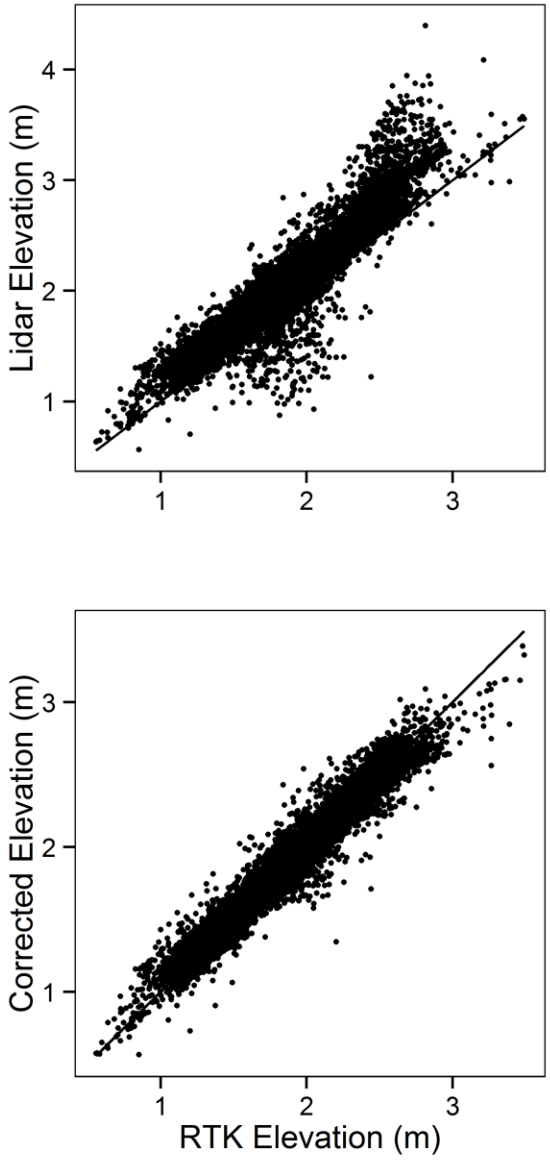

Figure 2.3. Positive bias in lidar DEM before Lidar Elevation Adjustment using NDVI (LEAN) correction (top) and after LEAN correction (bottom), with a 1:1 line. Units in m, NAVD88.

Table 2.3. Uncorrected lidar data root mean squared error (RMSE), initial mean error (ME), and fundamental vertical accuracy (FVA), 95th Percentile Error (PE, with standard deviation) from the training data, and mean (SD) Normalized Difference Vegetation Index (NDVI) for 17 study sites along the Pacific coast of the United States. Lidar error was calculated by subtracting RTK-GPS elevations from a 1-m lidar DEM for each study site. Sites where the skewness of the error distribution exceeds [-0.5, 0.5] are denoted with *.

Site	RMSE	ME	FVA	PE	NDVI Mean (SD)
Pacific Northwest					
Grays Harbor	0.466	0.419	0.912	0.871 (0.017)	0.228 (0.156)
Willapa*	0.392	0.382	0.768	0.501 (0.008)	0.203 (0.101)
Siletz*	0.304	0.269	0.596	0.434 (0.010)	0.410 (0.067)
Bull Island*	0.145	0.078	0.284	0.476 (0.15)	0.138 (0.099)
Bandon*	0.118	0.016	0.232	0.243 (0.004)	0.289 (0.127)
PNW Mean	0.285	0.233	0.560	0.505 (0.011)	0.254 (0.057)
San Francisco Bay					
Petaluma*	0.289	0.282	0.566	0.382 (0.004)	0.259 (0.058)
Black John	0.278	0.264	0.546	0.418 (0.011)	0.222 (0.053)
San Pablo	0.265	0.253	0.520	0.374 (0.003)	0.385 (0.094)
Fagan	0.256	0.242	0.502	0.376 (0.006)	0.339 (0.094)
Coon Island	0.273	0.260	0.535	0.401 (0.007)	0.348 (0.075)
China Camp	0.233	0.228	0.457	0.309 (0.003)	0.155 (0.047)
Corte Madera	0.182	0.228	0.357	0.367 (0.008)	0.218 (0.068)
SFB Mean	0.254	0.251	0.498	0.375 (0.006)	0.275 (0.070)
Southern California					
Morro*	0.109	0.082	0.214	0.216 (0.002)	0.011 (0.137)
Mugu	0.155	0.154	0.303	0.266 (0.003)	0.238 (0.142)
Seal Beach*	0.168	0.147	0.329	0.295 (0.003)	0.347 (0.123)
Newport	0.183	0.140	0.358	0.352 (0.008)	0.235 (0.126)
Tijuana*	0.113	0.084	0.221	0.209 (0.006)	0.239 (0.074)
SCA Mean	0.145	0.121	0.285	0.268 (0.004)	0.214 (0.120)
Overall Mean	0.231	0.208	0.453	0.382 (0.007)	0.251 (0.097)

Table 2.4. Lidar Elevation Adjustment using NDVI (LEAN) corrected DEM accuracy statistics for 17 tidal marshes along the Pacific coast of the United States. Root mean squared error (RMSE) for LEAN-corrected DEMs using all RTK-GPS points, Mean RMSE (standard deviation) from 100-fold cross-validation, mean error (ME), fundamental vertical accuracy (FVA), 95th Percentile Error (PE, with SD), and percent improvement in PE (Imp.). Sites where the skewness of the error distribution exceeds [-0.5, 0.5] are denoted with *.

Site	RMSE (All Pnts)	RMSE Mean	ME	FVA	PE Mean	Imp.	Mud-flat Elev (m)
Pacific Northwest							
Grays Harbor	0.118	0.121 (0.005)	1.77E-15	0.236	0.231 (0.010)	73.4	2.1
Willapa	0.079	0.072 (0.011)	5.50E-16	0.141	0.126 (0.015)	74.9	2.2
Siletz*	0.090	0.092 (0.006)	-5.86 E-15	0.181	0.182 (0.019)	58.0	2.3
Bull Island*	0.076	0.080 (0.006)	-2.01E-16	0.156	0.150 (0.009)	42.5	1.7
Bandon	0.069	0.071 (0.004)	8.93E-16	0.138	0.139 (0.007)	42.6	1.5
PNW Mean	0.086	0.087 (0.006)	0.000	0.170	0.166 (0.013)	58.3	-
San Francisco Bay							
Petaluma*	0.056	0.069 (0.028)	2.00E-15	0.135	0.110 (0.009)	71.2	1.3
Black John	0.071	0.081 (0.012)	3.01E-15	0.158	0.136 (0.014)	67.4	1.3
San Pablo	0.070	0.075 (0.011)	1.04E-14	0.146	0.142 (0.014)	62.1	1.3
Fagan	0.064	0.070 (0.013)	3.36E-15	0.138	0.127 (0.013)	66.3	1.3
Coon Island*	0.070	0.071 (0.004)	-9.86E-15	0.140	0.144 (0.011)	64.0	1.3
China Camp	0.051	0.054 (0.004)	7.74E-16	0.106	0.099 (0.008)	67.9	1.3
Corte Madera	0.057	0.062 (0.009)	-1.77E-15	0.122	0.150 (0.012)	59.0	1.3
SFB Mean	0.063	0.069 (0.012)	0.000	0.135	0.130 (0.012)	65.4	-
Southern California							
Morro	0.056	0.057 (0.003)	1.06E-15	0.112	0.113 (0.008)	47.8	1.3
Mugu	0.049	0.049 (0.001)	-5.94E-16	0.096	0.107 (0.005)	59.7	1.3
Seal Beach	0.074	0.074 (0.002)	7.39E-15	0.146	0.149 (0.006)	49.6	1.3
Newport*	0.102	0.104 (0.008)	-5.61E-16	0.203	0.211 (0.019)	40.0	1.2
Tijuana*	0.064	0.065 (0.004)	-1.94E-15	0.127	0.123 (0.011)	41.1	1.3
SCA Mean	0.069	0.070 (0.004)	0.000	0.137	0.142 (0.010)	47.6	-
Overall Mean	0.072	0.076 (0.008)	0.000	0.138	0.143 (0.011)	58.1	-

Table 2.5. Estimated error for alternative methods for correcting lidar digital terrain models. Mean Error Correction (MEC) root mean error squared (RMSE, m; with standard deviation), 5 m minimum bin gridding (MBG) RMSE (m; SD), and 5 m MBG mean error (m; SD) are reported from the 100-fold cross-validation models.

Site	MEC RMSE	MBG RMSE	MBG Mean Error
Pacific Northwest			
Grays Harbor	0.204 (0.010)	0.360 (0.014)	0.271 (0.012)
Willapa	0.089 (0.010)	0.312 (0.020)	0.227 (0.014)
Siletz	0.101 (0.006)	0.226 (0.012)	0.089 (0.008)
Bull Island	0.092 (0.007)	0.259 (0.020)	-0.062 (0.011)
Bandon	0.141 (0.008)	0.258 (0.019)	-0.075 (0.011)
PNW mean	*0.125 (0.008)*	*0.283 (0.016)*	*0.090 (0.011)*
San Francisco Bay			
Petaluma	0.064 (0.004)	0.286 (0.020)	0.162 (0.015)
Black John	0.089 (0.006)	0.245 (0.026)	0.153 (0.022)
San Pablo	0.080 (0.005)	0.259 (0.025)	0.113 (0.019)
Fagan	0.083 (0.004)	0.224 (0.016)	0.077 (0.014)
Coon Island	0.084 (0.004)	0.288 (0.021)	0.105 (0.016)
China Camp	0.054 (0.003)	0.251 (0.022)	0.106 (0.014)
Corte Madera	0.063 (0.007)	0.278 (0.013)	0.114 (0.014)
SFB mean	*0.074 (0.005)*	*0.262 (0.021)*	*0.119 (0.016)*
Southern California			
Morro	0.072 (0.004)	0.213 (0.012)	-0.051 (0.006)
Mugu	0.064 (0.002)	0.209 (0.006)	0.135 (0.006)
Seal Beach	0.081 (0.002)	0.315 (0.011)	-0.083 (0.008)
Newport	0.118 (0.010)	0.240 (0.022)	0.000 (0.011)
Tijuana	0.075 (0.002)	0.229 (0.021)	-0.033 (0.013)
SCA mean	*0.082 (0.005)*	*0.241 (0.015)*	*-0.007 (0.009)*

DISCUSSION

Consistent with previous studies, we found that lidar overestimated tidal marsh surface elevation at all our study sites. The bias ranged from 0.11-0.47 m (RMSE), which at the high end exceeds values for sites in South Carolina (0.15 m; Schmid et al. 2011) and Georgia (0.23 m; Hladik and Alber 2012), but is less than the bias found in a Florida marsh along the Gulf of Mexico (0.65 m, Medeiros et al. 2015). Lidar bias in our study varied by study region, likely because each region has distinct dominant vegetation communities (Table 2.1) with different canopy heights and densities (Schmid et al. 2011, Hladik and Alber 2012, McClure et al. 2016). Additionally, lidar was acquired in different seasons, which may also explain regional differences in initial error.

The LEAN model reduced positive bias in lidar DEMs 40-75% across the 17 tidal marshes, with low variation in final RMSE (Fig. 2.4). By relying on a statistical approach to lidar error correction, LEAN was insensitive to temporal mismatches between NDVI and lidar datasets, evidenced by the low standard deviation in final RMSE across sites (0.018 m; an 82% reduction in RMSE variation across sites). LEAN successfully reduced lidar error across a wide variety of dominant marsh vegetation communities while maintaining high spatial resolution, and the mean RMSE of 0.072 m across all our sites is lower than previous attempts to correct lidar in tidal marshes. In comparisons with other correction methods, the accuracy of our LEAN model was followed by MEC (0.096 m RMSE), VC (0.10 m RMSE, for China Camp and Coon Island), and MBG (0.271 m RMSE). Unexpectedly, MBG resulted in increased mean RMSE across sites, likely due to the addition of channel and mudflat features within the 5 m pixels. Because we modeled total lidar elevation errors, LEAN accounts for both random sensor error and the

systematic influence of dense vegetation canopies. Our focus was to correct the positive bias across the marsh platform as our RTK-GPS dataset did not include points within channels or on mudflats; additional work is warranted to address lidar error in these important marsh features.

LEAN (RMSE of 0.051 m) outperformed two prior efforts to correct lidar at China Camp that used vegetation correction methods. Schile et al. (2014) used the mean error for the dominant species (*Salicornia pacifica*) to correct the lidar DEM and achieved a RMSE of 0.12 m. McClure et al. (2016) used a more detailed vegetation map and correction factors for five species of plants to create a modified DEM with a RMSE of 0.098 m. LEAN likely outperforms VC methods because NDVI captures variation in both plant canopy height and aboveground biomass that can influence lidar reflectance and canopy penetration. More important than the relatively small improvements in accuracy is that LEAN does not require time-consuming vegetation surveys and airborne photo interpretation or expensive hyperspectral data to develop correction factors for individual species or communities, making LEAN relatively easy and inexpensive to implement.

The temporal mismatch between the RTK-GPS surveys and lidar acquisition is a potential source of uncertainty. Annual changes in tidal marsh elevations, however, occur at the millimeter-scale (2-8 mm/yr at our study sites, Thorne et al. 2015, Thorne et al. 2016) and the amount of instrument error in both the RTK-GPS (~2 cm) and lidar (>4 cm) is too large to robustly detect marsh elevation changes over relatively short time periods. A greater temporal mismatch is not necessarily an issue, provided the RTK-GPS surveys occur after the lidar acquisition; adjustments to the original lidar DEM using

LEAN can be interpreted as both correcting for dense vegetation and updating the DEM for changes in surface elevation.

Lidar-derived DEMs corrected using LEAN can be confidently used in mid-term (2050) SLR projections. NOAA recommends that DEMs used in sea-level rise (SLR) projections should be at least twice as accurate (using the 95% confidence interval, RMSE*1.96) as the SLR increment being modeled (NOAA 2010). Mean SLR projections for our study regions and the recommended DEM accuracies for 2030, 2050 and 2100 are provided (Table 2.6). The uncorrected lidar appears to have sufficient accuracy for 100-year projections across our SCA sites, but not our SFB or PNW sites illustrating that uncorrected lidar should be used with caution for assessing flooding risk to tidal marshes and other coastal zones without a correction for vegetation. Technological and analysis advances are necessary before lidar is capable of the accuracy needed for short-term (2030) projections, especially for areas with relatively low SLR projections as in the PNW.

Reliance on unadjusted lidar has consequences for both short and long term ecological applications for low slope tidal marshes. In the short term, LEAN-adjusted DEMs can correct projections of inundation frequency during the 24-hour tide cycle. For example, at three representative sites the estimate of inundation duration for the mean elevation of each site ranged from 1.3 to 4 times longer using the LEAN adjusted DEM versus uncorrected lidar (results not shown). Small changes in duration of inundation may change productivity (Janousek et al. 2016) and community composition of marsh plants (Kirwan and Guntenspergen 2012, Langley et al. 2013), and affect wildlife that

rely on intertidal habitats for nesting, foraging, and refugia (Shaughnessy et al. 2012, Takekawa et al. 2012).

In the long term, unadjusted DEMs can bias predictions of marsh persistence under SLR. Models like the Sea Level Affecting Marshes Model (SLAMM; Craft et al. 2009), Marsh Equilibrium Model (MEM; Morris et al. 2002), and Wetland Accretion Model for Ecosystem Resilience (WARMER; Swanson et al. 2013) all require an initial DEM with accurate starting elevation upon which to make future elevation projections under SLR. Sensitivity analysis of WARMER results indicate that 30-50% of the variance in final elevation is due to initial elevation (Thorne et al. 2015, Thorne et al. 2016). In comparing WARMER projections for 2110 with uncorrected DEMS and LEAN adjusted DEMs for three of our study sites (Grays Harbor, Petaluma, and Tijuana), we found WARMER predicted a loss of high marsh habitat 30 years earlier at Grays Harbor with the LEAN adjustment. At Petaluma, high marsh classified with the lidar DEM was reclassified as mid marsh with the LEAN DEM, and the transition to mudflat was predicted to be 10 years earlier, and at Tijuana the amount of habitat currently classified as high marsh was reduced by 46%, illustrating the importance of correcting lidar for marsh vegetation (results not shown, marsh classifications from Thorne et al. 2015 and Thorne et al. 2016).

LEAN was also robust to variation in NAIP image availability. We found that LEAN calibrated with NAIP imagery from years other than those of the lidar data performed as well as the LEAN corrections using lidar data and NAIP imagery from the same year. Due to the variance in correlation of NDVI between images, however, a LEAN model should not be calibrated with a NAIP image from one year and projected

using a different year. Theoretically, the shorter the timespan between lidar and NAIP (or NDVI) data acquisitions, the more accurate the model corrections; however, the results seem robust to differences of several years, likely due site-specific model calibration and low interannual variation of marsh perennials. In addition, NAIP images may be acquired during high tides or cloudy conditions in some years which will affect NDVI values, thus the capability of LEAN to use images from any recent year is especially useful.

We suggest taking at least 40 RTK-GPS points per vegetation class (± mean elevation and ± mean NVDI) to produce a robust DEM using LEAN, and up to 60 per class if the marsh has greater spatial variation in plant density and height. This number of sample points (~120) would also be sufficient to run a cross-validation for assessing model performance. In addition, separate model calibrations should be performed in areas that have very different dominant vegetation. For instance, we recommend modeling salt, brackish, and freshwater marshes within an estuary separately as the relationship between lidar error and NDVI may vary across these different marsh types. From the power analysis, we found no relationship between marsh area and number of RTK-GPS needed for LEAN calibration. While our sites were generally small in area, this result highlights the importance of capturing the variation in NDVI and initial lidar DEM with the RTK-GPS surveys rather than ensuring a specific density of points. Additional RTK-GPS points should be collected in areas with complex vegetation communities and high variability in NDVI. Finally, to avoid errors related to lidar DEM resolution, we advise surveying elevation at least 1 pixel (m) away from areas with steep slope such as channels and scarps.

CONCLUSION

Airborne lidar provides valuable elevation data by generating thousands of data points per hectare. However, some correction to lidar DEMs is required to offset the positive bias caused by the dense vegetation canopy in tidal marshes. The LEAN method for correcting lidar data requires a relatively small dataset of ground elevation points for calibration and a spatial map indicative of vegetation density (e.g., NDVI). The power analysis showed that on average approximately 120 RTK-GPS points were necessary for a robust LEAN model.

LEAN could be applied to other habitat types where dense vegetation obstructs the ground surface and high vertical accuracy is needed. So long as a sufficient number of RTK-GPS data are available, our statistical approach to lidar correction should be robust. The flat terrain and dynamic coastal landscape necessitates that tidal marsh DEMs be highly accurate to be useful across ecological, geomorphological, and engineering applications. NDVI derived from commercially available satellite images could be used in place of the NAIP airborne images to expand our method to areas in the world not covered by NAIP imagery.

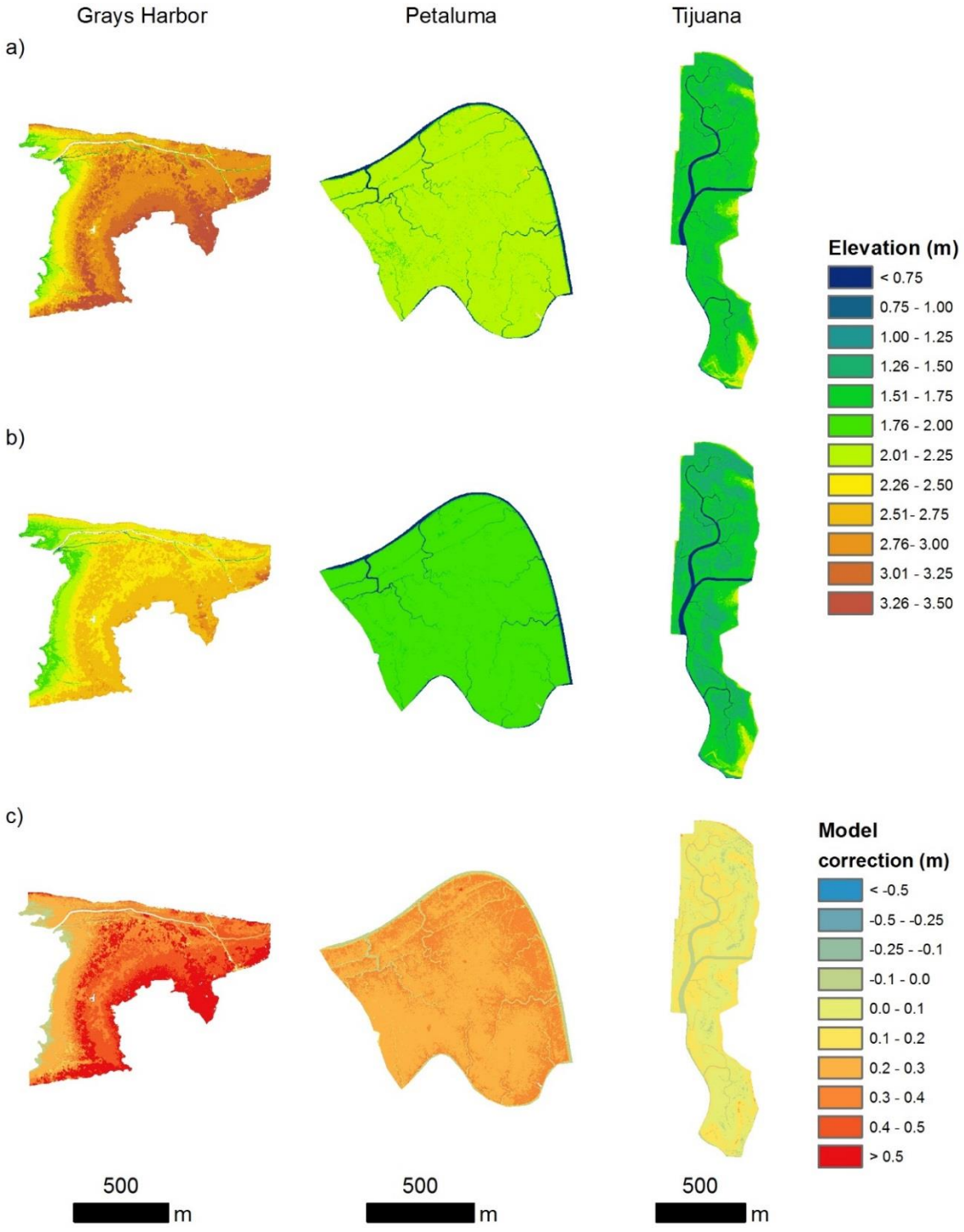

Figure 2.4. Example results from each region (Pacific Northwest: Grays Harbor; San Francisco Bay: Petaluma; Southern California: Tijuana. (a) Uncorrected lidar digital terrain model (DEM; (b) model adjusted DEM, and (c) total adjustment. Elevation in m, National Vertical Datum of 1988.

Table 2.6. Sea-level rise (SLR) projections (National Research Council 2012) and recommended digital elevation model accuracy (root mean squared error [RMSE]) for San Francisco Bay (SFB), Southern California (SCA), and Pacific Northwest (PNW) study sites.

	SLR Projection (cm)		RMSE (cm)	
Year	SFB/SCA	PNW	SFB/SCA	PNW
2030	14.4	6.8	3.8	1.7
2050	28.0	17.2	7.1	4.3
2100	91.9	63.3	23.2	16.0

ACKNOWLEDGMENTS

The authors would like to thank all the technicians who helped collect the RTK-GPS data for this study, including C. Freeman, K. Powelson, K. Lovett, L. Curry, P. Elson, T. Henner, and T. Bui. Thanks also to A. Nolin, C. Janousek and J. Vogeler for valuable conversations, comments, and insight. E. Harrington and C. Malachowski provided editorial assistance on earlier drafts of the manuscript. Special thanks to L. Schile for providing the vegetation corrected DEMs of China Camp and Coon Island for comparisons to LEAN. We would also like to thank DOI U.S. Geological Survey, Western Ecological Research Center, National Climate Change and Wildlife Science Center, the National Oceanic and Atmospheric Administration EESLR program (grant ID NA15NOS4780171), Northwest Climate Science Center (NWCSC), Southwest Climate Science Center, U.S. Fish & Wildlife Service North Pacific and California Landscape Conservation Cooperatives, Oregon State University and the NWCSC fellowship for

funding support. Any use of trade, product, or firm names in this publication is for descriptive purposes only and does not imply endorsement by the U.S. government.

LITERATURE CITED

Adam, E., O. Mutanga, and D. Rugege. 2010. Multispectral and hyperspectral remote sensing for identification and mapping of wetland vegetation: A review. Wetlands Ecology and Management 18:281–296.

Butzeck, C., A. Eschenbach, A. Gröngröft, K. Hansen, S. Nolte, and K. Jensen. 2015. Sediment Deposition and Accretion Rates in Tidal Marshes Are Highly Variable Along Estuarine Salinity and Flooding Gradients. Estuaries and Coasts 38:434–450.

Cahoon, D. R., and D. J. Reed. 1995. Relationships amoung marsh surface topography, hydroperoid, and soil accretion in a deteriorating Louisana salt marsh. Journal of Coastal Research 11:357–369.

Chavez, P. S. J. 1988. An improved dark-object subtraction technique for amtopshiec scattering correction of multispectral data. Remote Sensing of Environment 24:459–479.

Craft, C., J. Clough, J. Ehman, S. Jove, R. Park, S. Pennings, H. Guo, and M. Machmuller. 2009. Forecasting the effects of accelerated sea-level rise on tidal marsh ecosystem services. Frontiers in Ecology and the Environment 7:73–78.

Federal Geographic Committee. 1998. Geospatial positioning accuracy standards part 3: National standard for spatial data accuracy. FGDC-STD-007 3-1998, http://www.fgdc.gov/standards/projects/FGDC-standards-projects/accuracy/part3/chapter3.

Filella, I., J. Peñuelas, L. Llorens, and M. Estiarte. 2004. Reflectance assessment of seasonal and annual changes in biomass and CO2 uptake of a Mediterranean shrubland submitted to experimental warming and drought. Remote Sensing of Environment 90:308–318.

Flood, M (ed.). 2004. Vertical accuracy reporting for lidar data, version 1.0. ASPRS Lidar Committee (PAD), 20p. http://asprs.org/a/society/committee/lidar/Downloads/Vertical_Accuracy_Reporting_for_Lidar_Data.pdf

Foxgrover, B. A. C., D. P. Finlayson, and B. E. Jaffe. 2011. 2010 Bathymetry and Digital Elevation Model of Coyote Creek and Alviso Slough, South San Francisco Bay, California. U.S. Geological Survey Open File Report:20.

Gamon, J. A., C. B. Field, M. L. Goulden, K. L. Griffin, A. Hartley, G. Joel, J. Penuelas,

and R. Valentini. 1995. Relationships Between NDVI, Canopy Structure, and Photosynthesis in Three Californian Vegetation Types. Ecological Applications 5:28–41.

Hackney, C. T., S. Brady, L. Stemmy, M. Boris, C. Dennis, T. Hancock, M. O'Bryon, C. Tilton, and E. Barbee. 1996. Does intertidal vegetation indicate specific soil and hydrologic conditions. Wetlands 16:89–94.

Hladik, C., and M. Alber. 2012. Accuracy assessment and correction of a LIDAR-derived salt marsh digital elevation model. Remote Sensing of Environment 121:224–235.

Hodgson, M. E., and P. Bresnahan. 2004. Accuracy of Airborne Lidar-Derived Elevation : Empirical Assessment and Error Budget. Photogrammetric engineering and remote sensing 70:331–339.

Janousek, C. N., Buffington, K. J., Thorne, K. M., Gutenspergen, G. R., Takekawa, J. Y., Dugger B. D. 2016. Potential effects of sea-level rise on plant productivity:species-specific responses in northeast Pacific tidal marshes. *Marine Ecology Progress Series*, 548: 111-125.

Kane, V. R., R. J. McGaughey, J. D. Bakker, R. F. Gersonde, J. A. Lutz, and J. F. Franklin. 2010. Comparisons between field- and LiDAR-based measures of stand structural complexity. Canadian Journal of Forest Research 40:761–773.

Kirwan, M. L., and G. R. Guntenspergen. 2012. Feedbacks between inundation, root production, and shoot growth in a rapidly submerging brackish marsh. Journal of Ecology 100:764–770.

Kirwan, M., and S. Temmerman. 2009. Coastal marsh response to historical and future sea-level acceleration. Quaternary Science Reviews 28:1801–1808.

Kolker, A. S., S. L. Goodbred, S. Hameed, and J. K. Cochran. 2009. High-resolution records of the response of coastal wetland systems to long-term and short-term sea-level variability. Estuarine, Coastal and Shelf Science 84:493–508.

Langley, A. J., T. J. Mozdzer, K. A. Shepard, S. B. Hagerty, and J. Patrick Megonigal. 2013. Tidal marsh plant responses to elevated CO2, nitrogen fertilization, and sea level rise. Global Change Biology 19:1495–1503.

Maune, D. F., Maitra, J. B., and McKay, E. J. 2007. Accuracy standards & guidelines. In: Maune D. (ed.), Digital Elevation Model Technologies and Applications. The DEM Users Manual, 2nd Edition. Bethesda, Maryland: American Society for Photogrammetry and Remote Sensing, pp. 65-97.

Medeiros, S., S. Hagen, J. Weishampel, and J. Angelo. 2015. Adjusting Lidar-Derived Digital Terrain Models in Coastal Marshes Based on Estimated Aboveground Biomass Density. Remote Sensing 7:3507–3525.

Mitasova, H., M. F. Overton, J. J. Recalde, D. J. Bernstein, and C. W. Freeman. 2009. Raster-Based Analysis of Coastal Terrain Dynamics from Multitemporal Lidar Data.

Journal of Coastal Research 252:507–514.

Montané, J. M., and R. Torres. 2006. Accuracy Assessment of Lidar Saltmarsh Topographic Data Using RTK GPS. Photogrammetric Engineering & Remote Sensing:961–967.

Morris, J. T., P. V. Sundareshwar, C. T. Nietch, B. Kjerfve, and D. R. Cahoon. 2002. Responses of coastal wetlands to rising sea level. Ecology 83:2869–2877.

Myneni, R. B., F. G. Hall, P. J. Sellers, and A. L. Marshak. 1995. Interpretation of spectral vegetation indexes. IEEE Transactions on Geoscience and Remote Sensing 33:481–486.

National Research Council. 2012. Sea-Level Rise for the Coasts of California, Oregon, and Washington: Past, Present, and Future.

National Digital Elevation Program (NDEP). 2004. Guidelines for Digital Elevation Data, Version 1.0. 10 May 2004, 93 p. http://www.ndep.gov/NDEP_Elevation_Guidelines_Ver1_10_May2004.pdf

National Oceanic and Atmospheric Administration (NOAA). 2010. Technical considerations or the use of geospatial data in sea level change mapping and assessment. Silver Spring, Maryland: U.S. Department of Commerce, NOAA NOA Technical Report, NOAA National Ocean Service, 141 p. http://www.csc.noaa.gov/digitalcoast/_/pdf/SLC_Technicial_Considerations_Document.pdp.

Parrish, C. E., Rogers, J. N., and Calder, B. R. 2014. Assessment of waveform features for lidar uncertainty modeling in a coastal salt marsh environment. *IEEE Geoscience and Remote Sensing Letters*, 11:2, 569-573.

Pennings, S. C., R. M. Callaway, N. Apr, and M. C. Way. 1992. Salt Marsh Plant Zonation: The Relative Importance of Competition and Physical Factors. Ecology 73:681–690.

Pettorelli, N., J. O. Vik, A. Mysterud, J. M. Gaillard, C. J. Tucker, and N. C. Stenseth. 2005. Using the satellite-derived NDVI to assess ecological responses to environmental change. Trends in Ecology and Evolution 20:503–510.

Rosso, P. H., S. L. Ustin, and A. Hastings. 2005. Mapping marshland vegetation of San Francisco Bay, California, using hyperspectral data. International Journal of Remote Sensing 26:5169–5191.

Sadro, S., M. Gastil-Buhl, and J. Melack. 2007. Characterizing patterns of plant distribution in a southern California salt marsh using remotely sensed topographic and hyperspectral data and local tidal fluctuations. Remote Sensing of Environment 110:226–239.

Schile, L. M., J. C. Callaway, J. T. Morris, D. Stralberg, V. Thomas Parker, and M. Kelly. 2014. Modeling tidal marsh distribution with sea-level rise: Evaluating the

role of vegetation, sediment, and upland habitat in marsh resiliency. PLoS ONE 9.

Schmid, K. A., B. C. Hadley, and N. Wijekoon. 2011. Vertical Accuracy and Use of Topographic LIDAR Data in Coastal Marshes. Journal of Coastal Research 275:116–132.

Shaughnessy, F. J., W. Gilkerson, J. M. Black, D. H. Ward, and M. Petrie. 2012. Predicted eelgrass response to sea level rise and its availability to foraging Black Brant in Pacific coast estuaries. Ecological Applications 22:1743–1761.

Silvestri, S., A. Defina, and M. Marani. 2005. Tidal regime, salinity and salt marsh plant zonation. Estuarine, Coastal and Shelf Science 62:119–130.

Swanson, K. M., J. Z. Drexler, D. H. Schoellhamer, K. M. Thorne, M. L. Casazza, C. T. Overton, J. C. Callaway, and J. Y. Takekawa. 2013. Wetland Accretion Rate Model of Ecosystem Resilience (WARMER) and Its Application to Habitat Sustainability for Endangered Species in the San Francisco Estuary. Estuaries and Coasts 37:476–492.

Takekawa, J. Y, Thorne, K. M., Buffington, K. J., Spragens, K. A., Swanson, K. M., Drexler, J. Z., Schoellhamer, D. H., Overton, C. T., and Casazza, M. L. 2013. Final report for sea-level rise response modeling for San Francisco Bay estuary tidal marshes. U. S. Geological Survey Open File Report 2013-1081, 161 p.

Takekawa, J. Y., I. Woo, K. M. Thorne, K. J. Buffington, N. Nur, M. L. Casazza, and J. T. Ackerman. 2012. Chapter 12: Bird communities: effects of fragmentation, disturbance, and sea level rise on population viability. Pages 175–194Ecology, Conservation, and Restoration of Tidal Marshes: The San Francisco Estuary.

Thorne, K. M., B. D. Dugger, K. J. Buffington, C. M. Freeman, C. N. Janousek, K. W. Powelson, G. R. Gutenspergen, and J. Y. Takekawa. 2015. Marshes to mudflats—Effects of sea-level rise on tidal marshes along a latitudinal gradient in the Pacific Northwest: U.S. Geological Survey Open-File Report 2015-1204, 54 p. plus appendixes, http://dx.doi.org/10.3133/ofr20151204.

Thorne, K. M., G. M. MacDonald, R. F. Ambrose, K. J. Buffington, C. F. Freeman, C. N. Janousek, L. N. Brown, J. R. Holmquist, G. R. Gutenspergen, K. W. Powelson, P. L. Barnard, and J. Y. Takekawa. 2016. Effects of climate change on tidal marshes along a latitudinal gradient in California: U.S. Geological Survey Open-File Report 2016-1125, 75 p., http://dx.doi.org/10.3133/ofr20161125.

Improving Projections of Tidal Marsh Persistence under Climate Change with Remote Sensing and Site-Specific Data

CHAPTER 3

USING THE LANDSAT ARCHIVE TO ASSESS VARIATION IN PLANT PEAK BIOMASS AND GROWTH PHENOLOGY IN PACIFIC NORTHWEST TIDAL MARSHES

Kevin J. Buffington, Bruce D. Dugger, and Karen M. Thorne

ABSTRACT

Tidal marsh plant sensitivity to climate change impacts beyond sea-level rise has not been well established. Plant biomass is critical in the biogeomorphic feedback that occurs in marshes, which helps maintain marsh elevation relative to sea-level, as well as sequestering carbon. Furthermore, the phenology range of peak biomass has not been well documented in tidal marshes even though it may have important ecological consequences. We used the Landsat archive to assess how recent climate variation has affected biomass production and plant phenology across three maritime tidal marshes in the Pacific Northwest of the United States. We developed models of annual phenology using the Tasseled Cap Greenness (TCG) vegetation index and up to 29 years of images. We harvested biomass across 30 Landsat pixels to validate the relationship between TCG and aboveground biomass, and developed a significant model with reasonably high predictive power ($r^2 = 0.72$). We then assessed relationships between both peak biomass and peak day of year (DOYP) and 94 climate and sea-level metrics using generalized linear models and Akaike Information Criterion model selection. We found peak biomass was positively related to total annual precipitation, while the best predictor for DOYP was average temperature in May, with DOYP 4.5 days earlier per degree C. Our study shows how plants in maritime tidal marshes respond to interannual climate variation and demonstrates the utility of time-series remote sensing data to assess ecological responses to climate change.

INTRODUCTION

Tidal marshes are among the world's most productive ecosystems (Mitsch and Gosselink 2007) and they are among the most vulnerable to climate change. Climate change will impact coastal ecosystems through sea-level rise, increasing temperatures, and changing precipitation patterns (Scavia et al. 2002, Day et al. 2008), risking the loss of ecosystem services (Barbier et al. 2011) such as carbon storage (Chmura et al. 2003) and alteration of habitat composition important to wetland wildlife (Takekawa et al. 2012). Changes in tidal marsh plant community composition are already apparent and are projected to continue (Jarrell et al. 2016, Ward et al. 2016, Thorne et al. 2015, Thorne et al. 2016). However, the sensitivity of tidal marsh plants to changes in climate is not well understood (e.g., Osland et al. 2016).

A change in peak biomass and phenology of plant growth are two possible consequences of climate change in coastal tidal marshes (Cleland et al. 2007, Kirwan et al. 2009, Morisette et al. 2009, Walther 2010). Shifting phenology can lead to temporal mismatches between producers and consumers with ecosystem-wide consequences (Stenseth et al. 2002, Visser and Both 2005). Wildlife and fish communities may experience the effects of shifting phenology indirectly through changes in the abundance and composition of the invertebrate community, which may be more closely tied to the green-up of emergent vegetation (Baxter et al. 2005). Furthermore, mismatch between plant green-up and migrant arrival can reduce breeding success in migratory birds (e.g., Aubry et al. 2013). Changes in plant biomass not only influences the energy available to herbivores, it also plays a critical role in the biogeomorphic feedbacks that maintain marsh surface elevation with rising sea levels (Morris et al. 2002). For example,

increased aboveground biomass can stimulate sediment deposition by increased sediment trapping and reduced water velocities (Leonard and Luther 1995). In a fertilization experiment of *Spartina alterniflora*, Morris et al. (2002) found a 150% increase in sedimentation rate when aboveground biomass increased 320%. While the interannual variation in aboveground biomass in natural systems is much lower, these results demonstrate the important role that aboveground biomass plays in tidal marsh vulnerability to sea-level rise.

By examining how tidal marsh plants have responded to recent climatic variation, we can gain insight into how sensitive they may be to future changes in climate and how existing interactions between plants and species that rely on them might change. Across the Pacific coast of the United States, the El Nino-Southern Oscillation (ENSO) generates substantial interannual variation in temperature and precipitation (Gershunov and Barnett 1998), which may influence the timing of the growing season and aboveground biomass production. ENSO-driven variation has been used to assess the climate sensitivity of forests, salmon, and water resources (e.g., Parson et al. 2003), however, the sensitivity of tidal marsh plant phenology to climate variation has not been well explored.

Remote sensing is an alternative to more expensive field-based methods for monitoring vegetation at broad spatial and temporal scales (Goetz and Dubayah 2011). Moderate resolution satellite sensors such as Landsat offer sufficient detail to examine ecosystem patterns and the 16-day revisit time allows the study of annual phenology patterns (e.g., Fisher et al. 2006, Melaas et al. 2013, Mo et al. 2015). Additionally, the Landsat archive provides a global dataset for analysis of temporal trends over the last 45

years allowing researchers to retroactively investigate the roll of past climate on marsh plant vegetation.

We use the Landsat archive (1984-2015) to explore the relative influences of climate and sea level on tidal marsh aboveground biomass and phenology in three maritime tidal marshes in the Pacific Northwest of the United States. Specifically, our goals were to: 1) calibrate a model of aboveground tidal marsh plant biomass with field sampling; 2) determine the most important climate drivers of aboveground biomass and phenology; and 3) demonstrate the utility of Landsat and cloud computing for near-real time monitoring of coastal systems.

METHODS

Study sites

Our study sites included four Pacific Northwest tidal marshes: three outer coast sites (Bandon National Wildlife Refuge [NWR] on the Coquille river [hereafter Bandon], Grays Harbor NWR, north of Bowerman airport [Grays], Willapa Bay NWR, near Tarlett slough [Willapa]) and a Puget Sound site (Nisqually NWR [Nisqually]; Figure 3.). Tidal marshes can be defined into different marsh communities based on inundation rates; low marsh (lowest elevation of vegetation to inundation under 50% of high tides), mid marsh (25-50% inundation), and high marsh (3-25% inundation; Thorne et al. 2015). The marshes have broadly similar plant communities, with *Sarcocornia pacifica, Jaumea carnosa, and Carex lyngbyei* dominant in the low marsh, *Distichlis spicata*, *Triglochin maritima*, and *Agrostis stolonifera* found in the mid marsh, and *Deschampsia cespitosa*, *Juncus balticus*, and *Potentilla anserine* found in the high marsh (Thorne et al. 2015).

The Pacific Northwest experiences a maritime climate with cool, wet winters and warm, dry summers. Interannual climatic variation primarily is driven by cyclic patterns of sea surface temperature (ENSO and PDO), where El Nino tends to bring warmer temperatures and less precipitation, and La Nina cooler temperatures and greater precipitation (Gershunov and Barnett 1998).

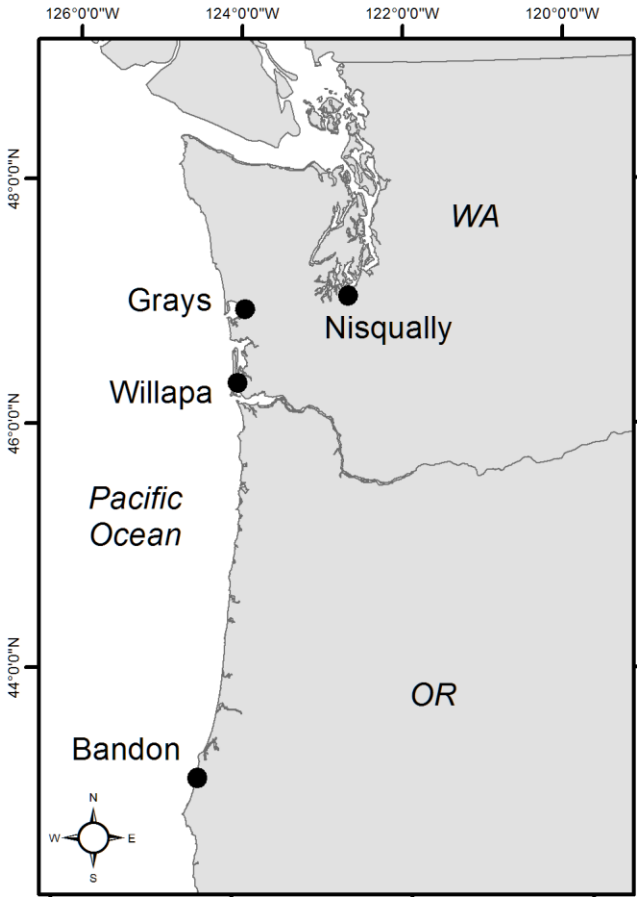

Figure 3.1. Map of study site locations along the Pacific coast.

Landsat Imagery

Landsat images (30 × 30 m resolution) were obtained and processed via Google Earth Engine (GEE). GEE provides access to the Landsat archive with cloud computing capabilities that facilitate online batch processing of the entire archive without having to

download the original images. We employed several steps to calibrate Landsat imagery so the spectral data were comparable through time and to ensure only high quality images were included in the dataset. The period of study (1984-2015) included images collected by different Landsat Sensors (Thematic Mapper/Enhanced Thematic Mapper Plus [TM/ETM+] and Operational land Imager [OLI]). To account for differences in spectral and radiometric resolution we harmonized the OLI images to TM/ETM+ images using a standard set of coefficients (Roy et al. 2016). For our analysis, we used the surface reflectance products from the USGS that were calculated using the Landsat Ecosystem Disturbance Adaptive Processing System (LEDAPS) algorithm (Masek et al. 2008). From surface reflectance we calculated Tasseled Cap Greenness (TCG; Kauth and Thomas 1976), which is a principal component transformation of six Landsat bands and correlates closely with photosynthetic activity. Unlike the widely used Normalized Difference Vegetation Index, TCG does not saturate in dense vegetation (Mutanga and Skidmore 2004) making it suitable for biomass estimation in productive tidal marshes. We removed cloud and cloud shadows within the Landsat images using the 'cfmask' product from the USGS (Zhu and Woodcock 2012).

We also wanted to compare the effect of additional quality control steps on the peak TCG and day of peak TCG. We visually inspected every image and removed images that had incomplete cloud and cloud shadow masking for each study site. Because water reduces the spectral signal of vegetation through the absorption of electromagnetic energy, we used hourly sea level data from nearby NOAA gauges and site-specific sea level thresholds to remove images acquired during high tide (tidesandcurrents.noaa.gov). Due to the high tide range at our sites water levels can rise and drop substantially within

one hour. To avoid removing too many images from the data set, we improved the temporal resolution of the water level data by interpolating the hourly data to 15 minutes using an exact interpolation method (natural spline) over five hour intervals. Two sets of time-series stacks of Landsat images (every image and QC images) were then extracted from GEE for each study site by year and used for the phenology and biomass analysis. Of the 3754 Landsat images available for the three sites, 1465 had less than 50% cloud cover and were included in the final analysis (every image), while an additional 202 were removed due to high tides or incomplete cloud masking (QC images). We used a paired t-test to assess whether the image QC steps significantly changed the biomass and DOY model results.

Abiotic Drivers of Biomass and Phenology

We assessed the relative influence of climate and sea level on peak TCG (TCGP) and day of peak TCG (DOYP) using an annual phenology model and time-series stacks of Landsat images. We modeled annual phenology for each pixel by fitting a Gaussian function ('nls' function in R) to TCG values and the day of the year the image was obtained (e.g., Mo et al. 2015),

$$TCG = B + Ae^{-(X-\mu)^2/2\sigma^2} \quad \text{Eq. 1}$$

where B is the background TCG value during winter, A is the amplitude of TCG during the growing season, μ is the day of peak TCG (DOYP), and σ is the standard deviation and controls the width of the curve. Considering these four parameters, we set a minimum requirement of five images per year to fit the phenology function. To protect against producing outlier metrics, we constrained the parameters to a range of reasonable

values derived from a regression fit that included images from all years. Additionally, we calculated Efron's pseudo r^2 ([-∞ - 1]; e.g., Mo et al. 2015) and used a threshold of 0.4 for the nonlinear regression to protect subsequent analysis from poor quality phenology models. Using a lidar-derived DEM, corrected for vegetation bias with the LEAN method (Chapter 2, Buffington et al. 2016) and standardized for tidal range using z* (z* = [z – MSL]/[MHHW – MSL]; where MSL: mean sea level, MHHW: mean higher high water; Swanson et al. 2013), we selected marsh areas that were between z* 0.9 and 1.0 for the final analysis. This elevation range represented the mid-high marsh transition zone (z*= 1.0 is MHHW). We then calculated the median of TCGP and DOYP by year across each site.

To examine how TCGP and DOYP varied with climate and sea level we gathered annual and seasonal datasets representing five categories of explanatory variables: temperature, precipitation, drought, ENSO, and sea level. We used gridded monthly datasets of temperature and precipitation from PRISM (PRISM, 2016) for 1984-2015. For each study site we extracted mean, min, and max temperature, and total precipitation for each year by month and season (winter: JFM, spring: AMJ, summer: JAS, fall: OND), and calculated mean and standard deviation of monthly mean temperature during the growing season (April-September). We considered mean annual and seasonal drought indices, including the Self-Calibrating Palmer's Drought Severity Index (SCPDSI; Wells et al. 2004), the Standardized Precipitation Index (SPI; Mckee et al. 1993) and the Standardized Precipitation Evapotranspiration Index (SPEI; Vicente-Serrano et al. 2010). SCPDSI represents the relative water deficit and is a function of eight climatic variables including evapotranspiration, temperature, and precipitation. SPI compares total

precipitation within a given time period to the historic average, while SPEI incorporates the effect of temperature on evapotranspiration rates into the index. We also considered the multivariate ENSO index (MEI) and the Pacific Decadal Oscillation (PDO), summarized globally by year and season, and the annual Oceanic Nino Index (ONI).

Sea level tidal datums were calculated using data from nearby NOAA tide gauges and site-specific water level data (Thorne et al 2015). We used a second-order polynomial to predict the offset in water level height between the NOAA gauge and each site, and then applied the offset to the historic NOAA water level data. Annual and seasonal mean high water (MHW) and mean higher high water (MHHW) tidal datums were then calculated from the adjusted water level data. Altogether, we obtained 94 climate and sea level variables to analyze with TCGP and DOYP.

Biomass model

To validate our assumption of the relationship between TCG and aboveground biomass, we developed a model using TCG from Landsat imagery and alive aboveground plant biomass using samples collected from plots at Willapa during the summer of 2016. To ensure sampling sites included a range of biomass values, the marsh at Willapa was stratified into five 'greenness' classes based on a one-dimensional 'natural Jenks' classification of a summer 2015 Landsat-derived TCG image. Six 30 × 30m Landsat pixels were randomly selected from each greenness class for a total of 30 pixels. The center of each sampling pixel was located in the field with a submeter GPS (Trimble GeoExplorer 3000) and three 25 × 50 cm (0.125 m^2) biomass plots were established, separated by seven m (Figure 3.2). For each plant species in a plot we estimated percent cover and measured maximum height (0.01 m) at the center and corners of the plot. We

clipped aboveground biomass in each plot and separately bagged living and dead vegetation. In the lab, all biomass and litter samples were washed to remove sediment and algae, oven-dried in paper bags at 60 °C until constant mass (~4 days), and then weighed to a precision of 0.01 g. The aboveground biomass values were adjusted by the vegetated fraction (divided by the percent of vegetated ground in the field survey) and then averaged within each sample pixel for further analysis.

We used a cloud-free Landsat 8 OLI surface reflectance image at Willapa (obtained May 31, 2016) to calibrate the biomass model from field surveys (July 11-14, 2016). Our goal was to calculate the average aboveground biomass (g m^{-2}) for each pixel; to do this we first needed the proportion of vegetated area in each calibration pixel. We used unsupervised K-means cluster analysis (Hartigan and Wong 1979) to classify a 2013 1 m National Agriculture Inventory Program (NAIP) image into vegetated/unvegetated (1/0), aggregated to a 30 m resolution, and divided by 900 (the number of 1 meter NAIP pixels within a 30 m Landsat pixel). Mean biomass values for each sampled pixel were then multiplied by the proportion of vegetated area from the NAIP analysis, log-transformed, and used as the dependent variable in models to predict biomass using TCG. We used leave one out cross-validation (LOOCV, Efron 1982) to estimate the root mean squared error (RMSE) of predicted biomass.

Model Development and Analysis

We used a two-tier approach for model development including an initial variable reduction/selection step. Willapa was originally included in the phenology and biomass analyses, however it was removed due to the low number of cloud-free images that were available for the period of years in the study. First, for each dependent variable, we used

generalized linear models (GLMs) to find the top explanatory variable within each category of weather variable. We controlled for inherent differences among study sites by including site as an explanatory variable in all models, and our 'null' model was the single factor model with site. The top predictor in each category was then included in the second modeling stage. In the second stage, we limited model complexity to three explanatory variables in additive models, including every possible combination in the model set. Due to correlation between the oceanic indices and local climate we did not include the ENSO and PDO indices in models with predictors from the other categories. Fourteen models were considered for TCGP and sixteen models were considered for DOYP (Table 3.2). We compared among models using AIC values and model weights, considering any model within two AIC values of the top model competitive, and we evaluated the magnitude and direction of effects using parameter estimates and their 95% confidence limits (Burnham and Anderson 2002). We assessed relative variable importance of the predictors in the top model with the 'calc.relimp' function (library: relaimpo, type:'lmg').

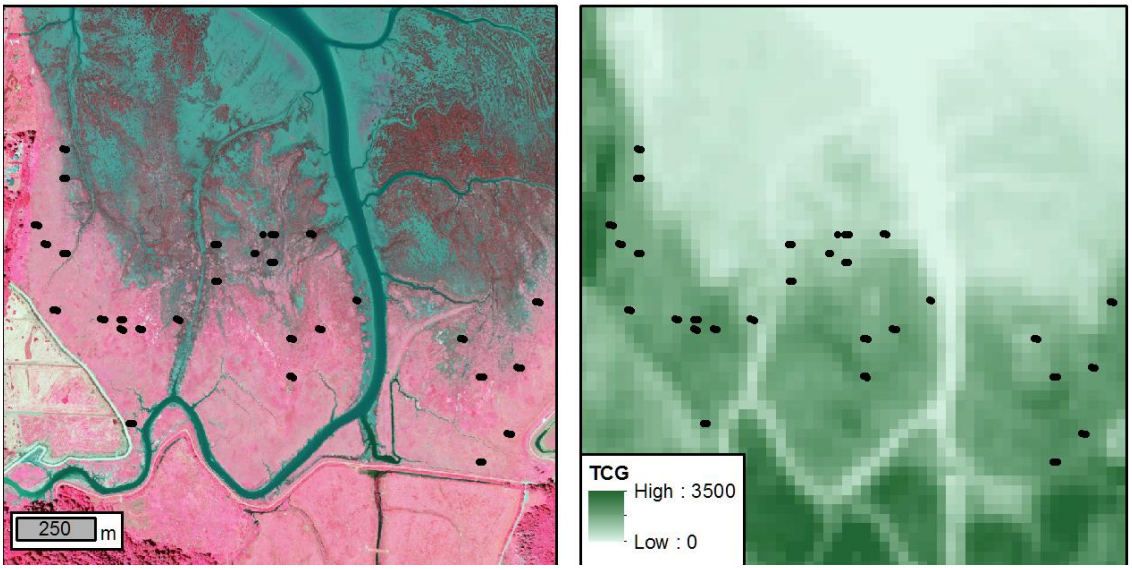

Figure 3.2. Locations of biomass clip plots Willapa NWR. False color NAIP imagery (left) and Landsat 8 Tasseled Cap Greenness (TCG, right).

RESULTS

Log-transformed plant biomass at Willapa was significantly related to log-transformed TCG ($r^2 = 0.71$; $F_{1,28} = 71.6$; $p < 0.0001$; Figure 3.3). We calculated an RMSE of 73.6 g using LOOCV. The 6-week disparity between field sampling and a cloud-free image means there was a potential of underestimating aboveground biomass with the TCG model. We estimated the day of peak TCG at Willapa was DOY 175 (SE = 4.4). The cloud-free calibration image was acquired on DOY 152 and our field sampling occurred on DOY 193-196. Based on the 2016 TCG phenology model and difference in predicted TCG between the image calibration and field sampling, we potentially underestimated peak biomass by 2%. There was no difference between the complete time series image stacks and the QC stacks for either TCGP ($t_{79} = 1.24$, $p = 0.22$) or DOYP ($t_{79} = 1.78$, $p = 0.08$), so we choose to use the complete stacks for the phenology and climate

modeling because that provided an additional seven years of data for the Grays study site. We used an average (range) of 19.0 (7-42), 12.9 (5-24), and 16.3 (5-34) images per year at Bandon, Grays, and Nisqually, respectively (Fig. 3.4).

During the years of our study, plant peak biomass varied by 42% (752 – 1064 g m^{-2}) at Bandon and 46% (762 – 1116 g m^{-2}) at Nisqually. We did not apply the TCG/biomass calibration to Grays because the range of TCGP values at Grays were higher than the TCG values that occurred during calibration at Willapa. Given the observed correlation between biomass and TCG at Willapa and the long history of using vegetation metrics as indicators of biomass (see reviews: Verstraete et al. 1996, Moran et al. 1997), we are confident that the relative changes in TCG observed at Grays are indicative of changes in aboveground biomass. However, for consistency across sites we choose to use TCGP rather than predicted peak biomass for the subsequent climate analysis.

For analysis of TCGP, the single best explanatory variable from each category of weather variables was total annual precipitation, annual SPEI, spring minimum temperature, spring MHHW, and summer PDO. The top multivariate model had a model weight of 0.69 and included site, minimum spring temperature, total annual precipitation, and the interaction with site and spring minimum temperature (Table 3.2). In the best model, study site accounted for the most variation (80%), followed by annual precipitation (17%) the interaction between spring minimum temperature and site (1.6%) and spring minimum temperature (1%). TCGP was greater overall at Grays and increased with annual precipitation at all sites (Fig. 3.5). The influence of minimum spring

temperature varied with site, with a negative relationship at Grays but no relationship at the other two sites.

Median DOYP ranged 34 days at Bandon, 29 days at Grays and 40 days at Nisqually. Across sites and years, DOYP ranged 42 days but on average was not significantly different across sites within each year ($F_{5,68} = 0.95$, $p = 0.45$). For analysis of DOYP, the single best explanatory variable from each category of weather variables was summer precipitation, annual SPEI, May mean temperature, annual MHHW, and annual PDO. There were seven competitive models that had a combined model weight of 0.99. All models included May mean temperature and the confidence limits around the parameter estimate did not include zero. The confidence limits around the parameter estimates for all other explanatory variables in the competitive model set overlapped zero, suggesting they had a very weak influence. The top model included May mean temperature, annual MHHW, and the interaction between site and May mean temperature. In the best model, May mean temperature accounted for the most variation (58%), followed by site (21%), annual MHHW (11%), and the interaction between site and May mean temperature (8.9%). Increased May mean temperature and annual MHHW resulted in earlier DOYP and across sites, DOYP averaged 4.5 (SE = 0.71) days earlier with each degree increase in mean May temperature.

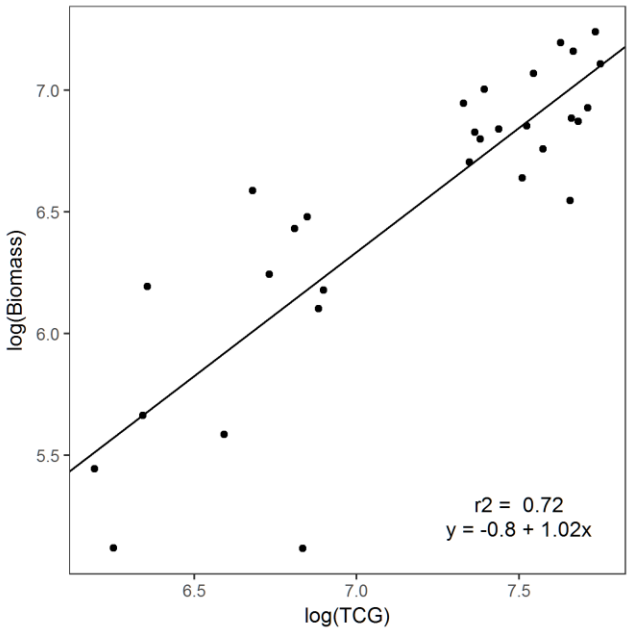

Figure 3.3. Relationship between alive aboveground biomass and Tasseled Cap Greenness (TCG) derived from a 2016 Landsat 8 image of Willapa Bay, Washington.

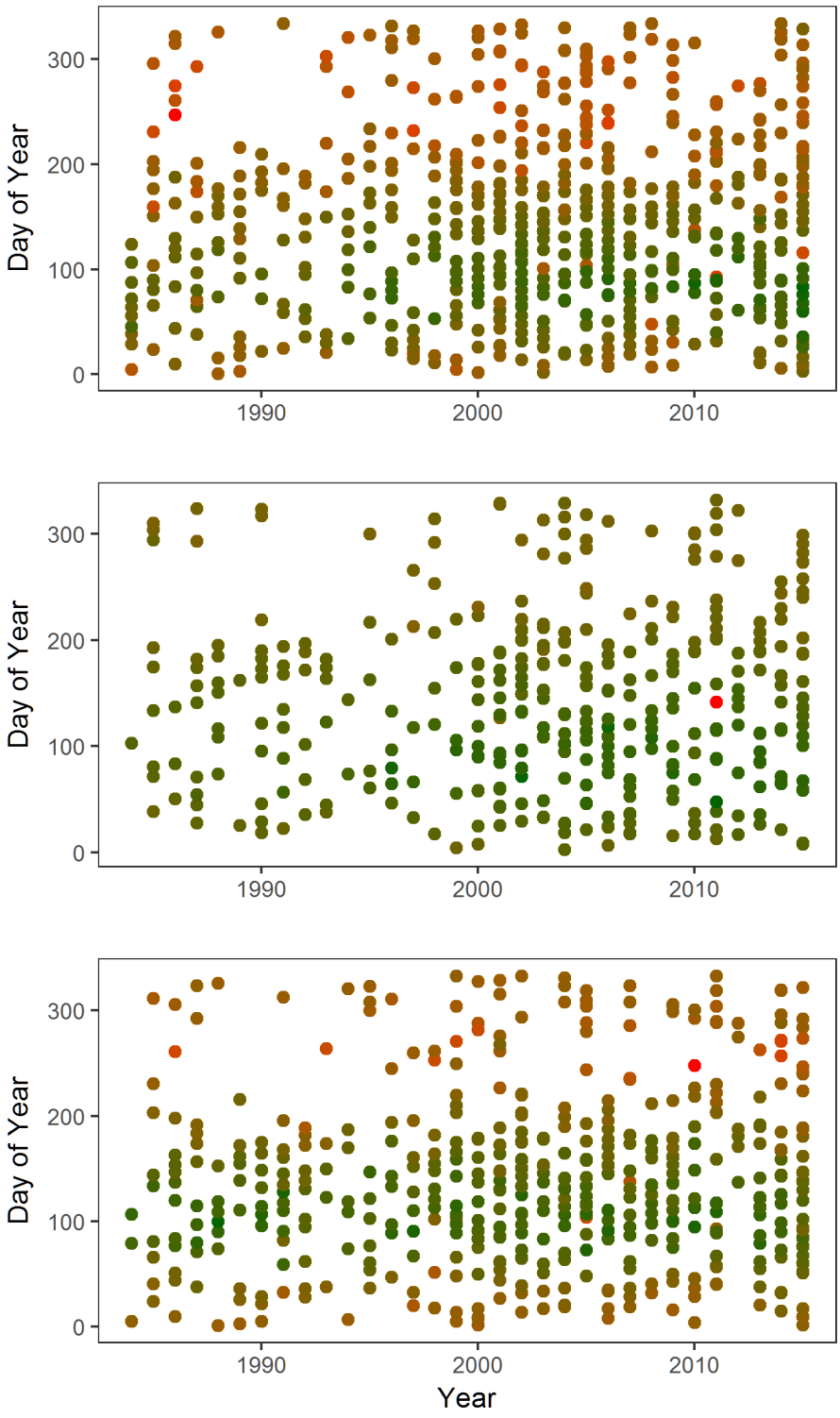

Figure 3.4. Schematic of Landsat scenes with less than 50% cloud cover for the study period (1984-2015; top-bottom, Bandon, Grays, Nisqually). Years with at least five images were included in the phenology models. Colors indicate mean Tasseled Cap Greenness for the study area, with low values in red and high values in green.

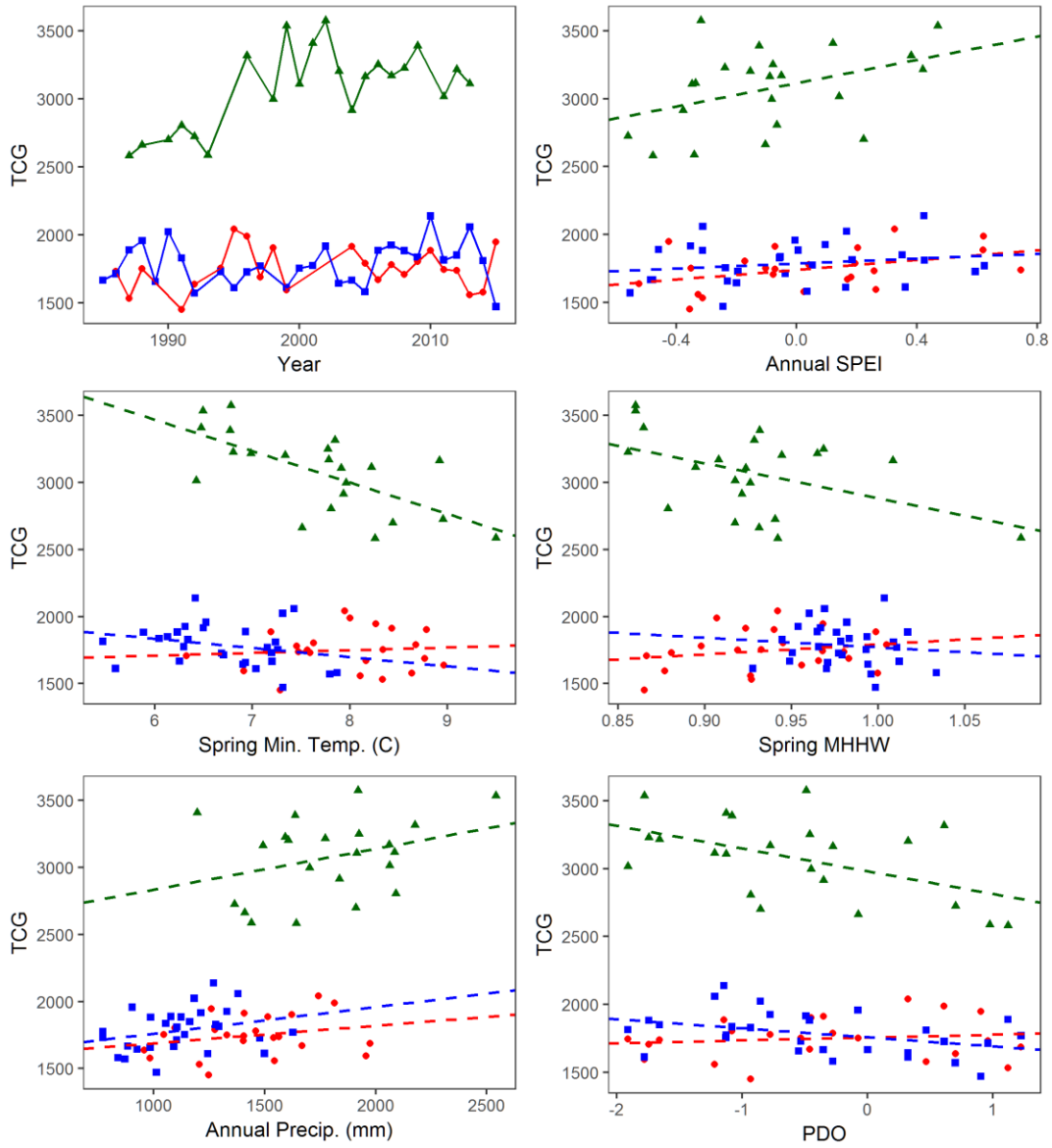

Figure 3.5. Relationship between peak TCG and environmental drivers for the three Pacific Northwest study sites. Each point represents one year. SPEI is the Standardized Precipitation Evapotranspiration Index where negative values indicate deeper drought. (Bandon, red circles; Nisqually, blue squares; Grays, green triangles)

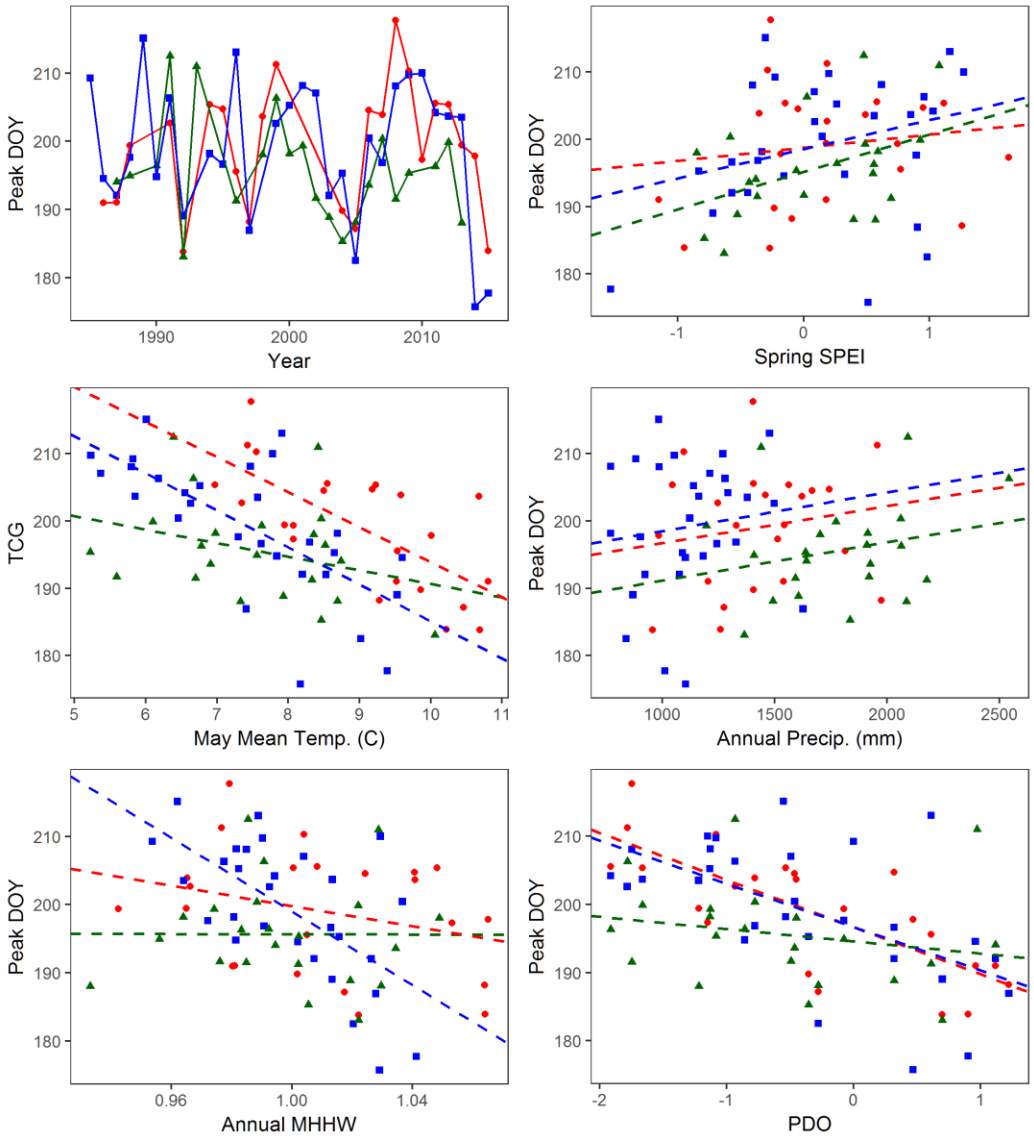

Figure 3.6. Relationship between day of peak biomass and significant abiotic drivers. MHHW is mean higher high water. (Bandon, red circles; Nisqually, blue squares; Grays, green triangles)

Table 3.1. Mean (±SD) peak biomass, peak TCG, day of peak TCG, climate, and sea level metrics for three Pacific Coast mid-high elevation tidal marshes from 1984-2015. Precipitation and monthly temperature is from PRISM, and the sea level data is from NOAA water level gauges that were calibrated to site-specific conditions.

	Nisqually	Grays	Bandon
Peak Biomass (g m^{-2})	928 ± 83.4	-	908 ± 80.4
Peak TCG	1785 ± 157	3076 ± 298	1747 ± 152
DOY Peak TCG (Days)	199.2 ± 10.1	195.6 ± 7.5	199.1 ± 9.1
Annual Mean Temp. (C)	10.8 ± 0.6	10.4 ± 0.6	11.0 ± 0.6
Annual Precip. (mm)	1125 ± 208	1805 ± 324	1408 ± 315
Spring MHW (z*)	0.82 ± 0.03	0.73 ± 0.05	0.77 ± 0.05

Table 3.2. Results from GLM models that predict peak TCG and climate in three mid-high elevation Pacific Coast tidal marshes.

Model[abc]	k	Log-likelihood	Deviance	ΔAIC	weight
Site + Temp + *PPT* + *Site*Temp*	7	-483.24	2036460	0	0.69
Site + Temp + *Site*Temp*	6	-485.39	2158573	2.31	0.22
Site + Temp + Tide + *Site*Temp*	7	-485.26	2150725	4.04	0.09
Site	3	-498.29	3059039	22.11	0

[a]*italics indicates confidence intervals for the parameter estimate did not overlap zero.*
[b]Temp = mean minimum spring temperature; PPT = total annual precipitation; Tide = spring mean higher high water; SPEI = annual average standardized precipitation evapotranspiration index.
[c]AIC value for the best model = 982.48.

Table 3.3. Results from GLM models that relate weather and tide variables to the day of peak biomass in three mid-high elevation Pacific Coast tidal marshes.

Model[abc]	k	Log-likelihood	Deviance	ΔAIC	weight
Site + *Temp* + Tide + Site*Temp	7	-246.42	3381.614	0	0.22
Site + *Temp* + Site*Temp	6	-247.7	3501.084	0.57	0.17
Site + *Temp* + SumPPT + Site*Temp	7	-246.8	3417.077	0.77	0.15
Site + *Temp* + Tide	5	-248.94	3620.638	1.05	0.13
Site + *Temp* + MHHW	5	-248.94	3620.638	1.05	0.13
Site + *Temp*	4	-250.19	3744.942	1.55	0.1
Site + *Temp* + SumPPT	5	-249.28	3653.841	1.73	0.09
Site + *PDO* + *Site*PDO*	6	-250.78	3804.313	6.72	0.01
Site	3	-266.86	5875.221	32.88	0

[a]*italics indicates confidence intervals for the parameter estimate did not overlap zero.*
[b]Temp = mean May temperature; SumPPT = total summer precipitation; Tide = annual mean higher high water; PDO = annual Pacific Decadal Oscillation.
[c]AIC value for the best model = 508.83.

DISCUSSION

Our study is the first to examine climate drivers of plant phenology and biomass across maritime tidal marshes in the PNW. We found that PNW tidal marsh plants occupying a narrow elevation range also respond to annual variation in climate. Specifically, TCGP and DOYP varied with annual precipitation and spring temperature, respectively. Additionally, we were able to detect subtle changes in biomass with time-series remotely sensed data.

Greater biomass was associated with increased annual precipitation. Direct precipitation on the marsh can reduce pore water salinity, alleviating salt stress and lead to increased biomass production (Ustin et al. 1982, Noe and Zedler 2000, Dunton et al. 2001). This effect depends on the ambient salinity conditions, however, with a stronger influence in hypersaline soils that are prevalent in Californian salt marshes. Alternatively,

too much precipitation can hinder biomass production by waterlogging the soils (Hanson et al. 2016). Given the direction of the significant response and the dominance of salt-sensitive graminoids in the plant communities we studied (Thorne et al. 2015), we hypothesize that soil salinity hinders overall biomass production at our study sites. Studies of marshes in other climates support our findings. Across semi-arid Texan tidal marshes, biomass was positively related to precipitation (Dunton et al. 2001), while drought conditions negatively affected biomass in *Spartina alterniflora* in a subtropical marsh in Georgia (O'Donnell and Schalles 2016). Projected shifts in the timing of precipitation and freshwater flow due to climate change across the PNW, along with increased saltwater intrusion, may negatively impact biomass production of graminoids in favor of more salt-tolerant forbs (e.g., *Sarcorcornia pacifica*), altering the function and community structure of maritime tidal marshes. Additional studies linking soil salinity, tides, and precipitation patterns across PNW marshes would help elucidate the underlying mechanisms of biomass production and competition between plant communities.

We predicted that warmer temperatures would result in higher marsh biomass, as found in experimental manipulations (e.g., Charles and Dukes 2009), and in latitudinal studies of *Spartina* (Kirwan et al. 2009), however, we found no relationship between temperature at two sites and a negative relationship at the third. Instead, biomass increased with increased precipitation. The negative relationship of minimum spring temperature and biomass at Grays is difficult to understand. While we limited our study to a narrow elevation range to control for vegetation community, the much higher TCG values and different relationship between biomass and temperature suggest different species are dominant at our Grays site than at Bandon and Nisqually. Contrary to other

studies (e.g., Kirwan and Guntenspergen 2012, Janousek et al. 2016) we did not find a relationship between biomass and inundation, however our narrow elevation range, focus on peak biomass, and the relatively small range of variation in the tidal datum metrics are likely reasons for the absence of a significant relationship.

We found that interannual variation in abiotic characteristics resulted in variation in time of peak biomass of 34 days. Mo et al. (2015) used three years of Landsat imagery and phenology models to compare subtropical tidal marsh responses to extreme precipitation across Louisiana and found that drought delayed the peak of the growing season by two months; in our study, less precipitation was related to an earlier growing season, although temperature had a greater overall influence. Higher mean temperature in May lead to a significantly earlier peak of the growing season across our sites. Increasing temperatures due to climate change is resulting in earlier growing seasons in ecosystems around the world (Linderholm 2006), thus this result was not unexpected. Through induction, our results suggest that the mid-high marsh plants in the Pacific Northwest are limited in growth by salt stress and respond to warmer temperatures by altering their phenology rather than increasing aboveground biomass production; however, these findings should be confirmed through manipulation experiments in the field.

Changes in plant phenology can have impacts of marsh dependent wildlife and fish species through phenological mismatches (Canepuccia et al. 2010, Takekawa et al. 2012). Phenology mismatches due to climate change have been documented in other ecosystems, including forests and grasslands (reviewed in Walther 2010); however, the phenology shifts in tidal marshes are not well studied in general and ecological studies of the consequences are rare in tidal marshes (although see Thorne et al. 2012). The

direction and magnitude of responses can vary by trophic level (Doi et al. 2008, Ovaskainen et al. 2013, Schwartzberg et al. 2014), with plants tending to have a larger response to abiotic changes than higher trophic levels, with potentially broad ecological consequences. Additional studies on the impacts of phenological shifts on tidal marsh communities are warranted.

For the phenology modeling at our mid-high tidal marsh sites, removal of the high tide images and images with incomplete cloud and shadow masking did not make a significant difference in predicted TCGP or DOYP. While there was a statistically significant reduction in pseudo r^2 in the complete image dataset (0.88 vs. 0.86), in practice, we felt the gain in number of years added to our dataset outweighed the negligible difference in model performance. These results suggest that the Gaussian model regressions were robust to reductions in TCG value caused by water and imperfect cloud masking. Previous studies have noted the influence of standing water on the spectral signature (e.g., Byrd et al. 2014) and in more sparsely vegetated tidal areas (e.g., low marsh) there may have been a greater decrease in median TCG than at our mid-high elevation sites.

We found a strong relationship between Landsat-derived TCG and aboveground biomass at Willapa. We are aware of few studies that have predicted tidal marsh biomass using Landsat. In a tidal brackish marsh in the San Francisco Bay Delta, Byrd et al. (2016) achieved an R^2 of 0.57 when predicting aboveground biomass with spectral indices from Landsat 8 images and accounting for vegetated area. Differences in model performance likely reflect differences in the relationship among different plant communities, but also methodology. By accounting for the vegetated area within each

Landsat pixel using high resolution NAIP imagery we were able to predict biomass at the native 30 m resolution across the entire site. Accounting for the vegetated fraction is particularly important in marshes, where channels and ponds fragment the vegetation, causing a mixed spectral signal.

Calibration of satellite images in coastal areas with high cloud cover is a challenge. The paucity of cloud-free 2016 Landsat images at Willapa meant we had to rely on a calibration image taken six weeks prior to field sampling. However, through phenology modeling using the median TCG value in the available images we found that peak biomass likely occurred between sampling and the calibration image, reducing the amount of uncertainty in our biomass predictions. To fill in the gaps in our phenology model for Willapa, we also investigated the availability of cloud-free Sentinel-2A MultiSpectral Instrument images (European Space Agency, 10 m resolution), however, the study site was obscured by clouds in all summer 2016 images. When Sentinel-2B comes online later in 2017, the Sentinel program will have a 5-day revisit schedule; when combined with Landsat 7 & 8 (combined 8 day revisit) the chances of cloud-free image acquisition will be further increased and the opportunity for robust time-series analysis will be enhanced.

Finally, the combination of Landsat images and the Google Earth Engine analytical platform provides an important tool that can facilitate monitoring of ecosystems subject to change and evaluation of threats of sea-level rise and climate change. The cloud computing power of Google Earth Engine allowed us to consider over 3,700 Landsat images for this study. GEE was particularly useful considering the small size of our study sites as we did not need to download and process entire Landsat images,

saving months of analysis time. While other tidal marsh phenology studies have used Landsat for analysis, they have been limited either in the number of years analyzed (3; Mo et al. 2015) or in the number of sites (1; O'Donnell and Schalles; 28 years); GEE facilitated analysis over 32 years and 3 spatially distinct sites. GEE also allows for rapid analysis of new images in context with historic imagery and for the rapid assessment of ecosystem change, further improving the utility of Landsat and other remotely sensed data for landscape monitoring. The ~2°C range of variation in annual mean temperature over the last 32 years suggests that the historic ENSO-related variation is a reasonable proxy for near-term climate change (2.0-2.8°C by 2050, Dalton et al. 2017). Further integration of time-series remote sensing datasets and biological monitoring is important for expanding our understanding of ecological responses to climate change.

ACKNOWLEDGMENTS

We would like to thank B. Drucker, K. Miller, K. Kemp, M. Monnin, Y. Zhiqiang, J. Vogeler, A. Nolin, C. Freeman, A. Goodman, and C. Janousek for their assistance and support in this project. Funding support was provided by the DOI U.S. Geological Survey, Western Ecological Research Center, National Climate Change and Wildlife Science Center, the National Oceanic and Atmospheric Administration EESLR program (grant ID NA15NOS4780171), Northwest Climate Science Center (NWCSC), Southwest Climate Science Center, U.S. Fish & Wildlife Service North Pacific, Oregon State University and the NWCSC fellowship. Any use of trade, product, or firm names in this publication is for descriptive purposes only and does not imply endorsement by the U.S. government.

LITERATURE CITED

Aubry, L. M., R. F. Rockwell, E. G. Cooch, R. W. Brook, C. P. H. Mulder, and D. N. Koons. 2013. Climate change, phenology, and habitat degradation: Drivers of gosling body condition and juvenile survival in lesser snow geese. Global Change Biology 19:149–160.

Barbier, E. B., S. D. Hacker, C. Kennedy, E. W. Koch, A. C. Stier, and B. R. Silliman. 2011. The value of estuarine and coastal ecosystem services. Ecological Monographs 81:169–193.

Baxter, C. V., K. D. Fausch, and W. C. Saunders. 2005. Tangled webs: Reciprocal flows of invertebrate prey link streams and riparian zones. Freshwater Biology 50:201–220.

Buffington, K. J., B. D. Dugger, K. M. Thorne, and J. Y. Takekawa. 2016. Statistical correction of lidar-derived digital elevation models with multispectral airborne imagery in tidal marshes. Remote Sensing of Environment 186:616–625.

Byrd, K. B., J. L. O'Connell, S. Di Tommaso, and M. Kelly. 2014. Evaluation of sensor types and environmental controls on mapping biomass of coastal marsh emergent vegetation. Remote Sensing of Environment 149:166–180.

Byrd, K. B., L. Windham-myers, T. Leeuw, B. Downing, J. T. Morris, and M. C. Ferner. 2016. Forecasting tidal marsh elevation and habitat change through fusion of Earth observations and a process model. Ecosphere 7:1–27.

Canepuccia, A. D., J. Alberti, J. Pascual, G. Alvarez, J. Cebrian, and O. O. Iribarne. 2010. ENSO episodes modify plant/terrestrial-herbivore interactions in a southwestern Atlantic salt marsh. Journal of Experimental Marine Biology and Ecology 396:42–47.

Charles, H., and J. S. Dukes. 2009. Effects of warming and altered precipitation on plant and nutrient dynamics of a New England salt marsh. Ecological Applications 19:1758–1773.

Chmura, G. L., S. C. Anisfeld, D. R. Cahoon, and J. C. Lynch. 2003. Global carbon sequestration in tidal, saline wetland soils. Global Biogeochemical Cycles 17:12.

Cleland, E. E., I. Chuine, A. Menzel, H. A. Mooney, and M. D. Schwartz. 2007. Shifting plant phenology in response to global change. Trends in Ecology and Evolution 22:357–365.

Dalton, M. M., K. D. Dello, L. Hawkins, P. W. Mote, and D. E. Rupp. 2017. The Third Oregon Climate Assessment Report.

Day, J. W., R. R. Christian, D. M. Boesch, A. Yáñez-Arancibia, J. Morris, R. R. Twilley, L. Naylor, L. Schaffner, and C. Stevenson. 2008. Consequences of climate change

on the ecogeomorphology of coastal wetlands. Estuaries and Coasts 31:477–491.

Doi, H., O. Gordo, and I. Katano. 2008. Heterogeneous intra-annual climatic changes drive different phenological responses at two trophic levels. Climate Research 36:181–190.

Dunton, K. H., B. Hardegree, and T. E. Whitledge. 2001. Response of Estuarine Marsh Vegetation to Interannual Variations in Precipitation. Estuaries 24:851–861.

Efron, B. 1982. The Jackknife, the Bootstrap and other resampling plans. In *CBMS-NSF regional conference series in applied mathematics 1982*. Philadelphia, PA: Society for Industrial and Applied Mathematics (SIAM).

Fisher, J. I., J. F. Mustard, and M. A. Vadeboncoeur. 2006. Green leaf phenology at Landsat resolution: Scaling from the field to the satellite. Remote Sensing of Environment 100:265–279.

Gabler, C. A., M. J. Osland, J. B. Grace, C. L. Stagg, R. H. Day, S. B. Hartley, N. M. Enwright, A. S. From, M. L. McCoy, and J. L. McLeod. 2017. Macroclimatic change expected to transform coastal wetland ecosystems this century. Nature Climate Change 7:142–147.

Gershunov, A., and T. Barnett. 1998. Interdecadal modultion of ENSO teleconnections. Bulletin of the American Meteorological Society 79:2715–2726.

Goetz, S., and R. Dubayah. 2011. Advances in remote sensing technology and implications for measuring and monitoring forest carbon stocks and change. Carbon Management 2:231–244.

Hanson, A., R. Johnson, C. Wigand, A. Oczkowski, E. Davey, and E. Markham. 2016. Responses of Spartina alterniflora to Multiple Stressors: Changing Precipitation Patterns, Accelerated Sea Level Rise, and Nutrient Enrichment. Estuaries and Coasts 39:1376–1385.

Hartigan, J. A. and M. A. Wong. 1979. A K-means clustering algorithm. Applied Statistics 28, 100–108.

Janousek, C., K. Buffington, K. Thorne, G. Guntenspergen, J. Takekawa, and B. Dugger. 2016. Potential effects of sea-level rise on plant productivity: species-specific responses in northeast Pacific tidal marshes. Marine Ecology Progress Series 548:111–125.

Jarrell, E. R., A. S. Kolker, C. Campbell, and M. J. Blum. 2016. Brackish Marsh Plant Community Responses to Regional Precipitation and Relative sea-Level Rise. Wetlands 36:607–619.

Kauth, R. J and G.S. Thomas. 1976. The tasseled Cap -- A Graphic Description of the Spectral-Temporal Development of Agricultural Crops as Seen by LANDSAT. Proceedings of the Symposium on Machine Processing of Remotely Sensed Data, Purdue University of West Lafayette, Indiana, pp. 4B-41 to 4B-51.

Kirwan, M. L., and G. R. Guntenspergen. 2012. Feedbacks between inundation, root production, and shoot growth in a rapidly submerging brackish marsh. Journal of Ecology 100:764–770.

Kirwan, M. L., G. R. Guntenspergen, and J. T. Morris. 2009. Latitudinal trends in Spartina alterniflora productivity and the response of coastal marshes to global change. Global Change Biology 15:1982–1989.

Leonard, L. A., and M. E. Luther. 1995. Flow hydrodynamics in tidal marsh canopies. Limnology and Oceanography 40:1474–1484.

Linderholm, H. W. 2006. Growing season changes in the last century. Agricultural and Forest Meteorology 137:1–14.

Masek, J. G., C. Huang, R. Wolfe, W. Cohen, F. Hall, J. Kutler, and P. Nelson. 2008. North American forest disturbance mapped from a decadal Landsat record. Remote Sensing of Environment 112:2914–2926.

Mckee, T. B., N. J. Doesken, and J. Kleist. 1993. The relationship of drought frequency and duration to time scales. AMS 8th Conference on Applied Climatology:179–184.

Melaas, E. K., M. A. Friedl, and Z. Zhu. 2013. Detecting interannual variation in deciduous broadleaf forest phenology using Landsat TM/ETM+ data. Remote Sensing of Environment 132:176–185.

Mitsch, W J, J. G. Gosselink, Wetlands; John Wiley and Sons: Hoboken, NJ, USA, 2007.

Mo, Y., B. Momen, and M. S. Kearney. 2015. Quantifying moderate resolution remote sensing phenology of Louisiana coastal marshes. Ecological Modelling 312:191–199.

Moran, M. S., Y. Inoue, and E. M. Barnes. 1997. Opportunities and limitations for image-based remote sensing in precision crop management. Remote Sensing of Environment 61:319–346.

Morisette, J. T., A. D. Richardson, A. K. Knapp, J. I. Fisher, E. A. Graham, J. Abatzoglou, B. E. Wilson, D. D. Breshears, G. M. Henebry, J. M. Hanes, and L. Liang. 2009. Tracking the rhythm of the seasons in the face of global change: Phenological research in the 21 st century. Frontiers in Ecology and the Environment 7:253–260.

Morris, J. T., P. V. Sundareshwar, C. T. Nietch, B. Kjerfve, and D. R. Cahoon. 2002. Responses of coastal wetlands to rising sea level. Ecology 83:2869–2877.

Mutanga, O., and A. K. Skidmore. 2004. Narrow band vegetation indices overcome the saturation problem in biomass estimation. International Journal of Remote Sensing 25:3999–4014.

Noe, G. B., and J. B. Zedler. 2000. Differential effects of four abiotic factors on the germination of salt marsh annuals. American Journal of Botany 87:1679–1692.

O'Donnell, J. P. R., and J. F. Schalles. 2016. Examination of abiotic drivers and their influence on Spartina alterniflora biomass over a twenty-eight year period using Landsat 5 TM satellite imagery of the Central Georgia Coast. Remote Sensing 8:477–499.

Osland, M. J., N. M. Enwright, R. H. Day, C. A. Gabler, C. L. Stagg, and J. B. Grace. 2016. Beyond just sea-level rise: Considering macroclimatic drivers within coastal wetland vulnerability assessments to climate change. Global Change Biology 22:1–11.

Ovaskainen, O., S. Skorokhodova, M. Yakovleva, A. Sukhov, and A. Kutenkov. 2013. Community level phenological response to climate change. Proceedings of the National Academy of Sciences 110:13434–13439.

Parson, E. A., P. W. Mote, A. F. Hamlet, W. S. Keeton, D. Lettenmaier, N. Mantua, E. L. Miles, D. W. Peterson, D. L. Peterson, R. Slaughter, and A. K. Snover. 2003. Forests for climatic change: The water, salmon and forests of the Pacific Northwest. Climate Change 61:45–88.

PRISM Climate Group, Oregon State University, http://prism.oregonstate.edu

Roy, D. P., V. Kovalskyy, H. K. Zhang, E. F. Vermote, L. Yan, S. S. Kumar, and A. Egorov. 2016. Characterization of Landsat-7 to Landsat-8 reflective wavelength and normalized difference vegetation index continuity. Remote Sensing of Environment 185:57–70.

Scavia, D., J. C. Field, D. F. Boesch, R. W. Buddemeier, V. Burkett, D. R. Cayan, M. Fogarity, M. A. Harwell, R. W. Howarth, C. Mason, D. J. Reed, T. C. Royer, A. H. Sallenger, and J. G. Titus. 2002. Climate Change Impacts on U. S. Coastal and Marine Ecosystems. Estuaries 25:149–164.

Schwartzberg, E. G., M. A. Jamieson, K. F. Raffa, P. B. Reich, R. A. Montgomery, and R. L. Lindroth. 2014. Simulated climate warming alters phenological synchrony between an outbreak insect herbivore and host trees. Oecologia 175:1041–1049.

Stenseth, N. C., A. Mysterud, and G. Ottersen. 2002. Ecological effects of climate fluctuations. Science 297:1292–1296.

Swanson, K. M., J. Z. Drexler, D. H. Schoellhamer, K. M. Thorne, M. L. Casazza, C. T. Overton, J. C. Callaway, and J. Y. Takekawa. 2013. Wetland Accretion Rate Model of Ecosystem Resilience (WARMER) and Its Application to Habitat Sustainability for Endangered Species in the San Francisco Estuary. Estuaries and Coasts 37:476–492.

Takekawa, J. Y., I. Woo, K. M. Thorne, K. J. Buffington, N. Nur, M. L. Casazza, and J. T. Ackerman. 2012. Chapter 12: Bird communities: effects of fragmentation, disturbance, and sea level rise on population viability. Pages 175–194Ecology,

Conservation, and Restoration of Tidal Marshes: The San Francisco Estuary.

Thorne, K. M., J. Y. Takekawa, and D. L. Elliott-Fisk. 2012. Ecological Effects of Climate Change on Salt Marsh Wildlife: A Case Study from a Highly Urbanized Estuary. Journal of Coastal Research 285:1477–1487.

Ustin, S. L., R. W. Pearcy, and D. E. Bayer. 1982. Plant Water Relations in a San Francisco Bay Salt Marsh. Botanical Gazette 143:368–373.

Verstraete, M. M., B. Pinty, R. B. Myneni, and M. M. Verstraete. 1996. Potential and limitations of information extraction on the terrestrial biosphere from satellite remote sensing. Remote Sensing of Environment 58:201–214.

Vicente-Serrano, S. M., S. Beguería, and J. I. López-Moreno. 2010. A multiscalar drought index sensitive to global warming: The standardized precipitation evapotranspiration index. Journal of Climate 23:1696–1718.

Visser, M. E., and C. Both. 2005. Shifts in phenology due to global climate change : the need for a yardstick Shifts in phenology due to global climate change: the need for a yardstick. Proceedings of the Royal Society B 272:2561–2569.

Walther, G.-R. 2010. Community and ecosystem responses to recent climate change. Philosophical Transactions of the Royal Society B: Biological Sciences 365:2019–24.

Ward, R. D., N. G. Burnside, C. B. Joyce, K. Sepp, and P. A. Teasdale. 2016. Improved modelling of the impacts of sea level rise on coastal wetland plant communities. Hydrobiologia 774:203–216.

Wells, N., S. Goddard, and M. J. Hayes. 2004. A self-calibrating Palmer Drought Severity Index. Journal of Climate 17:2335–2351.

Zhu, Z., and C. E. Woodcock. 2012. Object-based cloud and cloud shadow detection in Landsat imagery. Remote Sensing of Environment 118:83–94.

Improving Projections of Tidal Marsh Persistence under Climate Change with Remote Sensing and Site-Specific Data

CHAPTER 4

PACIFIC NORTHWEST TIDAL MARSH ACCRETION RATES AND THE VALUE OF SITE-SPECIFIC DATA

Kevin J. Buffington, Bruce D. Dugger, and Karen M. Thorne

ABSTRACT

Tidal marshes are vulnerable to alteration due to climate change, particularly accelerating sea-level rise (SLR) and changes in freshwater flow. In the Pacific Northwest (PNW) relatively little is known about the variation of accretion rates across estuaries and relative marsh vulnerability to SLR into the future. To understand the spatial variability in accretion rates across tidal marshes we measured vertical accretion rates using soil cores and radioisotope dating for eight PNW estuaries. Mean vertical accretion was 4.5 mm yr^{-1} (SD = 2.2), however there were significant differences among tidal marshes, highlighting the importance of measuring accretion rates at a local scale. To determine the landscape characteristics that were associated with measured accretion rates we assessed a suite of physical, climatic, and land use characteristics across each watershed and found that mean annual fluvial discharge into the estuary was the best predictor for net accretion rates in the tidal marsh. Finally, to test our assumption that site-specific data is needed to understand tidal marsh accretion rates and vulnerability from SLR, we ran a process-based elevation model at a tidal marsh in Puget Sound and compared results when the model was run with accretion rates from other marshes in our study. This comparison showed that under a moderate SLR scenario (+63 cm after 100 years), differences in final elevation varied up to 41% (50 cm) depending on the source of the accretion rate data. Our study highlights the spatial variability in accretion rates and the need for site-specific ground data when assessing SLR vulnerabilities for tidal wetlands.

INTRODUCTION

Tidal marshes are an important ecological component of estuaries that provide valuable ecosystem services (Craft et al. 2009), support endemic species (Greenberg et al. 2006), and sequester carbon belowground (Chmura et al. 2003, Bridgham et al. 2006, Callaway et al. 2012). Human development and habitat modification have impacted tidal marshes worldwide (Kennish 2002) and accelerating sea-level rise (SLR) due to climate change is synergistically increasing tidal marsh vulnerability (van der Wal and Pye 2004, Torio and Chmura 2013). Within the broader estuarine watershed, land use changes, resource extraction, and human development can also negatively affect the underlying processes that facilitate tidal marsh sediment accretion (Mattheus et al. 2009, Kirwan et al. 2011, Weston 2014), further influencing marsh vulnerability to SLR through altered freshwater flows and delivery of suspended sediment and nutrients (Nixon et al. 1996).

Models used to forecast tidal marsh persistence to sea-level rise are sensitive to estimates of sediment accretion rates. For example, a comprehensive sensitivity analysis of the Wetland Accretion Rate Model for Ecosystem Resilience (WARMER) marsh elevation model found that after the rate of sea-level rise, model predictions were most sensitive to sediment accumulation or accretion rate (Swanson et al. 2015). Additionally, experiments with multiple marsh elevation models found that suspended sediment concentration (SSC) and tidal range are key parameters for estimating tidal marsh persistence under sea-level rise (Kirwan et al. 2010)**,** and models that account for mudflat width and tidal marsh area have shown the importance of local sediment supply in long-term marsh persistence (Mariotti and Fagherazzi 2013).

The rate of sediment deposition and accretion in a tidal marsh is a function of both local and watershed-scale processes. At the local scale, relative elevation to sea-level (Morris et al. 2002, Kirwan and Murray 2007), fetch (Day et al. 1998, Kolker et al. 2009), and distance from marsh edge (van Proosdij et al. 2006) influence deposition rates across the marsh. Marine currents and waves can deliver larger grained sediments (sand) to tidal marshes, however sand transport up-estuary is typically limited to high-energy storms and tsunamis (de Groot et al. 2011). At the watershed-scale, rates of mineral transport from terrestrial sources are variable and dependent on watershed characteristics such as slope and elevation (Milliman and Syvitski 1992), however, direct links between the watershed and tidal marsh accretion are lacking. Additional characteristics, such as land use and cover, climate, and weather extremes may also play a role in shaping long-term tidal marsh vulnerability to sea-level rise but have yet to be evaluated.

Estimates of accretion rates are necessary for accurate projections of marsh persistence to sea-level rise, however these data are relatively sparse. Of 35 major estuaries with tidal marshes in Washington and Oregon, only five have published data on accretion rates (Thom 1992) and none have elevation data necessary to calibrate models of marsh evolution and sea-level rise. When site- or estuary-specific data are not available to calibrate marsh process elevation models, the best available data from nearby sites or regional means have been used (e.g., Glick et al. 2007); however, the accuracy of such an approach has not been validated. Furthermore, there has been no effort to evaluate or understand the variation in accretion rates across PNW estuaries specifically. Recognizing the degree of spatial variation in accretion rates is important for assessing

relative vulnerability to sea-level rise across the landscape, and making robust projections of future marsh elevation change under changing environmental conditions.

In this study we measure the accretion rates for tidal marshes in eight maritime estuaries in Oregon and Washington located within PNW of the United States. We then determine how accretion rates vary with climatic and landscape factors and explore how climate and watershed characteristics relate to mineral and organic accumulation rates across the estuaries. Finally, we use a case study to illustrate the value of site-specific accretion data when projecting marsh elevation under sea-level rise.

METHODS

Study Sites

Our study covered eight sites and included five outer coast sites (Bandon National Wildlife Refuge [NWR] on the Coquille river [hereafter Bandon], Bull Island in Coos Bay [Coos Bay], Siletz NWR [Siletz], Tarlet Slough marsh in southern Willapa Bay NWR [Willapa], Grays Harbor NWR, north of Bowerman airport [Grays Harbor]) and three Puget Sound sites (Skokomish River delta [Skokomish], Nisqually NWR [Nisqually], and Port Susan Bay in the Whidbey Basin of Puget Sound, on the Stillaguamish river delta [Port Susan]; Fig. 4.1). We selected sites that are conservation priorities (NWRs) from a range of estuarine types (drowned river, bar built, river delta) to encompasses the potential variation in sea-level rise vulnerability. Sampled marshes ranged in size from 29 to 97 ha, with a mean area of 68 ha. All sites have relatively rural watersheds, however, much of all watersheds have been extensively logged since European settlement (Jiang et al. 2004). All of the study estuaries have been modified to

some degree over the last 150 years. Over 80% of the tidal marsh habitats across Puget Sound have been lost due to human modifications (Collins 1997, Dean et al. 2001); tidal marsh restoration projects are ongoing at Port Susan (Yang et al. 2010), Nisqually (Ellings 2011) and Skokomish (SWAT 2016). Willapa Bay has lost 64% of the tidal wetland habitat (Coastal Resources Alliance, 2007), while Grays Harbor has lost 60% (Boule and Bierly 1987). In Oregon, Siletz Bay has lost 47% of historic tidal wetland habitat (USFWS 2012b), the Coquille River (Bandon) has lost 95% (USFWS 2012a), and Coos Bay has lost nearly 30% (Borde et al. 2003). Estuary modifications slowed by the mid-1970s due to increased state and federal oversight and permitting requirements (Adamus et al. 2005). Additionally, there are large dams are present within the Nisqually, Skokomish and Grays Harbor watersheds, influencing fluvial discharge. Across the PNW, rainfall and fluvial discharge are strongly seasonal with high flows in the winter and low flows in the summer (Hickey and Banas 2003). Marsh plant communities are broadly similar across sites with *Sarcocornia pacifica*, *Jaumea carnosa* and *Carex lyngbyei* dominate in low marsh and *Deschampsia cespitosa*, *Triglochin maritima*, *Juncus balticus*, and *Potentilla anserina* common across the mid and high marsh (Thorne et al. 2015).

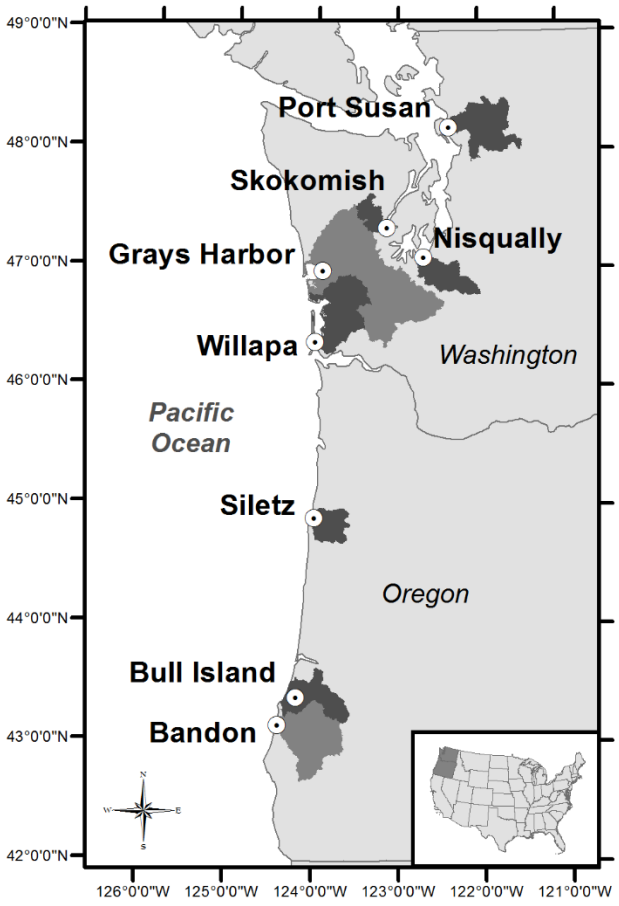

Figure 4.1. Locations of the eight study estuaries and their respective watersheds (shaded areas).

Data collection and processing

Soil cores were collected in winter of 2013/14 at each study site. We used a 50-cm long, 5 cm diameter Russian peat corer (http://www.aquaticresearch.com/russian_peat_borer.htm) to collect one core at low, mid and high elevations in each estuary. We stratified each site into low, mid and high elevation zones using mean high water (MHW) and mean higher high water (MHHW) tidal datum elevations (Thorne et al. 2015). Cores were taken at sampling stations that

were placed along a transect spanning the elevation gradient, separated by at least 150 m, and away from marsh channels. If soil compaction was greater than 2 cm a replacement core was taken. In the lab, cores were cut into 1-cm discs. We calculated bulk density (BD) for each disc by drying samples at 80ºC until constant mass and dividing by the known volume of the disc (10 cm^3; Blake and Hartge 1986). We estimated percentage organic matter (OM) of each disc using loss on ignition (muffle furnace at 450ºC for 8 hrs).

We calculated the historic accretion rate for each sediment core using the Cesium-137 radioisotope. Each disc was placed in a high-purity germanium detector at the Oregon State University Radiation Center for 24 hours, enumerating the gamma radioactivity at the ^{137}Cs energy level (662 keV). The ^{137}Cs activity was then normalized for detection geometry and detection efficiency using calibration standards, and divided by sample mass. The sediment disc with the highest ^{137}Cs activity was assumed to correlate to the cessation of atmospheric nuclear detonations in 1963 (Ritchie and Mchenry 1990); the depth of this disc was divided by 50 (the number of years since the 1963) to calculate the accretion rate in mm yr^{-1}.

The mass-based annual organic matter accumulation rate (R_{OM}, g cm^{-2} yr^{-1}) for each core was calculated as:

$$R_{om} = \frac{\sum_d^1 ob}{n} \qquad \text{Eq. 1}$$

where, *d* is the depth (cm) of peak ^{137}Cs activity, *o* is the proportion organic matter in the sample, *b* is the bulk density of the sample (g cm^{-3}), and *n* is the number of years (50). Mineral accumulation rates were calculated with a similar equation, where *o* is instead the proportion mineral matter in the sample. We found the mineral and organic matter

density by calculating the mean density across all discs down to the ^{137}Cs horizon. We also calculated the total inventory of mineral and organic matter by multiplying the density of each by the depth of the ^{137}Cs horizon (Nyman et al. 1993). The total inventory of mineral and organic matter is a method to determine the relative amount of each within the soil column and is independent of the accretion rate.

Analysis

We used an analysis of variance (ANOVA) to test whether core characteristics varied across sites ($\alpha = 0.05$). We tested whether mineral or organic matter inventory best explained vertical accretion rates using an F-statistic and Moran's I (Moran 1950) to test if there was significant spatial autocorrelation in core characteristics across estuaries. We limited analysis of organic matter across cores to the top 20 cm, which is the approximate depth of the rooting zone.

To explore how explanatory variables influenced accretion rates, we used generalized linear models where the dependent variable was area-weighted mean vertical accretion for each estuary. The area-weighted mean accounts for unevenly distributed elevation across the marsh platform, providing a more accurate representation of vertical accretion across the entire marsh. Since cores were stratified by elevation related to a tidal datum, we used a DEM and found the area below MHW, between MHW and MHHW, and from MHHW to the edge of marsh vegetation. For this analysis we considered several mechanisms that may be responsible for driving variation in accretion rates, including geography, topography, rainfall, climate, and erosion-inducing landscape disturbances. The explanatory variables that relate to these potential mechanisms

included watershed area, watershed age, watershed discharge, precipitation, temperature, stream and road densities, and development.

We calculated the total area of each watershed below major dams (which were constructed prior to 1963) using HUC-10 boundaries obtained from the GeoSpatialDataGateway (https://gdg.sc.egov.usda.gov). For an estimate of geologic form and age of a watershed we used the integral of the hypsometric curve. The hypsometric curve describes the distribution of elevation by relative area and the integral [standardized 0-1] can be used to compare watershed geologic form and age, where higher values are indicative of younger, less eroded basins, and smaller values are indicative of older basins (Strahler 1952, Dowling et al. 1998). We calculated the hypsometric curve for each watershed with a 30 m resolution DEM (National Elevation Dataset) using the ArcGIS add-in 'CalHypso' (Pérez-Peña et al. 2009).

We calculated the proportion of each watershed that was developed, urbanized, and disturbed, using the results of the 2011 USGS GAP analysis. We hypothesized that different land cover types might influence sedimentation rates. For example, forest disturbance such as fires and logging, have the potential to promote erosion and increase downstream sediment concentrations (e.g., Beschta 1978). Human development and urbanization may also promote erosion through construction activities. In addition, as a metric of recent logging history we calculated the area of conifer trees 10–50 years old using PNW forest cover predictions from Jiang et al. (2004). We also calculated stream and road densities using the National Hydrography Dataset and the 2015 TIGER line shapefiles for Oregon and Washington (2015 TIGER/Line Shapefiles). We calculated the total length within each watershed and divided by watershed area. We hypothesized that

higher stream and road densities would increase mineral accumulation rates due to increased erosion potential. We estimated mean annual watershed discharge (cfs) using USGS stream gauge data and the area ratio method (e.g., Archfield and Vogel 2010) to scale up stream discharge from gauged sub basins to the entire watershed of each estuary by multiplying the discharge of a gauged basin by the ratio of ungauged basin area to gauged basin area.

We obtained 30-year average precipitation and temperature data from PRISM (PRISM Climate Group), and used the centroid of each study site to sample the 800 m resolution gridded data. We calculated mean and maximum annual average temperature, and mean annual and mean growing season precipitation (e.g., Chmura and Hung 2004, Charles and Dukes 2009). Annual mean precipitation volume was also calculated for each watershed by multiplying the watershed area by the average annual precipitation across the watershed. Tidal range and historic rates of sea-level rise were obtained from nearby NOAA tidal gauges (noaa.tidesandcurrents.gov).

Our sample included eight estuaries (n = 8), we therefore limited our a priori model set to single-variable models and the null model. We ranked model performance using Akaike's Information Criterion correction for small sample sizes (AICc) and model weights (w), considering all models within 2 AIC values of the best model competitive, and we evaluated the direction and strength of variable effects using parameter estimates and their confidence intervals (Anderson and Burnham 2002). All analyses were conducted in R (www.r-project.org) and ArcGIS (ESRI, Redlands, CA). Watershed characteristics for each estuary are provided in Appendix B, S1.

Finally, we used the Wetland Accretion Rate Model for Ecosystem Resilience (WARMER; Swanson et al., 2013) to illustrate the value of collecting site-specific data for making projections about marsh persistence with sea-level rise. WARMER is a cohort model that captures the dominant processes that control tidal marsh elevation, including mass-based mineral and organic matter deposition, decomposition, compaction, and relative sea-level rise. Functions for sediment deposition are based the relationship between inundation frequency and elevation, while organic deposition is a unimodal function based on Morris et al. (2002). The amplitudes of the sediment and organic accumulation functions are calibrated from rates determined from soil cores. We choose Nisqually as our focal study site because it had a site-specific mean accretion rate that was near the PNW mean. We ran WARMER for Nisqually using the soil core data from the other study sites keeping the remaining model parameters constant (Tables 4.1, 4.2). Since relative elevation is crucial in controlling accretion rates, we set the elevation of the calibration cores after controlling for differences in tide range between Nisqually and the other sites. We ran WARMER at a range of initial elevations (20-cm intervals) and used linear interpolation to create a continuous surface of marsh elevation from the results at 10 year increments. We calculated the percent difference in mean elevation under a moderate sea-level rise scenario (+63 cm by the year 2110; National Research Council 2012), and a paired t-test of the final elevation of each model run compared to the final elevation of the Nisqually results. We also translated the elevation projections into marsh habitat zones based on field surveys (Thorne et al. 2015), and compared percent cover of the habitat zones across the model results. For the initial elevation, we used a lidar-

derived DEM that was corrected for vertical bias caused by vegetation using the LEAN method (Chapter 2, Buffington et al. 2016).

RESULTS

We found ^{137}Cs peaks that corresponded to the 1963 horizon for all but two soil cores. The mean vertical accretion rate across sites was 4.5 mm yr^{-1} (SD = 2.2). Using the area-weighted average we found a mean vertical accretion rate of 4.3 mm yr^{-1} (SD = 2.1). There were significant differences across sites in vertical accretion ($F_{7,14} = 17.7$, $p < 0.0001$), mineral accumulation ($F_{7,14} = 4.4$, $p = 0.009$), and organic matter accumulation ($F_{7,14} = 3.5$, $p = 0.02$). Grays Harbor, Port Susan, and Willapa were similar to each other but had significantly higher vertical accretion rates than Coos, Nisqually, Bandon, Skokomish, and Siletz (Table 4.3). Across all sites there was no trend in accretion rate with elevation (standardized for tidal range; Fig. 2). Accretion rates were better explained by the mineral inventory than organic matter across all cores ($F_{1,20} = 8.98$, $p = 0.007$), and there was no significant spatial autocorrelation between estuaries and their weighed average accretion rate ($p = 0.67$), mineral accumulation rate ($p = 0.65$), or organic matter accumulation rate ($p = 0.32$).

There was significant variation in the amount of soil organic matter (top 20 cm) across sites, ($F_{7,16} = 3.93$, $p < 0.011$). Siletz and Skokomish had significantly more organic matter while Port Susan had the least (Table 4.4). Mean organic matter content in the top 20 cm was not significantly different by elevation class, ($F_{2,21} = 1.61$, $p = 0.22$). However, an ANOVA with ‘site’ and ‘elevation’ as categorical predictors for organic

matter content was significant (r^2 = 0.61, $F_{9,14}$ = 5.1, p = 0.004), indicating extent of spatial variation across a site (within marsh) differed among study sites (across estuaries). Across all sites and cores, average organic matter content was 12.6%. Mean bulk density for the entire depth of each core was not significantly different between elevation classes ($F_{2,14}$ = 2.17, p = 0.15), and only marginal across sites ($F_{7,14}$ = 2.34, p=0.08; BD~Site+Elev: r^2 = 0.34, $F_{9,14}$ = 2.3, p = 0.078). Complete depth profiles of organic matter content and bulk density for all cores are provided in Appendix B, S2.

Mean annual watershed discharge (*D,* cfs) was the best single-variable model, predicting a positive relationship with vertical accretion (w_i = 0.89; $acc = 0.14 + 7.54e^{-5} \times D$; Table 4.5) and mineral accumulation (w_i = 0.77; $m = -391.87 + 0.46 \times D$; Appendix B, S3). Tidal range (T_R) was the top predictor and had a positive relationship with organic matter accumulation (w_i = 0.46; $om = -19.74 + 267.4 \times T_R$; Appendix B, S3). For each analysis, no other models were competitive.

The different sources of accretion rate data used to calibrate future projections of marsh elevation with sea-level rise at Nisqually resulted in projections that were significantly different (p < 0.0001) than the projections calibrated with site-specific data (Fig. 4.3). Port Susan and Skokomish represent the range of accretion rates found in this study, thus we use those sites to discuss the WARMER comparison results. The higher accretion rate from Port Susan resulted in a mean elevation that was 34 cm higher after 100 years than the site-specific accretion rate. The lower accretion rate from Skokomish resulted in a mean elevation that was 16 cm lower than the mean elevation using the rate from Nisqually. The range of error in using accretion rates from nearby sites was 41%, or 50 cm, after 100 years. With site-specific accretion data from Nisqually and a 63-cm

increase in sea level, WARMER projected 55% of the marsh will be mid marsh, 38% low marsh, and a 61% loss in high marsh (Fig. 4.4). Using the higher accretion rates from Port Susan, WARMER projected 91% high marsh and 8% mid, while with the lower rates from Skokomish the projections were 18% mid, 72% low and less that 1% high marsh.

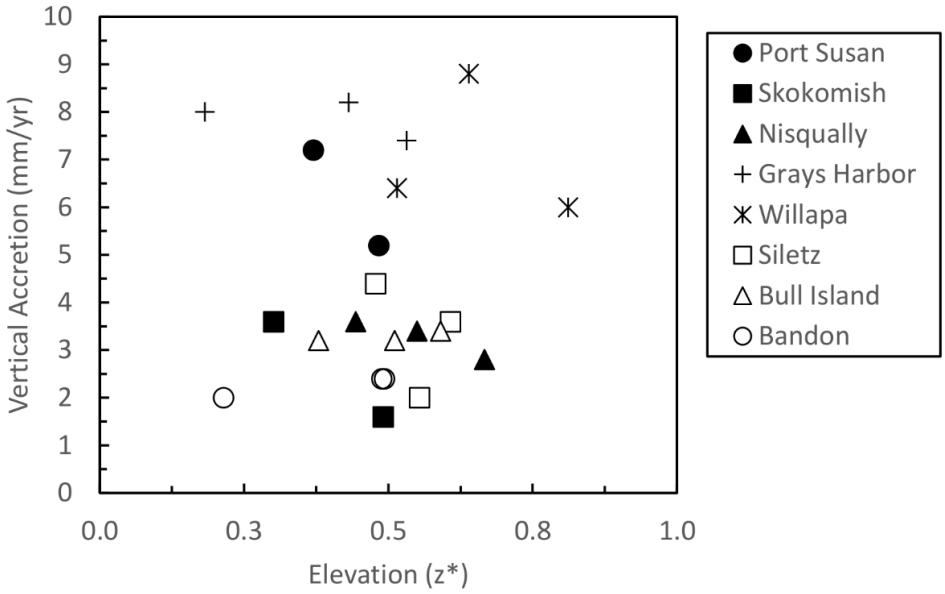

Figure 4.2. Vertical accretion rate (mm yr^{-1}) for each Cesuim-137 dated soil core by standardized elevation (z*) for 22 soil cores collected in eight estuaries in Oregon and Washington in winter 2013-14. z* is calculated by normalizing elevation relative to mean sea level by the elevation of mean higher high water.

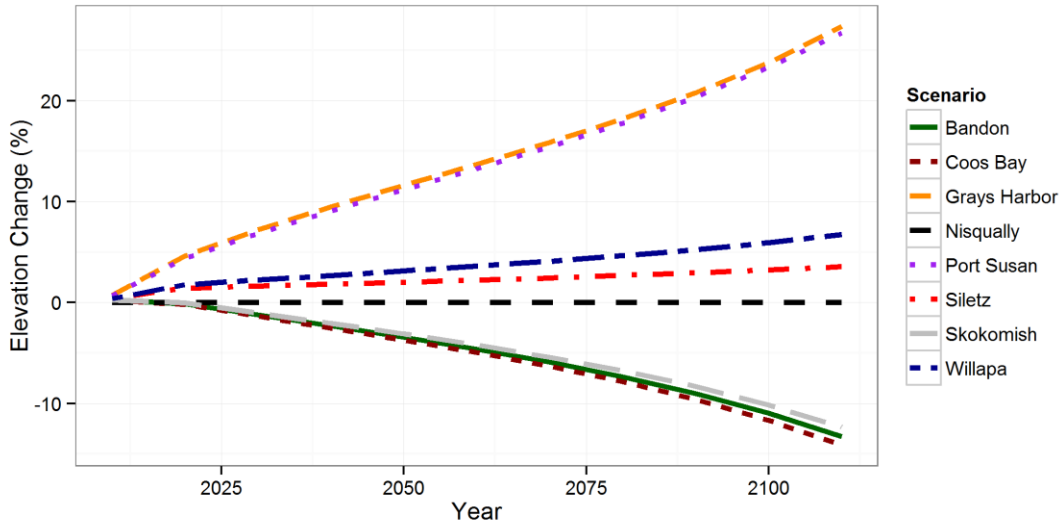

Figure 4.3. Comparison of 100-year Wetland Accretion Rate Model for Ecosystem Resilience elevation projections for Nisqually using accretion data (mineral and organic matter accumulation rates) that was estimated from soil cores at each study site (scenarios). A moderate sea-level rise scenario (+63 cm over 100 years) was used and all other model parameters were held constant.

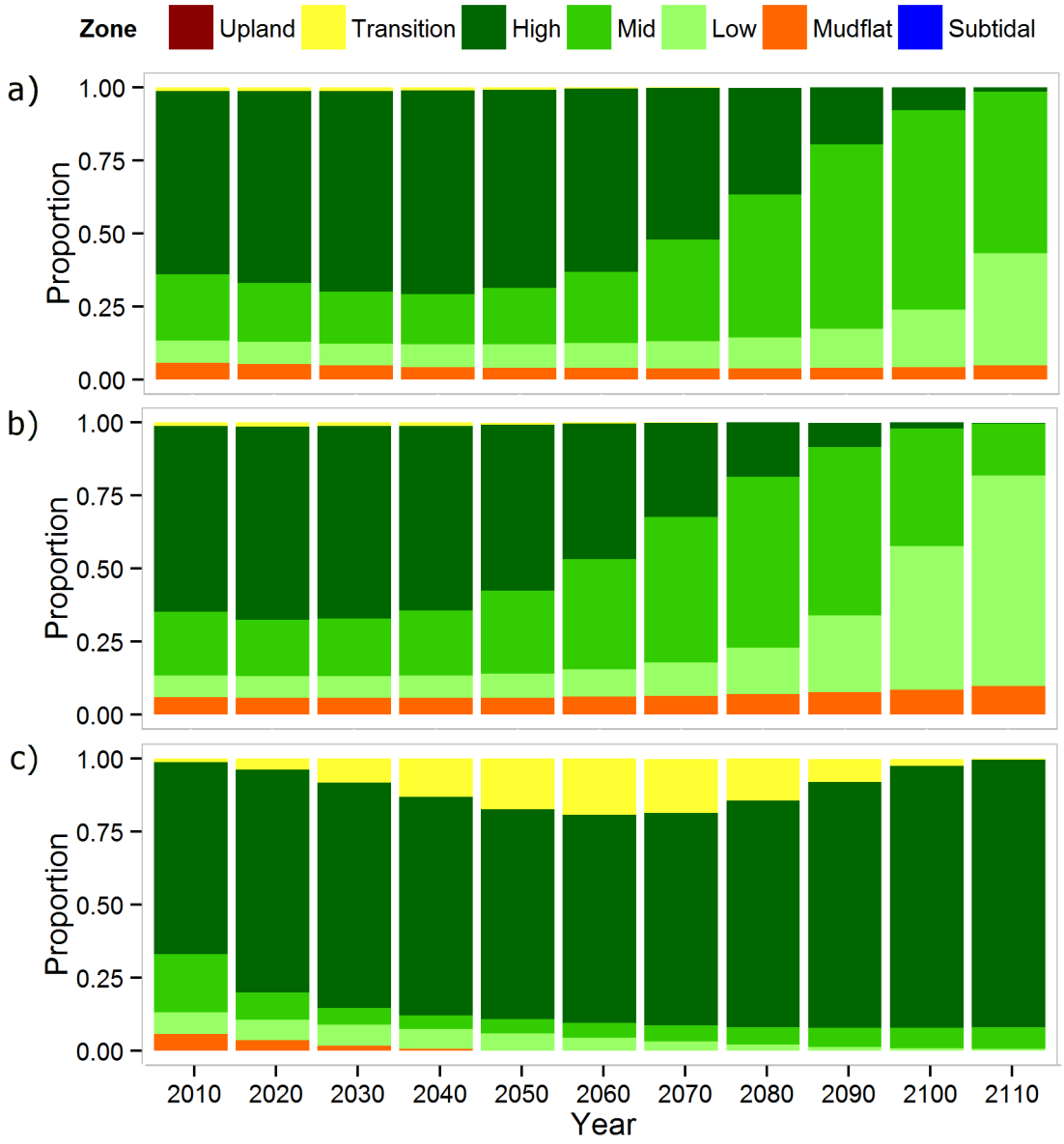

Figure 4.4. Marsh habitat zones from Wetland Accretion Rate Model for Ecosystem Resilience elevation projections at Nisqually with a 63-cm increase in sea level over 100 years. Site-specific accretion rates (a), Skokomish accretion rates (b), Port Susan accretion rates (c).

Table 4.1. WARMER model parameters from Nisqually that were held constant for each run. Values calculated from analysis of a mid-elevation soil core.

Model Parameter	Value
Elevation of Peak Biomass (cm, MSL)	175
Minimum Elevation of Vegetation (cm, MSL)	105
Root:Shoot	1.95
Porosity Surface (%)	94
Porosity Depth (%)	88
Refractory Carbon (%)	59.7
Maximum Astronomical Tide (cm, MSL)	286
Historic Sea-Level Rise (mm/yr)	1.97
Organic Matter Density (g/cm^3)	1.14
Mineral Density (g/cm^3)	2.61

Table 4.2 WARMER model parameters changed for each comparison. Calibrated sediment accumulation is reported at the elevation of mean sea level (MSL).

Site	Sediment Accumulation Rate ($g\ m^{-2}\ yr^{-1}$)	Max. Aboveground Organic Accumulation ($g\ m^{-2}\ yr^{-1}$)
Port Susan	9334	302
Nisqually	2400	120
Skokomish	912	98
Grays Harbor	8026	134
Willapa	3379	198
Siletz	2984	143
Coos Bay	988	57
Bandon	1045	63

Table 4.3. Vertical accretion, mineral accumulation and carbon sequestration rates as determined by Cesuim-137 dating for soil cores sampled at low, mid and high elevations. The weighted mean is based on marsh area and core sampling location.

	Low	Mid	High	Mean (SD)	Weighted Mean
Vertical accretion (mm yr^{-1})					
Port Susan	--	7.2	5.2	6.2 (1.4)	6.7
Nisqually	3.6	3.4	2.8	3.3 (0.4)	3.3
Skokomish	--	1.6	2.8	2.2 (0.8)	2.5
Grays H.	8.0	8.2	7.4	7.9 (0.4)	7.3
Willapa	6.4	8.8	6.0	7.1 (1.5)	6.4
Siletz	4.4	3.6	2.0	3.3 (1.2)	2.7
Coos	3.2	3.2	3.4	3.3 (0.1)	3.3
Bandon	2.0	2.4	2.4	2.3 (0.2)	2.3
Mineral accumulation (g m^{-2} yr^{-1})					
Port Susan	--	3895	3536	3716 (254)	3690
Nisqually	1500	650	925	1025 (434)	720
Skokomish	--	305	215	260 (63)	315
Grays H.	3432	1411	6158	3667 (2382)	2765
Willapa	2732	3711	565	2336 (1610)	2331
Siletz	978	1076	529	861 (292)	654
Bull Island	290	390	451	377 (81)	315
Bandon	281	327	780	463 (276)	290
Organic Accumulation (g m^{-2} yr^{-1})					
Port Susan	--	163	143	154 (26)	157
Nisqually	72	125	88	96 (39)	109
Skokomish	--	98	61	81 (35)	91
Grays H.	164	109	136	138 (46)	116
Willapa	171	161	81	141 (70)	155
Siletz	190	182	96	159 (79)	118
Coos	48	67	79	65 (20)	53
Bandon	53	70	88	65 (35)	48

Table 4.4. Average (standard deviation) percentage organic matter in the rooting zone (top 20 cm) and overall bulk density from low, mid and high marsh soil cores across Pacific Northwest estuaries (n = 20). Elevation zones were determined by site-specific tidal datums.

	Organic Matter (%)			Bulk Density (g cm^{-3})		
	Low	Mid	High	Low	Mid	High
Port Susan	2.2 (0.5)	7.2 (1.3)	5.6 (1.1)	0.28 (0.25)	0.23 (0.11)	0.20 (0.14)
Nisqually	5.2 (0.7)	23.1 (3.7)	11.2 (6.8)	0.42 (0.14)	0.23 (0.08)	0.39 (0.16)
Skokomish	13.0 (2.0)	24.9 (2.9)	27.1 (6.8)	0.28 (0.10)	0.23 (0.08)	0.2 (0.11)
Grays Harbor	11.0 (1.4)	15.6 (2.1)	5.1 (5.7)	0.28 (0.10)	0.10 (0.05)	0.62 (0.33)
Willapa	11.4 (2.9)	10.5 (1.6)	30.9 (3.2)	0.42 (0.12)	0.27 (0.07)	0.10 (0.03)
Siletz	21.1 (3.8)	20.9 (5.3)	18.7 (4.6)	0.27 (0.10)	0.36 (0.10)	0.35 (0.14)
Coos	24.1 (2.7)	22.3 (4.4)	22.6 (5.9)	0.10 (0.04)	0.15 (0.08)	0.16 (0.07)
Bandon	20.9 (4.1)	6.7 (5.6)	19.0 (2.2)	0.20 (0.23)	0.32 (0.08)	0.41 (0.17)

Table 4.5. Predictors of vertical accretion (using the area-weighted mean) for sediment cores collected in eight estuaries in Oregon and Washington from single-variable generalized linear models. Raw values used for these models are in Appendix B, Table 1.

Predictors	Resid. Df	Log-likelihood	AICc	ΔAICc	weight
Discharge	6	8.57	-5.15	0	0.89
Hypsometric Integral	6	5.03	1.95	7.1	0.03
Watershed Precip Vol	6	4.95	2.09	7.24	0.02
Intercept-Only	7	1.69	3.02	8.17	0.01

DISCUSSION

Our results are the first attempt to measure accretion rates with sediment cores along elevation gradients across multiple Pacific Northwest tidal marshes to better understand variability in accretion, the physical drivers of accretion rates, and the sensitivity of sea-level rise vulnerability assessments. The range of accretion rates we measured in all cores across all study sites (2.3 – 7.3 mm yr^{-1}) had accretion rates that were greater than the historical sea-level rise rates, which ranged from 0.4 mm yr^{-1} at Willapa to 2.1 mm yr^{-1} in Puget Sound (NOAA, tidesandcurrents.noaa.gov). Our estimates of accretion are comparable to those measured by Thom (1992; 2.3 - 6.6 mm yr^{-1}); whose study included tidal marshes in two of our focal estuaries (Nisqually and Grays Harbor). Thom (1992) calculated an average accretion rate at Nisqually of 2.8 mm yr^{-1} and 6.6 mm yr^{-1} at a marsh along the Elk River at the southern side of Grays Harbor, similar to the rates we found for those estuaries. While all our study sites appear to be keeping pace with the current rate of sea-level rise, disruptions to the sediment supply, changes in freshwater discharge to the estuary (Elsner et al. 2010) or accelerated sea-level

rise anticipated after 2050 due to climate change (National Research Council 2012) pose risks to their long-term persistence.

Accretion rates varied significantly across estuaries with mean annual watershed freshwater discharge as the best watershed-scale predictor of both accretion and mineral accumulation rates. Previous studies have found that sediment loads increase with fluvial discharge (Milliman and Syvitski 1992, Milliman 2001, Weston 2014), and the relationship between suspended sediment concentrations (SSC) and marsh accretion rates has been well established through empirical studies and numerical modeling (e.g., Temmerman et al. 2004, French 2006, Butzeck et al. 2014). Links between watershed discharge and marsh accretion rates, however, have not been explicitly tested. There has been a focus on the SSC of the water column during tidal inundation, however SSC can be a misleading metric for marsh stability as eroding marshes can produce high SSCs (Ganju et al. 2015). From a watershed-scale perspective, we suggest that SSC is a proximate factor in tidal marsh accretion and that freshwater discharge (and sediment supply) into the estuary is the important factor influencing tidal marsh longevity, at least in estuaries with ample supplies of erodible fine sediment and strong fluvial influence. However, little work has been done on linking SSC in channels with measured marsh surface accretion rates. While researchers have recognized the importance of sufficient SSCs for marsh persistence with sea-level rise (e.g., Kirwan et al. 2010), our results indicate that changes in discharge and sediment supply (e.g., Ganju et al. 2015) related to human influences (e.g., dams; Weston 2014) or precipitation (Rosencranz et al. 2016) are also important to consider for a holistic understanding of tidal marsh vulnerability.

Watershed-scale disturbances have influenced discharge and sediment loads across PNW estuaries. Human activities in watersheds have altered sediment delivery in other regions. For example, water retention behind dams is correlated with a decline in suspended sediment concentrations (Weston 2014), hydraulic gold mining and European settlement in the 1800s has been linked to marsh expansion (Watson and Byrne 2013), and road construction and logging has increased erosion, sediment transport, and peak discharge rates (Beschta 1978, Jones and Grant 1996). Additional monitoring and linking of fluvial SSC and surface elevation tables (SETs) are needed across the PNW to better evaluate the long-term impacts of land use and climate change on tidal marsh accretion processes (e.g., Nisqually restoration; Barber 2014).

The relationship between organic matter accumulation and tide range is difficult to understand, but may be related to soil flushing. More frequent inundation would reduce soil salinities and promote biomass production, leading to increased rates of organic accumulation. However, marshes tend to increase in elevation with greater tidal ranges, thus it is not clear if increased inundation frequency is a reasonable assumption. Unfortunately, water salinity data was not available at every site, thus it was not possible to explore salinity as a potential mechanism. Salinity in the summer, when freshwater flow is lowest, may be a particularly useful metric to understanding variation in organic matter across Pacific Northwest marshes.

The mineral and organic inventory results indicate that variation in accretion was more related to the accumulation of mineral sediment than organic matter. Overall, percent organic matter in the root zone and at depth was low in comparison to pickleweed (*Sarcocornia* spp) dominated marshes in the San Francisco Bay, California (Callaway et

al. 2012). Furthermore, these results contrasts with the high organic matter contributions in East Coast and Gulf Coast marshes of the United States (Nyman et al. 1993, Callaway et al. 1997, Chmura and Hung 2004, Kearney and Turner 2016), and underscores sediment supply and delivery as critical factors for PNW marsh accretion.

Through comparison of WARMER model projections under a range of accretion rate scenarios, we demonstrated that site-specific measures of accretion are needed for accurate projections of marsh elevations with sea-level rise. There was significant variation in soil core characteristics and no spatial autocorrelation in accretion rates across sites and elevations illustrating that approaches of using nearest neighbor estuaries or a regional mean of accretion when site specific data is not available are not likely accurate. For example, we found that the higher accretion rate from Port Susan increased mean elevation at Nisqually by 26% in the 100-year simulation, while the lower rate from Skokomish reduced mean elevation by 14%, compared to using accretion rates from Nisqually (Fig. 4.3). After 100 years all of the high marsh habitat at Nisqually was projected to be lost using site-specific accretion data, while projections using the Port Susan accretion rates show high marsh covering 91% of the area (Fig. 4.4). The use of regional mean accretion rates can significantly alter model projections and interpretations, with implications for short- and long-term resource management.

CONCLUSION

We measured vertical accretion in tidal marshes across eight PNW estuaries and found that they all have accretion rates greater than the current sea-level rise rate. There was also significant variation across the estuaries. The variation in accretion was related

to fluvial discharge rates into the estuaries, which deliver sediments to the estuary for redistribution and deposition onto the marsh platform. Fluvial discharge rates are influenced by human activities and may further be altered by changes in freshwater availability and timing of flows due to climate change in the PNW. Integration of soil core-based accretion rates from additional estuaries across the PNW and in other climates is warranted to validate the model with discharge and explore the generality of the relationship. Exploration of hydrologic model climate change projections for PNW watersheds in this context would provide additional information about future sediment supplies to estuaries. From our model comparison, we found site-specific data are critical for accurate projections of marsh elevation into the future under sea-level rise scenarios. While there is much uncertainty in the rate of sea-level rise, site-specific accretion data helps reduce the overall uncertainty associated with future projections. Finally, holistic knowledge on the variation in sediment supply is required for the long-term management of tidal marshes facing an uncertain future.

ACKNOWLEDGMENTS

The authors would like to thank J. Takekawa, K. Schmidt, C. Freeman, M. Zarzycki, M. Monnin, S. Pearlstein, L. Shakari and S. Blakely for assistance in the field and the lab. Special thanks to L. Minc for access to the OSU Radiation Center. We would also like to thank DOI U.S. Geological Survey, Western Ecological Research Center, National Climate Change and Wildlife Science Center, the National Oceanic and Atmospheric Administration EESLR program (grant ID NA15NOS4780171), Northwest Climate Science Center (NWCSC), Southwest Climate Science Center, U.S. Fish & Wildlife

Service North Pacific, Oregon State University and the NWCSC fellowship for funding support. Any use of trade, product, or firm names in this publication is for descriptive purposes only and does not imply endorsement by the U.S. government.

LITERATURE CITED

Adamus, P.R., J. Larsen, and R. Scranton. 2005. Wetland Profiles of Oregon's Coastal Watersheds and Estuaries. Part 3 of a Hydrogeomorphic Guidebook. Report to Coos Watershed Association, US Environmental Protection Agency, and Oregon Depart. of State Lands, Salem.

Archfield, S. A., and R. M. Vogel. 2010. Map correlation method: Selection of a reference streamgage to estimate daily streamflow at ungaged catchments. Water Resources Research 46:1–15.

Barber, A. 2014. Sediment and vegetation monitoring during a levee removal project on the Stillaguamish River Delta at By. Thesis.

Beschta, R. L. 1978. Long-term patterns of sediment production following road construction and logging in the Oregon Coast Range. Water Resources Research 14:1011–1016.

Blake, G. R., and K. H. Hartge. 1986. Bulk density. p. 363–375. In A. Klute (ed.) Methods of soil analysis. Part 1. 2nd ed. Agron. Monogr. 9. ASA and SSSA, Madison, WI.

Borde, A. B., R. M. Thom, S. Rumrill, and L. M. Miller. 2003. Geospatial habitat change analysis in Pacific Northwest coastal estuaries. Estuaries 26:1104–1116.

Boule, M. E. and K. F. Bierly. 1987. History of estuarine wetland development and alteration: what we wrought? Northwest Environmental Journal, 3:1, 43-61.

Bridgham, S. D., J. P. Megonigal, J. K. Keller, N. B. Bliss, and C. Trettin. 2006. The Carbon Balance of North American Wetlands. The Society of Wetland Scientists 26:889–916.

Buffington, K. J., B. D. Dugger, K. M. Thorne, and J. Y. Takekawa. 2016. Statistical correction of lidar-derived digital elevation models with multispectral airborne imagery in tidal marshes. Remote Sensing of Environment 186:616–625.

Butzeck, C., A. Eschenbach, A. Gröngröft, K. Hansen, S. Nolte, and K. Jensen. 2015. Sediment Deposition and Accretion Rates in Tidal Marshes Are Highly Variable Along Estuarine Salinity and Flooding Gradients. Estuaries and Coasts 38:434–450.

Callaway, A. J. C., R. D. Delaune, and W. H. P. Jr. 1997. Sediment Accretion Rates from Four Coastal Wetlands along the Gulf of Mexico. Journal of Coastal Research 13:181–191.

Callaway, J. C., E. L. Borgnis, R. E. Turner, and C. S. Milan. 2012. Carbon Sequestration and Sediment Accretion in San Francisco Bay Tidal Wetlands. Estuaries and Coasts 35:1163–1181.

Charles, H., and J. S. Dukes. 2009. Effects of warming and altered precipitation on plant and nutrient dynamics of a New England salt marsh. Ecological Applications 19:1758–1773.

Chmura, G. L., S. C. Anisfeld, D. R. Cahoon, and J. C. Lynch. 2003. Global carbon sequestration in tidal, saline wetland soils. Global Biogeochemical Cycles 17:12.

Chmura, G. L., and G. A. Hung. 2004. Controls on salt marsh accretion: A test in salt marshes of Eastern Canada. Estuaries 27:70–81.

Coastal Resources Alliance. 2007. Ranking of estuarine habitat restoration priorities in Willapa Bay, WA. Final report. 30 pp.

Collins, B., 1997. Effects of Land Use on the Stillaguamish River, Washington, ~1870 to ~1990: Implications for Salmonid Habitat and Water Quality and Their Restoration. Report to The Tulalip Tribes, Snohomish County, Stillaguamish Tribe, and Washington State Department of Ecology. University of Washington, Seattle, Washington.

Craft, C., J. Clough, J. Ehman, S. Jove, R. Park, S. Pennings, H. Guo, and M. Machmuller. 2009. Forecasting the effects of accelerated sea-level rise on tidal marsh ecosystem services. Frontiers in Ecology and the Environment 7:73–78.

Day, J. W., F. Scarton, A. Rismondo, D. Are, J. W. Day, F. Scarton, A. Rismondo, and D. Aret. 1998. Rapid Deterioration of a Salt Marsh in Venice Lagoon, Italy. Journal of Coastal Research 14:583–590.

Dean, T., Z. Ferdaña, J. White, and C. Tanner. 2001. Identifying and Prioritizing Sites for Estuarine Habitat Restoration in Puget Sound's Skagit River Delta. Puget Sound Research. People for Puget Sound and U.S. Fish and Wildlife Service

Ellings, C. 2011. Nisqually National Wildlife Refuge estuary restoration project monitoring framework. Unpublished draft report on file with the Nisqually National Wildlife Refuge, Olympia, WA.

Elsner, M. M., L. Cuo, N. Voisin, J. S. Deems, A. F. Hamlet, J. A. Vano, K. E. B. Mickelson, S. Y. Lee, and D. P. Lettenmaier. 2010. Implications of 21st century climate change for the hydrology of Washington State. Climatic Change 102:225–260.

French, J. 2006. Tidal marsh sedimentation and resilience to environmental change: Exploratory modelling of tidal, sea-level and sediment supply forcing in predominantly allochthonous systems. Marine Geology 235:119–136.

Ganju, N. K., M. L. Kirwan, P. J. Dickhudt, G. R. Guntenspergen, D. R. Cahoon, and K. D. Kroeger. 2015. Sediment transport-based metrics of wetland stability. Geophysical Research Letters 42:7992–8000.

Gelfenbaum G. and Kaminsky, G. 2002. Southwest Washington coastal erosion workshop report 2000. USGS Open-File Report 02-229, 308 pp.

Glick, P., Clough, J., and Nunley, B. 2007. Sea-level Rise and Coastal Habitats in the Pacific Northwest: An Analysis for Puget Sound, Southwestern Washington, and Northwestern Oregon, National Wildlife Federation, Seattle, Washington, 94 pp.

Greenberg, R., J. E. Maldonado, S. Droege, and M. V. McDonald. 2006. Tidal Marshes: A Global Perspective on the Evolution and Conservation of Their Terrestrial Vertebrates. BioScience 56:675–685.

de Groot, A. V., R. M. Veeneklaas, and J. P. Bakker. 2011. Sand in the salt marsh: Contribution of high-energy conditions to salt-marsh accretion. Marine Geology 282:240–254.

Hickey, B. M., and N. S. Banas. 2003. Oceanography of the U. S. Pacific Northwest Coastal Ocean and Estuaries with Application to Coastal Ecology. Estuaries 26:1010–1031.

Jiang, H., J. R. Strittholt, P. a. Frost, and N. C. Slosser. 2004. The classification of late seral forests in the Pacific Northwest, USA using Landsat ETM+ imagery. Remote Sensing of Environment 91:320–331.

Jones, J. A., and G. E. Grant. 1996. Peak flow response to clear-cutting and roads in small and large basin, western Cascades, Oregon. Water Resources Research 32:959–974.

Kearney, M. S., and R. E. Turner. 2016. Microtidal marshes: Can these widespread and fragile marshes survive increasing climate–sea level variability and human action? Journal of Coastal Research 319:686–699.

Kennish, M. J. 2002. Environmental threats and environmental future of estuaries. Environmental Conservation 29:78–107.

Kirwan, M. L., G. R. Guntenspergen, A. D'Alpaos, J. T. Morris, S. M. Mudd, and S. Temmerman. 2010. Limits on the adaptability of coastal marshes to rising sea level. Geophysical Research Letters 37:1–5.

Kirwan, M. L., and A. B. Murray. 2007. A coupled geomorphic and ecological model of tidal marsh evolution. Proceedings of the National Academy of Sciences of the United States of America 104:6118–6122.

Kirwan, M. L., A. B. Murray, J. P. Donnelly, and D. R. Corbett. 2011. Rapid wetland expansion during European settlement and its implication for marsh survival under modern sediment delivery rates. Geology 39:507–510.

Kolker, A. S., S. L. Goodbred, S. Hameed, and J. K. Cochran. 2009. High-resolution records of the response of coastal wetland systems to long-term and short-term sea-level variability. Estuarine, Coastal and Shelf Science 84:493–508.

Mariotti, G., and S. Fagherazzi. 2013. Critical width of tidal flats triggers marsh collapse in the absence of sea-level rise. Proceedings of the National Academy of Sciences of the United States of America 110:5353–6.

Mattheus, C. R., A. B. Rodriguez, and B. a. McKee. 2009. Direct connectivity between upstream and downstream promotes rapid response of lower coastal-plain rivers to land-use change. Geophysical Research Letters 36:1–6.

Milliman, J. D. 2001. River Inputs. Page (A. Thorpe and K. K. Turekian, Eds.) Encyclopedia of Ocean Sciences. 2nd edition. Academic Press, New York.

Milliman, J. D., and J. P. M. Syvitski. 1992. Geomorphic/Tectonic Control of Sediment Discharge to the Ocean: The Importance of Small Mountainous Rivers. The Journal of Geology 100:525–544.

Moran P. A. P. 1950. Notes on continuous stochastic phenomena. Biometrika 37: 17-23.

Morris, J. T., P. V. Sundareshwar, C. Nietch, B. Kjerfve, and D. R. Cahoon. 2002. Responses of coastal wetlands to rising sea level. Ecology 83:2869–2877.

National Research Council. 2012. Sea-Level Rise for the Coasts of California, Oregon, and Washington: Past, Present, and Future.

Nisqually Restoration. http://nisquallydeltarestoration.org/science_geomorphology_sedimentation.php, accessed 27 September 2016.

Nixon, A. S. W., J. W. Ammerman, L. P. Atkinson, V. M. Berounsky, G. Billen, C. Boicourt, W. R. Boynton, T. M. Church, D. M. Ditoro, R. Elmgren, J. H. Garber, R. A. Jahnke, N. J. P. Owens, M. E. Q. Pilson, and S. P. Seitzinger. 1996. The Fate of Nitrogen and Phosphorus at the Land-Sea Margin of the North Atlantic Ocean. Biogeochemistry 35:141–180.

Nyman, J. A., R. D. Delaune, H. H. Roberts, and W. H. Patrick. 1993. Relationship between vegetation and soil formation in a rapidly submerging coastal marsh. Marine Ecology Progress Series 96:269–279.

Pérez-Peña, J. V., J. M. Azañón, and A. Azor. 2009. CalHypso: An ArcGIS extension to calculate hypsometric curves and their statistical moments. Applications to drainage basin analysis in SE Spain. Computers and Geosciences 35:1214–1223.

PRISM Climate Group, Oregon State University, http://prism.oregonstate.edu, created 9 Oct 2015.

van Proosdij, D., R. G. D. Davidson-Arnott, and J. Ollerhead. 2006. Controls on spatial patterns of sediment deposition across a macro-tidal salt marsh surface over single tidal cycles. Estuarine, Coastal and Shelf Science 69:64–86.

Ritchie, J., and J. R. Mchenry. 1990. Application of Radioactive Fallout Cesium-137 for Measuring Soil Erosion and Sediment Accumulation Rates and Patterns : A Review. Journal of Environmental Quality 19:215–233.

Rosencranz, J. A., N. K. Ganju, R. F. Ambrose, S. M. Brosnahan, P. J. Dickhudt, G. R. Guntenspergen, G. M. MacDonald, J. Y. Takekawa, and K. M. Thorne. 2016. Balanced Sediment Fluxes in Southern California's Mediterranean-Climate Zone Salt Marshes. Estuaries and Coasts 39:1035–1049.

Swanson, K. M., J. Z. Drexler, C. Fuller, and D. H. Schoellhamer. 2015. Modeling tidal

freshwater marsh sustainability in the Sacramento-San Juaquin Delta under a broad suite of potential future scenarios. San Francisco Estuary and Watershed Science 13:217–220.

SWAT 2016. Skokomish Watershed Action Team, Skokomish Watershed Action Plan Update 2016. Available: http://hccc.wa.gov/content/salmon-recovery-planning

Temmerman, S., G. Govers, S. Wartel, and P. Meire. 2004. Modelling estuarine variations in tidal marsh sedimentation: response to changing sea level and suspended sediment concentrations. Marine Geology 212:1–19.

Thom, R. M. 1992. Accretion rates of low intertidal salt marshes in the Pacific Northwest. Wetlands 12:147–156.

TIGER/Line Shapefiles (machine readable data files), prepared by the U.S. Census Bureau, 2015.

Torio, D. D., and G. L. Chmura. 2013. Assessing Coastal Squeeze of Tidal Wetlands. Journal of Coastal Research 29:1049–1061.

U.S. Fish and Wildlife Service. 2012a. Bandon Marsh National Wildlife Refuge draft Comprehensive Conservation Plan and Environmental Assessment. U.S. Department of the Interior, Fish and Wildlife Service, Region 1, Portland, OR. 431 pp.

U.S. Fish and Wildlife Service. 2012b. Siletz Bay National Wildlife Refuge draft Comprehensive Conservation Plan and Environmental Assessment. U.S. Department of the Interior, Fish and Wildlife Service, Region 1, Portland, OR. 418 pp.

van der Wal, D., and K. Pye. 2004. Patterns, rates and possible causes of saltmarsh erosion in the Greater Thames area (UK). Geomorphology 61:373–391.

Watson, E. B., and R. Byrne. 2013. Late Holocene Marsh Expansion in Southern San Francisco Bay, California. Estuaries and Coasts 36:643–653.

Weston, N. B. 2014. Declining Sediments and Rising Seas: An Unfortunate Convergence for Tidal Wetlands. Estuaries and Coasts 37:1–23.

Yang, Z., K. L. Sobocinski, D. Heatwole, T. Khangaonkar, R. Thom, and R. Fuller. 2010. Hydrodynamic and ecological assessment of nearshore restoration: A modeling study. Ecological Modelling 221:1043–1053.

Improving Projections of Tidal Marsh Persistence under Climate Change with Remote Sensing and Site-Specific Data

CHAPTER 5

GENERAL CONCLUSIONS

Kevin J. Buffington

As climate change and sea-level rise threaten to change coastal ecosystems (Day et al. 2008), resource managers need improved techniques to assist in assessing their current conditions, understand historic sensitivities to climate variation, and help guide management decisions in the face of future change. The overall goal of my dissertation was to integrate remote sensing and field datasets to improve our understanding the vulnerability of Pacific Northwest tidal marshes to climate change and sea-level rise. I developed a novel technique for improving the accuracy of airborne lidar in dense vegetation (Chapter 2), which is necessary for robust assessments of the baseline elevation in tidal marshes, and for making future projections of elevation response to sea-level rise. I demonstrated the utility of time-series Landsat satellite imagery for monitoring changes in tidal marsh biomass and phenology due to variation in climate (Chapter 3). Finally, I found that tidal marsh accretion rates across the Pacific Northwest (PNW) vary considerably among sites, that variation is related to watershed discharge, accretion is dominated by mineral deposition, and the current rates of accretion in PNW marshes are greater than the current sea-level rise rate (Chapter 4).

Both accurate initial elevation data and local accretion rates are important for making assessments of current tidal marsh vulnerability to sea-level rise and for making projections into the future. To further assess how model results respond to uncertainty in these two important data inputs, I ran the Wetland Accretion Rate Model for Ecosystem Resilience (WARMER; Swanson et al. 2013) at Nisqually with uncorrected and LEAN-corrected DEMs, and with local and non-local accretion data. Using both the uncorrected DEM and non-local accretion data resulted in an error range for elevation of up to 50% (62 cm) compared to a LEAN-corrected DEM with site-specific data (Fig. 5.1). This

amount of uncertainty has important consequences for mapping current vegetation zones (e.g., low, mid, and high marsh communities), and for interpreting WARMER projections of the future. Using inundation frequency to define vegetation zones of current conditions (Thorne et al. 2015), I found substantial differences in vegetation maps between the uncorrected and LEAN-corrected DEMs at Nisqually, with 28% more 'transitional' vegetation in the uncorrected DEM (Fig. 5.2). These differences persist after a 100 year WARMER sea-level rise simulation, with 30% more high marsh projected with the uncorrected DEM. Combining uncorrected DEMs with non-local accretion data (from Grays Harbor, in this example) resulted in stark differences in the prevalence of vegetation in different elevation zones compared with the LEAN corrected DEM and local accretion (Fig. 5.2). These findings highlight the nonlinearities in tidal marsh systems that can lead to very different model projections if error in initial elevation and accretion rates are not controlled.

Differences in the relative abundance of low, mid, and high marsh can influence the suitability of future marsh conditions for wetland-dependent wildlife. For example, the relative abundance of suitable habitat for marsh-endemic species such as Ridgeway's Rail (*Rallus obsoletus*) and California Black Rail (*Laterallus jamaicensis coturniculus*) will change (Thorne et al. 2012). Ridgeway's rails use low marsh areas dominated by *Spartina spp* for nesting (Zedler 1993), while Black Rails favor high marsh habitat dominated by *Sarcocornia pacifica* (Tsao et al. 2009). Using an inundation (elevation)-based metric for marsh vegetation zones at China Camp, in San Francisco Bay (Thorne et al. 2015), I calculated that the current area of low marsh was underestimated by 220% when using uncorrected lidar compared with a LEAN DEM, and high marsh was

overestimated by nearly 100%. Under moderate 100 year sea-level rise (+93 cm), China Camp is projected to be dominated by low marsh species, with no high marsh remaining (Swanson et al. 2013). While elevation alone is an incomplete measure of habitat suitability of these species, these results demonstrate how a seemingly small vertical offset in elevation (23 cm, on average; Chapter 2) can impact estimates of suitable habitat area in tidal marshes. As demonstrated above at Nisqually, accurate initial elevation is critical when making projections into the future. Habitat suitability modeling efforts of species that live in habitat affected by hydrology need to carefully consider the error tolerances of baseline elevation data and the feasibility of adjustment algorithms like LEAN to refine projections.

While my work using soil cores to improve our ability to forecast marsh response to sea-level rise is useful, soil cores alone are likely not enough for complete calibration of tidal marsh elevation models. Changes in land use across the watershed and in precipitation regimes due to climate change can influence the rate of sediment delivery to the estuary (e.g., Wright and Schoellhamer 2004, Chapter 4). Integration of accretion data from soil cores, suspended sediment concentration monitoring, and surface elevation tables (SETs) into model projections would capture both the history of the tidal marsh, including rates of soil compaction and organic matter sequestration, and the current availability of sediment.

The integration of climate projections and stochastic drivers (storms, strong El Nino conditions) into future estimates of sediment availability (e.g., Ganju and Schoellhamer 2010) and accretion within marsh elevation models would potentially capture a broader range of future conditions and facilitate a more robust analysis of future

uncertainty. Movement away from using long-term average accretion rates for calibrating marsh elevation models, and using that data for validation instead, may expose additional sensitivities of marsh biogeomporhic processes that are important when considering historically rapid shifts in the abiotic environment due to climate change. For example, fluvial discharge, and hence sediment delivery, to estuaries along the Pacific coast is highly seasonal, however, little is understood about how potential changes in the timing of sediment delivery (because of earlier snow melt; Elsner et al. 2010) and altered plant phenology (due to climate change or ENSO, Chapter 3) may impact rates of sediment deposition and accretion in tidal marshes. Whether extending models like WARMER to include stochastic drivers or relying on more sophisticated modeling frameworks like Delft3D, there is a general lack of the necessary calibration and validation field data to extrapolate lessons learned from one site to others. The expansion of long-term suspended sediment monitoring programs (e.g., NOAA National Estuarine Research Reserves), coupled with SETs, would provide a valuable dataset for model parameterization. A next generation of tidal marsh models, coupled with local sediment and vegetation monitoring, would provide managers and scientists an improved guide for assessing existing tidal marsh vulnerability to sea-level rise, as well as provide better information regarding the necessity and feasibility of tidal marsh elevation enhancement (e.g., Ford et al. 1999) and restoration.

Around the world, tidal marshes have been impacted by human development (Kennish 2002, Torio and Chmura 2013) and extensive efforts are underway to restore tidal marsh function. As the rate of sea level rise increases it is important to build additional capacity into coastal systems if they are to continue providing historic

ecosystem functions. My findings in Chapter 4 suggest that estuaries with higher fluvial discharge may better support restoration projects as the underlying sediment supply may be greater. While other considerations, such as the availability of restorable land and initial elevation, are also important, these results suggest fluvial discharge may be a useful and readily available metric for ranking restoration priorities at the regional scale.

The effects of phenology in tidal marsh ecosystems has received relatively limited research attention. As they are subject to dynamic abiotic gradients, tidal marsh plants and wildlife may be particularly resilient to phenology shifts owing to broad phenotypic and behavioral plasticity (Wetson et al. 2012, Di Bella et al. 2014, Carus et al. 2016, Hunter et al. 2016). However, temporal and abundance mismatches between producer and consumer communities may have important, but subtle, effects on ecosystem functioning that may be further exacerbated by climate change and sea-level rise. Additionally, altered phenology may impact the net accumulation of carbon, with implications for carbon accounting and efforts to include tidal marshes in carbon markets (Sutton-Grier and Moore 2016). Further study into the effects of shifting phenology in coastal ecosystems is warranted, particularly in regard to potential effects on net accretion rates.

There are several limitations of this dissertation that are important to reiterate. The LEAN method was developed using site-specific elevation data, thus extrapolating model corrections to other marshes, especially those with different vegetation, should be done carefully. Further analysis, including a leave-one-site out sensitivity analysis across each region, is needed to determine the amount of uncertainty that is introduced by extrapolation. The Landsat time-series and phenology modeling analysis would benefit

from further validation of the timing of peak biomass with repeated field sampling across the growing season. This would ensure that the interpretation of the temporal Landsat spectral signal across Pacific Northwest marshes aligns with the field conditions. The accretion rates I found across the Pacific Northwest largely represent the sediment supply conditions of the last 50 years. Deployment of surface elevation tables and long-term monitoring would help determine whether accretion rates have changed due to watershed management practices or climate change.

Finally, monitoring and projecting tidal marsh responses to climate change requires accurate, site-specific data. Remote sensing data, including lidar and Landsat, offer a tremendous amount of information that can be used to improve our understanding of tidal marsh vulnerability and sensitivity to climate change, although both require careful calibration. Active monitoring of coastal systems with Landsat (and now Sentinel) and early identification of marsh response to sea-level rise may facilitate more proactive management strategies that promote tidal marsh persistence, as well as confirm model predictions about climate change impacts. Standardizing monitoring and modeling protocols across the landscape (e.g., Thorne et al. 2015, 2016) would give resource managers additional confidence in assessments of current and future conditions. Additional work is needed to capture the influence of stochastic events on long-term tidal marsh persistence, understand the influence of shifting plant phenology on accretion rates, move beyond long-term averages in models of tidal marsh vulnerability, as well as further integration of remote sensing products, fine-scale monitoring data, and marsh elevation models.

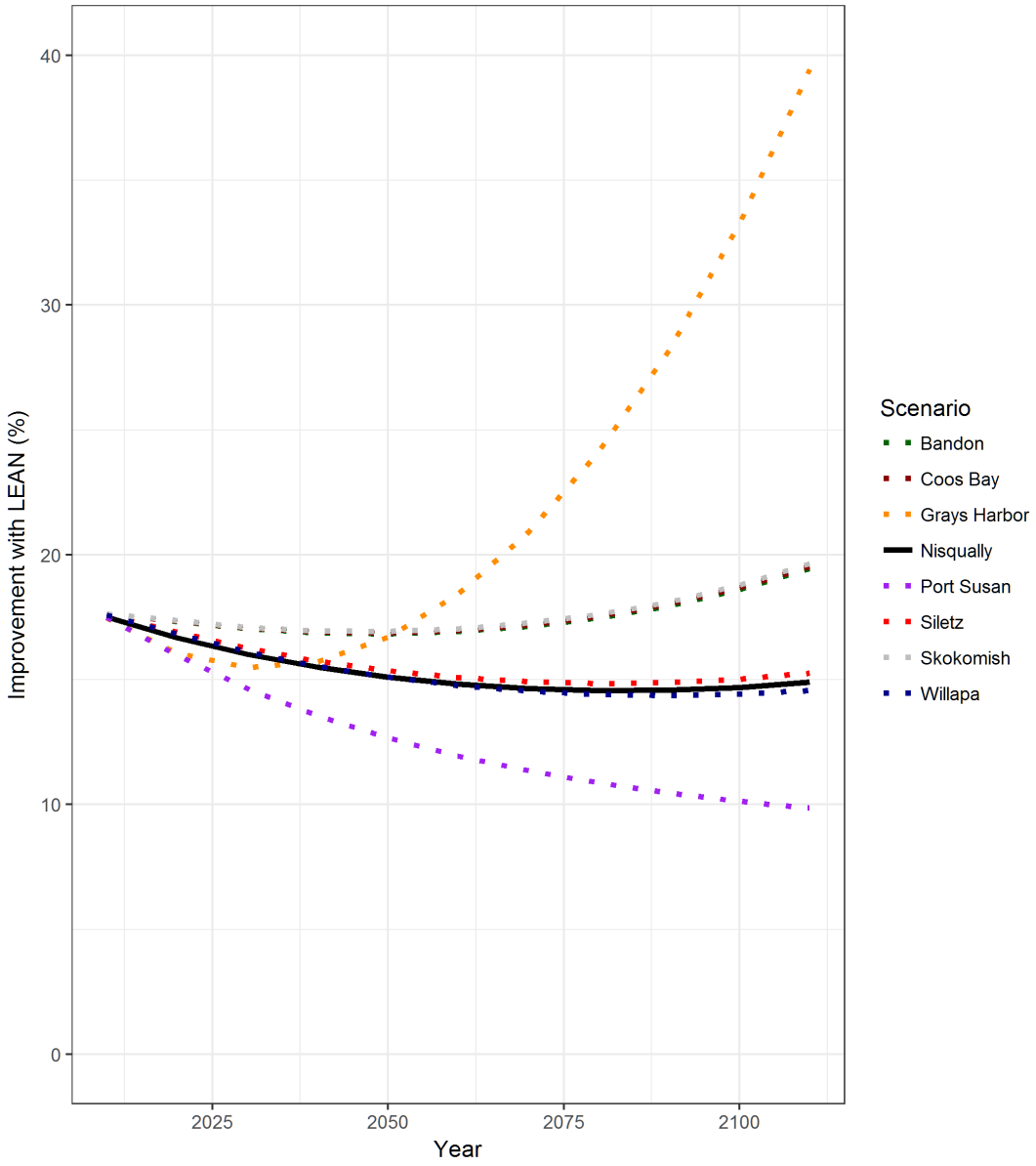

Figure 5.1. Wetland Accretion Rate Model for Ecosystem Resilience (WARMER) model improvement (%) in mean elevation when using the LEAN method to correct the lidar digital elevation model at Nisqually.

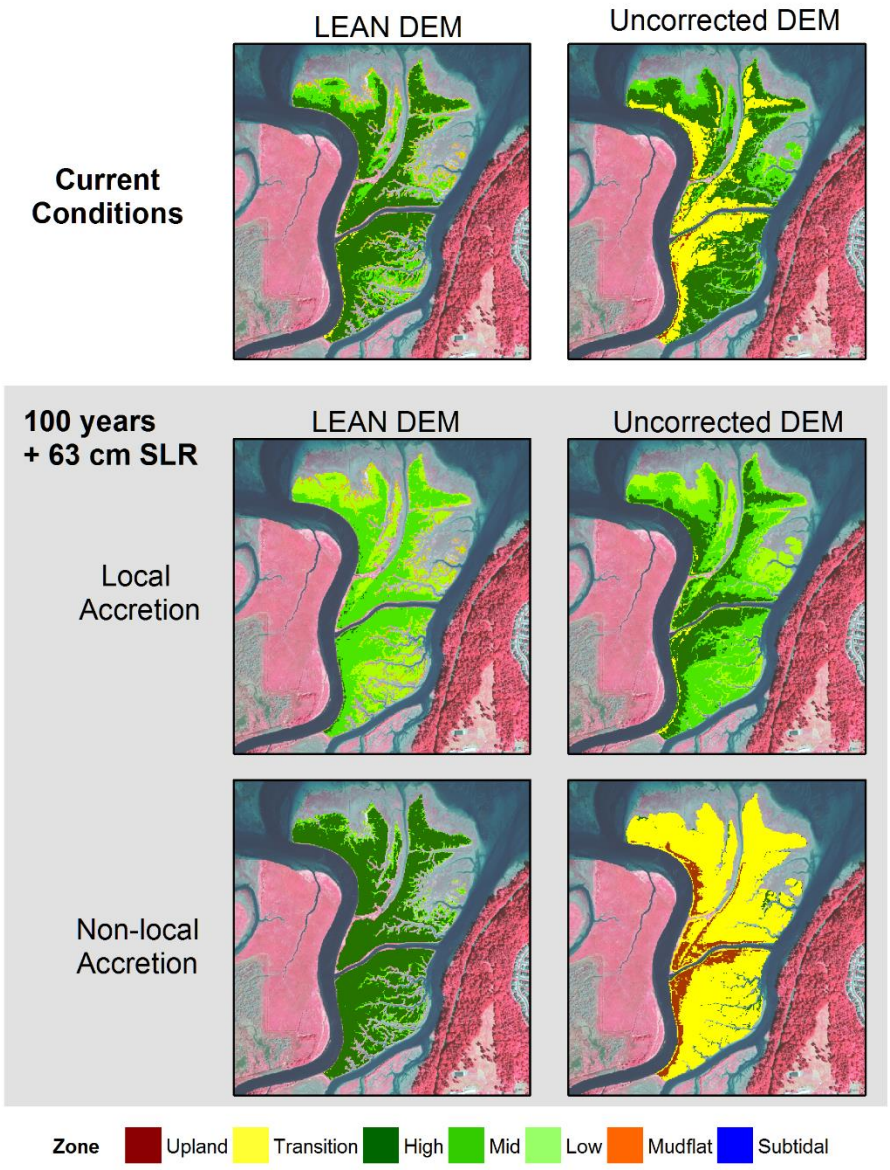

Figure 5.2. Effect of corrected elevations and local accretion data on current and future tidal marsh vegetation zones. 100-year WARMER projections used accretion rate data from Nisqually (Local) and Grays Harbor (Non-local). Vegetation zones were defined by inundation frequency (Thorne et al. 2015). The background is a 2013 false-color NAIP composite image.

LITERATURE CITED

di Bella, C. E., G. G. Striker, F. J. Escaray, F. A. Lattanzi, A. M. Rodríguez, and A. A. Grimoldi. 2014. Saline tidal flooding effects on Spartina densiflora plants from different positions of the salt marsh. Diversities and similarities on growth, anatomical and physiological responses. Environmental and Experimental Botany 102:27–36.

Callaway, A. J. C., R. D. Delaune, and W. H. P. Jr. 1997. Sediment Accretion Rates from Four Coastal Wetlands along the Gulf of Mexico. Journal of Coastal Research 13:181–191.

Callaway, J. C., E. L. Borgnis, R. E. Turner, and C. S. Milan. 2012. Carbon Sequestration and Sediment Accretion in San Francisco Bay Tidal Wetlands. Estuaries and Coasts 35:1163–1181.

Carus, J., M. Paul, and B. Schröder. 2016. Vegetation as self-adaptive coastal protection: Reduction of current velocity and morphologic plasticity of a brackish marsh pioneer. Ecology and Evolution 6:1579–1589.

Charles, H., and J. S. Dukes. 2009. Effects of warming and altered precipitation on plant and nutrient dynamics of a New England salt marsh. Ecological Applications 19:1758–1773.

Day, J. W., R. R. Christian, D. M. Boesch, A. Yáñez-Arancibia, J. Morris, R. R. Twilley, L. Naylor, L. Schaffner, and C. Stevenson. 2008. Consequences of climate change on the ecogeomorphology of coastal wetlands. Estuaries and Coasts 31:477–491.

Elsner, M. M., L. Cuo, N. Voisin, J. S. Deems, A. F. Hamlet, J. A. Vano, K. E. B. Mickelson, S. Y. Lee, and D. P. Lettenmaier. 2010. Implications of 21st century climate change for the hydrology of Washington State. Climatic Change 102:225–260.

Ford, M. A., D. R. Cahoon, and J. C. Lynch. 1999. Restoring marsh elevation in a rapidly subsiding salt marsh by thin-layer deposition of dredged material. Ecological Engineering 12:189–205.

Ganju, N. K., and D. H. Schoellhamer. 2010. Decadal-timescale estuarine geomorphic change under future scenarios of climate and sediment supply. Estuaries and Coasts 33:15–29.

Hunter, E. A., N. P. Nibbelink, and R. J. Cooper. 2016. Threat predictability influences seaside sparrow nest site selection when facing trade-offs from predation and flooding. Animal Behaviour 120:135–142.

Janousek, C., K. Buffington, K. Thorne, G. Guntenspergen, J. Takekawa, and B. Dugger. 2016. Potential effects of sea-level rise on plant productivity: species-specific responses in northeast Pacific tidal marshes. Marine Ecology Progress Series 548:111–125.

Kennish, M. J. 2002. Environmental threats and environmental future of estuaries. Environmental Conservation 29:78–107.

Kirwan, M. L., G. R. Guntenspergen, and J. T. Morris. 2009. Latitudinal trends in Spartina alterniflora productivity and the response of coastal marshes to global change. Global Change Biology 15:1982–1989.

Klemas, V. V. 2001. Remote sensing of landscape-level coastal environmental indicators. Environmental Management 27:47–57.

Masek, J. G., C. Huang, R. Wolfe, W. Cohen, F. Hall, J. Kutler, and P. Nelson. 2008. North American forest disturbance mapped from a decadal Landsat record. Remote Sensing of Environment 112:2914–2926.

Mo, Y., B. Momen, and M. S. Kearney. 2015. Quantifying moderate resolution remote sensing phenology of Louisiana coastal marshes. Ecological Modelling 312:191–199.

Nyman, J. A., R. D. Delaune, H. H. Roberts, and W. H. Patrick. 1993. Relationship between vegetation and soil formation in a rapidly submerging coastal marsh. Marine Ecology Progress Series 96:269–279.

O'Donnell, J. P. R., and J. F. Schalles. 2016. Examination of abiotic drivers and their influence on Spartina alterniflora biomass over a twenty-eight year period using Landsat 5 TM satellite imagery of the Central Georgia Coast. Remote Sensing 8.

Schumaker, N. H., A. Brookes, J. R. Dunk, B. Woodbridge, J. A. Heinrichs, J. J. Lawler, C. Carroll, and D. LaPlante. 2014. Mapping sources, sinks, and connectivity using a simulation model of northern spotted owls. Landscape Ecology 29:579–592.

Sutton-Grier, A. E., and A. Moore. 2016. Leveraging Carbon Services of Coastal Ecosystems for Habitat Protection and Restoration. Coastal Management 753:259–277.

Swanson, K. M., J. Z. Drexler, D. H. Schoellhamer, K. M. Thorne, M. L. Casazza, C. T. Overton, J. C. Callaway, and J. Y. Takekawa. 2013. Wetland Accretion Rate Model of Ecosystem Resilience (WARMER) and Its Application to Habitat Sustainability for Endangered Species in the San Francisco Estuary. Estuaries and Coasts 37:476–492.

Thorne, K. M., J. Y. Takekawa, D. L. Elliott-Fisk, and Thorne. 2012. Ecological Effects of Climate Change on Salt Marsh Wildlife: A Case Study from a Highly Urbanized Estuary. Journal of Coastal Research 28:1477–1487.

Thorne, K. M., Dugger, B. D., Buffington, K. J., Freeman, C. M., Janousek, C. N., Powelson, K. W., Gutenspergen, G. R., and Takekawa, J. Y., 2015. Marshes to mudflats—Effects of sea-level rise on tidal marshes along a latitudinal gradient in the Pacific Northwest: U.S. Geological Survey Open-File Report 2015-1204, 54 p. plus appendixes, http://dx.doi.org/10.3133/ofr20151204.

Thorne, K. M., MacDonald, G. M., Ambrose, R. F., Buffington, K. J., Freeman, C. M., Janousek, C. N., Brown, L. N., Holmquist, J. R., Gutenspergen, G. R., Powelson, K. W., Barnard, P. L., and Takekawa, J. Y., 2016. Effects of climate change on tidal marshes along a latitudinal gradient in California: U.S. Geological Survey Open-File Report 2016-1125, 75 p., http://dx.doi.org/10.3133/ofr20161125.

Torio, D. D., and G. L. Chmura. 2013. Assessing Coastal Squeeze of Tidal Wetlands. Journal of Coastal Research 29:1049–1061.

Tsao, D. C., J. Y. Takekawa, I. Woo, J. L. Yee, and J. G. Evens. 2009. Home Range, Habitat Selection, and Movements of California Black Rails at Tidal Marshes at San Francisco Bay, California. The Condor 111:599–610.

Wetson, A. M., C. Zorb, E. A. John, and T. J. Flowers. 2012. High phenotypic plasticity of Suaeda maritima observed under hypoxic conditions in relation to its physiological basis. Annals of Botany 109:1027–1036.

Wright, S. A., and D. H. Schoellhamer. 2004. Trends in the sediment yield of the Sacramento River, California, 1957 – 2001. San Francisco Estuary and Watershed Science 2:1–14.

Zedler, J. B. 1993. Canopy Architecture of Natural and Planted Cordgrass Marshes: Selecting Habitat Evaluation Criteria. Ecological Applications 3:123–138.

Zhang, H., and S. M. Gorelick. 2014. Coupled impacts of sea-level rise and tidal marsh restoration on endangered California clapper rail. Biological Conservation 172:89–100.

BIBLIOGRAPHY

Adamus, P.R., J. Larsen, and R. Scranton. 2005. Wetland Profiles of Oregon's Coastal Watersheds and Estuaries. Part 3 of a Hydrogeomorphic Guidebook. Report to Coos Watershed Association, US Environmental Protection Agency, and Oregon Depart. of State Lands, Salem.

Adam, E., O. Mutanga, and D. Rugege. 2010. Multispectral and hyperspectral remote sensing for identification and mapping of wetland vegetation: A review. Wetlands Ecology and Management 18:281–296.

Archfield, S. A., and R. M. Vogel. 2010. Map correlation method: Selection of a reference streamgage to estimate daily streamflow at ungaged catchments. Water Resources Research 46:1–15.

Aubry, L. M., R. F. Rockwell, E. G. Cooch, R. W. Brook, C. P. H. Mulder, and D. N. Koons. 2013. Climate change, phenology, and habitat degradation: Drivers of gosling body condition and juvenile survival in lesser snow geese. Global Change Biology 19:149–160.

Barber, A. 2014. Sediment and vegetation monitoring during a levee removal project on the Stillaguamish River Delta at By. Thesis.

Barbier, E. B., S. D. Hacker, C. Kennedy, E. W. Koch, A. C. Stier, and B. R. Silliman. 2011. The value of estuarine and coastal ecosystem services. Ecological Monographs 81:169–193.

Bawden, G. W., W. Thatcher, R. S. Stein, K. W. Hudnut, and G. Peltzer. 2001. Tectonic contraction across Los Angeles after removal of groundwater pumping effects. Nature 412:812–5.

Baxter, C. V., K. D. Fausch, and W. C. Saunders. 2005. Tangled webs: Reciprocal flows of invertebrate prey link streams and riparian zones. Freshwater Biology 50:201–220.

di Bella, C. E., G. G. Striker, F. J. Escaray, F. A. Lattanzi, A. M. Rodríguez, and A. A. Grimoldi. 2014. Saline tidal flooding effects on Spartina densiflora plants from different positions of the salt marsh. Diversities and similarities on growth, anatomical and physiological responses. Environmental and Experimental Botany 102:27–36.

Beschta, R. L. 1978. Long-term patterns of sediment production following road construction and logging in the Oregon Coast Range. Water Resources Research 14:1011–1016.

Blake, G. R., and K. H. Hartge. 1986. Bulk density. p. 363–375. In A. Klute (ed.) Methods of soil analysis. Part 1. 2nd ed. Agron. Monogr. 9. ASA and SSSA, Madison, WI.

Borde, A. B., R. M. Thom, S. Rumrill, and L. M. Miller. 2003. Geospatial habitat change analysis in Pacific Northwest coastal estuaries. Estuaries 26:1104–1116.

Boule, M.E. and K. F. Bierly. 1987. History of estuarine wetland development and alteration: what we wrought? Northwest Environmental Journal, 3:1, 43-61.

Bridgham, S. D., J. P. Megonigal, J. K. Keller, N. B. Bliss, and C. Trettin. 2006. The Carbon Balance of North American Wetlands. The Society of Wetland Scientists 26:889–916.

Buffington, K. J., B. D. Dugger, K. M. Thorne, and J. Y. Takekawa. 2016. Statistical correction of lidar-derived digital elevation models with multispectral airborne imagery in tidal marshes. Remote Sensing of Environment 186:616–625.

Butzeck, C., A. Eschenbach, A. Gröngröft, K. Hansen, S. Nolte, and K. Jensen. 2015. Sediment Deposition and Accretion Rates in Tidal Marshes Are Highly Variable Along Estuarine Salinity and Flooding Gradients. Estuaries and Coasts 38:434–450.

Byrd, K. B., J. L. O'Connell, S. Di Tommaso, and M. Kelly. 2014. Evaluation of sensor types and environmental controls on mapping biomass of coastal marsh emergent vegetation. Remote Sensing of Environment 149:166–180.

Byrd, K. B., L. Windham-myers, T. Leeuw, B. Downing, J. T. Morris, and M. C. Ferner. 2016. Forecasting tidal marsh elevation and habitat change through fusion of Earth observations and a process model. Ecosphere 7:1–27.

Cahoon, D. R., and D. J. Reed. 1995. Relationships amoung marsh surface topography, hydroperoid, and soil accretion in a deteriorating Louisana salt marsh. Journal of Coastal Research 11:357–369.

Callaway, A. J. C., R. D. Delaune, and W. H. P. Jr. 1997. Sediment Accretion Rates from Four Coastal Wetlands along the Gulf of Mexico. Journal of Coastal Research 13:181–191.

Callaway, J. C., E. L. Borgnis, R. E. Turner, and C. S. Milan. 2012. Carbon Sequestration and Sediment Accretion in San Francisco Bay Tidal Wetlands. Estuaries and Coasts 35:1163–1181.

Canepuccia, A. D., J. Alberti, J. Pascual, G. Alvarez, J. Cebrian, and O. O. Iribarne. 2010. ENSO episodes modify plant/terrestrial-herbivore interactions in a southwestern Atlantic salt marsh. Journal of Experimental Marine Biology and Ecology 396:42–47.

Carus, J., M. Paul, and B. Schröder. 2016. Vegetation as self-adaptive coastal protection: Reduction of current velocity and morphologic plasticity of a brackish marsh pioneer. Ecology and Evolution 6:1579–1589.

Charles, H., and J. S. Dukes. 2009. Effects of warming and altered precipitation on plant and nutrient dynamics of a New England salt marsh. Ecological Applications

19:1758–1773.

Chavez, P. S. J. 1988. An improved dark-object subtraction technique for amtopshiec scattering correction of multispectral data. Remote Sensing of Environment 24:459–479.

Chmura, G. L., S. C. Anisfeld, D. R. Cahoon, and J. C. Lynch. 2003. Global carbon sequestration in tidal, saline wetland soils. Global Biogeochemical Cycles 17:12.

Chmura, G. L., and G. A. Hung. 2004. Controls on salt marsh accretion: A test in salt marshes of Eastern Canada. Estuaries 27:70–81.

Church J. A., D. Monselesan, J. M. Gregory and B. Marzeion. 2013. Evaluating the ability of process based models to project sea-level change. Environ. Res. Lett. 8 014051 8pp.

Cleland, E. E., I. Chuine, A. Menzel, H. A. Mooney, and M. D. Schwartz. 2007. Shifting plant phenology in response to global change. Trends in Ecology and Evolution 22:357–365.

Coastal Resources Alliance. 2007. Ranking of estuarine habitat restoration priorities in Willapa Bay, WA. Final report. 30 pp.

Collins, B., 1997. Effects of Land Use on the Stillaguamish River, Washington, ~1870 to ~1990: Implications for Salmonid Habitat and Water Quality and Their Restoration. Report to The Tulalip Tribes, Snohomish County, Stillaguamish Tribe, and Washington State Department of Ecology. University of Washington, Seattle, Washington.

Craft, C., J. Clough, J. Ehman, S. Jove, R. Park, S. Pennings, H. Guo, and M. Machmuller. 2009. Forecasting the effects of accelerated sea-level rise on tidal marsh ecosystem services. Frontiers in Ecology and the Environment 7:73–78.

Dalton, M. M., K. D. Dello, L. Hawkins, P. W. Mote, and D. E. Rupp. 2017. The Third Oregon Climate Assessment Report.

Day, J. W., R. R. Christian, D. M. Boesch, A. Yáñez-Arancibia, J. Morris, R. R. Twilley, L. Naylor, L. Schaffner, and C. Stevenson. 2008. Consequences of climate change on the ecogeomorphology of coastal wetlands. Estuaries and Coasts 31:477–491.

Day, J. W., F. Scarton, A. Rismondo, D. Are, J. W. Day, F. Scarton, A. Rismondo, and D. Aret. 1998. Rapid Deterioration of a Salt Marsh in Venice Lagoon, Italy. Journal of Coastal Research 14:583–590.

Doi, H., O. Gordo, and I. Katano. 2008. Heterogeneous intra-annual climatic changes drive different phenological responses at two trophic levels. Climate Research 36:181–190.

Dunton, K. H., B. Hardegree, and T. E. Whitledge. 2001. Response of Estuarine Marsh Vegetation to Interannual Variations in Precipitation. Estuaries 24:851–861.

Efron, B. 1982. The Jackknife, the Bootstrap and other resampling plans. In *CBMS-NSF regional conference series in applied mathematics 1982*. Philadelphia, PA: Society for Industrial and Applied Mathematics (SIAM).

Ellings, C. 2011. Nisqually National Wildlife Refuge estuary restoration project monitoring framework. Unpublished draft report on file with the Nisqually National Wildlife Refuge, Olympia, WA.

Elsner, M. M., L. Cuo, N. Voisin, J. S. Deems, A. F. Hamlet, J. A. Vano, K. E. B. Mickelson, S. Y. Lee, and D. P. Lettenmaier. 2010. Implications of 21st century climate change for the hydrology of Washington State. Climatic Change 102:225–260.

Fagherazzi, S., P. L. Wiberg, S. Temmerman, E. Struyf, Y. Zhao, and P. a Raymond. 2013. Fluxes of water, sediments, and biogeochemical compounds in salt marshes. Ecological Processes 2:3.

Federal Geographic Committee. 1998. Geospatial positioning accuracy standards part 3: National standard for spatial data accuracy. FGDC-STD-007 3-1998, http://www.fgdc.gov/standards/projects/FGDC-standards-projects/accuracy/part3/chapter3.

Filella, I., J. Peñuelas, L. Llorens, and M. Estiarte. 2004. Reflectance assessment of seasonal and annual changes in biomass and CO2 uptake of a Mediterranean shrubland submitted to experimental warming and drought. Remote Sensing of Environment 90:308–318.

Fisher, J. I., J. F. Mustard, and M. A. Vadeboncoeur. 2006. Green leaf phenology at Landsat resolution: Scaling from the field to the satellite. Remote Sensing of Environment 100:265–279.

Flood, M (ed.). 2004. Vertical accuracy reporting for lidar data, version 1.0. ASPRS Lidar Committee (PAD), 20p. http://asprs.org/a/society/committee/lidar/Downloads/Vertical_Accuracy_Reporting_for_Lidar_Data.pdf

Ford, M. A., D. R. Cahoon, and J. C. Lynch. 1999. Restoring marsh elevation in a rapidly subsiding salt marsh by thin-layer deposition of dredged material. Ecological Engineering 12:189–205.

Foxgrover, B. A. C., D. P. Finlayson, and B. E. Jaffe. 2011. 2010 Bathymetry and Digital Elevation Model of Coyote Creek and Alviso Slough, South San Francisco Bay, California. U.S. Geological Survey Open File Report:20.

French, J. 2006. Tidal marsh sedimentation and resilience to environmental change: Exploratory modelling of tidal, sea-level and sediment supply forcing in predominantly allochthonous systems. Marine Geology 235:119–136.

Gabler, C. A., M. J. Osland, J. B. Grace, C. L. Stagg, R. H. Day, S. B. Hartley, N. M.

Enwright, A. S. From, M. L. McCoy, and J. L. McLeod. 2017. Macroclimatic change expected to transform coastal wetland ecosystems this century. Nature Climate Change 7:142–147.

Gamon, J. A., C. B. Field, M. L. Goulden, K. L. Griffin, A. Hartley, G. Joel, J. Penuelas, and R. Valentini. 1995. Relationships Between NDVI, Canopy Structure, and Photosynthesis in Three Californian Vegetation Types. Ecological Applications 5:28–41.

Ganju, N. K., M. L. Kirwan, P. J. Dickhudt, G. R. Guntenspergen, D. R. Cahoon, and K. D. Kroeger. 2015. Sediment transport-based metrics of wetland stability. Geophysical Research Letters 42:7992–8000.

Ganju, N. K., and D. H. Schoellhamer. 2010. Decadal-timescale estuarine geomorphic change under future scenarios of climate and sediment supply. Estuaries and Coasts 33:15–29.

Gelfenbaum G. and Kaminsky, G. 2002. Southwest Washington coastal erosion workshop report 2000. USGS Open-File Report 02-229, 308 pp.

Gershunov, A., and T. Barnett. 1998. Interdecadal modultion of ENSO teleconnections. Bulletin of the American Meteorological Society 79:2715–2726.

Glick, P., Clough, J., and Nunley, B. 2007. Sea-level Rise and Coastal Habitats in the Pacific Northwest: An Analysis for Puget Sound, Southwestern Washington, and Northwestern Oregon, National Wildlife Federation, Seattle, Washington, 94 pp.

Glick, P., B.A. Stein, and N.A. Edelson, editors. 2011. Scanning the Conservation Horizon: A Guide to Climate Change Vulnerability Assessment. National Wildlife Federation, Washington, D.C.

Goetz, S., and R. Dubayah. 2011. Advances in remote sensing technology and implications for measuring and monitoring forest carbon stocks and change. Carbon Management 2:231–244.

Greenberg, R., J. E. Maldonado, S. Droege, and M. V. McDonald. 2006. Tidal Marshes: A Global Perspective on the Evolution and Conservation of Their Terrestrial Vertebrates. BioScience 56:675–685.

Grinsted, A., J. C. Moore, and S. Jevrejeva. 2010. Reconstructing sea level from paleo and projected temperatures 200 to 2100 AD. Climate Dynamics 34:461–472.

de Groot, A. V., R. M. Veeneklaas, and J. P. Bakker. 2011. Sand in the salt marsh: Contribution of high-energy conditions to salt-marsh accretion. Marine Geology 282:240–254.

Hackney, C. T., S. Brady, L. Stemmy, M. Boris, C. Dennis, T. Hancock, M. O'Bryon, C. Tilton, and E. Barbee. 1996. Does intertidal vegetation indicate specific soil and hydrologic conditions. Wetlands 16:89–94.

Hanson, A., R. Johnson, C. Wigand, A. Oczkowski, E. Davey, and E. Markham. 2016. Responses of Spartina alterniflora to Multiple Stressors: Changing Precipitation Patterns, Accelerated Sea Level Rise, and Nutrient Enrichment. Estuaries and Coasts 39:1376–1385.

Hartigan, J. A. and M. A. Wong. 1979. A K-means clustering algorithm. Applied Statistics 28, 100–108.

Hickey, B. M., and N. S. Banas. 2003. Oceanography of the U. S. Pacific Northwest Coastal Ocean and Estuaries with Application to Coastal Ecology. Estuaries 26:1010–1031.

Hladik, C., and M. Alber. 2012. Accuracy assessment and correction of a LIDAR-derived salt marsh digital elevation model. Remote Sensing of Environment 121:224–235.

Hodgson, M. E., and P. Bresnahan. 2004. Accuracy of Airborne Lidar-Derived Elevation : Empirical Assessment and Error Budget. Photogrammetric engineering and remote sensing 70:331–339.

Hunter, E. A., N. P. Nibbelink, and R. J. Cooper. 2016. Threat predictability influences seaside sparrow nest site selection when facing trade-offs from predation and flooding. Animal Behaviour 120:135–142.

Janousek, C., K. Buffington, K. Thorne, G. Guntenspergen, J. Takekawa, and B. Dugger. 2016. Potential effects of sea-level rise on plant productivity: species-specific responses in northeast Pacific tidal marshes. Marine Ecology Progress Series 548:111–125.

Jarrell, E. R., A. S. Kolker, C. Campbell, and M. J. Blum. 2016. Brackish Marsh Plant Community Responses to Regional Precipitation and Relative sea-Level Rise. Wetlands 36:607–619.

Jiang, H., J. R. Strittholt, P. A. Frost, and N. C. Slosser. 2004. The classification of late seral forests in the Pacific Northwest, USA using Landsat ETM+ imagery. Remote Sensing of Environment 91:320–331.

Jones, J. A., and G. E. Grant. 1996. Peak flow response to clear-cutting and roads in small and large basin, western Cascades, Oregon. Water Resources Research 32:959–974.

Kane, V. R., R. J. McGaughey, J. D. Bakker, R. F. Gersonde, J. A. Lutz, and J. F. Franklin. 2010. Comparisons between field- and LiDAR-based measures of stand structural complexity. Canadian Journal of Forest Research 40:761–773.

Kauth, R. J and G.S. Thomas. 1976. The tasseled Cap -- A Graphic Description of the Spectral-Temporal Development of Agricultural Crops as Seen by LANDSAT. Proceedings of the Symposium on Machine Processing of Remotely Sensed Data, Purdue University of West Lafayette, Indiana, pp. 4B-41 to 4B-51.

Kearney, M. S., and R. E. Turner. 2016. Microtidal marshes: Can these widespread and

fragile marshes survive increasing climate–sea level variability and human action? Journal of Coastal Research 319:686–699.

Kennish, M. J. 2002. Environmental threats and environmental future of estuaries. Environmental Conservation 29:78–107.

Kirwan, M. L., and G. R. Guntenspergen. 2012. Feedbacks between inundation, root production, and shoot growth in a rapidly submerging brackish marsh. Journal of Ecology 100:764–770.

Kirwan, M. L., G. R. Guntenspergen, A. D'Alpaos, J. T. Morris, S. M. Mudd, and S. Temmerman. 2010. Limits on the adaptability of coastal marshes to rising sea level. Geophysical Research Letters 37:1–5.

Kirwan, M. L., G. R. Guntenspergen, and J. T. Morris. 2009. Latitudinal trends in Spartina alterniflora productivity and the response of coastal marshes to global change. Global Change Biology 15:1982–1989.

Kirwan, M. L., and A. B. Murray. 2007. A coupled geomorphic and ecological model of tidal marsh evolution. Proceedings of the National Academy of Sciences of the United States of America 104:6118–6122.

Kirwan, M. L., A. B. Murray, J. P. Donnelly, and D. R. Corbett. 2011. Rapid wetland expansion during European settlement and its implication for marsh survival under modern sediment delivery rates. Geology 39:507–510.

Kirwan, M., and S. Temmerman. 2009. Coastal marsh response to historical and future sea-level acceleration. Quaternary Science Reviews 28:1801–1808.

Klemas, V. 2013. Remote Sensing of Coastal Wetland Biomass: An Overview. Journal of Coastal Research 29:1016–1028.

Klemas, V. V. 2001. Remote sensing of landscape-level coastal environmental indicators. Environmental Management 27:47–57.

Kolker, A. S., S. L. Goodbred, S. Hameed, and J. K. Cochran. 2009. High-resolution records of the response of coastal wetland systems to long-term and short-term sea-level variability. Estuarine, Coastal and Shelf Science 84:493–508.

Langley, A. J., T. J. Mozdzer, K. A. Shepard, S. B. Hagerty, and J. Patrick Megonigal. 2013. Tidal marsh plant responses to elevated CO2, nitrogen fertilization, and sea level rise. Global Change Biology 19:1495–1503.

Leonard, L. A., and M. E. Luther. 1995. Flow hydrodynamics in tidal marsh canopies. Limnology and Oceanography 40:1474–1484.

Linderholm, H. W. 2006. Growing season changes in the last century. Agricultural and Forest Meteorology 137:1–14.

Mariotti, G., and S. Fagherazzi. 2013. Critical width of tidal flats triggers marsh collapse in the absence of sea-level rise. Proceedings of the National Academy of Sciences of

the United States of America 110:5353–6.

Masek, J. G., C. Huang, R. Wolfe, W. Cohen, F. Hall, J. Kutler, and P. Nelson. 2008. North American forest disturbance mapped from a decadal Landsat record. Remote Sensing of Environment 112:2914–2926.

Mattheus, C. R., A. B. Rodriguez, and B. a. McKee. 2009. Direct connectivity between upstream and downstream promotes rapid response of lower coastal-plain rivers to land-use change. Geophysical Research Letters 36:1–6.

Maune, D. F., Maitra, J. B., and McKay, E. J. 2007. Accuracy standards & guidelines. In: Maune D. (ed.), Digital Elevation Model Technologies and Applications. The DEM Users Manual, 2nd Edition. Bethesda, Maryland: American Society for Photogrammetry and Remote Sensing, pp. 65-97.

Mckee, T. B., N. J. Doesken, and J. Kleist. 1993. The relationship of drought frequency and duration to time scales. AMS 8th Conference on Applied Climatology:179–184.

Medeiros, S., S. Hagen, J. Weishampel, and J. Angelo. 2015. Adjusting Lidar-Derived Digital Terrain Models in Coastal Marshes Based on Estimated Aboveground Biomass Density. Remote Sensing 7:3507–3525.

Melaas, E. K., M. A. Friedl, and Z. Zhu. 2013. Detecting interannual variation in deciduous broadleaf forest phenology using Landsat TM/ETM+ data. Remote Sensing of Environment 132:176–185.

Milliman, J. D. 2001. River Inputs. Page (A. Thorpe and K. K. Turekian, Eds.) Encyclopedia of Ocean Sciences. 2nd edition. Academic Press, New York.

Milliman, J. D., and J. P. M. Syvitski. 1992. Geomorphic/Tectonic Control of Sediment Discharge to the Ocean: The Importance of Small Mountainous Rivers. The Journal of Geology 100:525–544.

Mitasova, H., M. F. Overton, J. J. Recalde, D. J. Bernstein, and C. W. Freeman. 2009. Raster-Based Analysis of Coastal Terrain Dynamics from Multitemporal Lidar Data. Journal of Coastal Research 252:507–514.

Mitsch,W.J, and J. G. Gosselink, Wetlands. John Wiley and Sons: Hoboken, NJ, USA, 2007.

Mo, Y., B. Momen, and M. S. Kearney. 2015. Quantifying moderate resolution remote sensing phenology of Louisiana coastal marshes. Ecological Modelling 312:191–199.

Montané, J. M., and R. Torres. 2006. Accuracy Assessment of Lidar Saltmarsh Topographic Data Using RTK GPS. Photogrammetric Engineering & Remote Sensing:961–967.

Moran P. A. P. 1950. Notes on continuous stochastic phenomena. Biometrika 37: 17-23.

Moran, M. S., Y. Inoue, and E. M. Barnes. 1997. Opportunities and limitations for image-

based remote sensing in precision crop management. Remote Sensing of Environment 61:319–346.

Morisette, J. T., A. D. Richardson, A. K. Knapp, J. I. Fisher, E. A. Graham, J. Abatzoglou, B. E. Wilson, D. D. Breshears, G. M. Henebry, J. M. Hanes, and L. Liang. 2009. Tracking the rhythm of the seasons in the face of global change: Phenological research in the 21 st century. Frontiers in Ecology and the Environment 7:253–260.

Morris, J. T., P. V. Sundareshwar, C. T. Nietch, B. Kjerfve, and D. R. Cahoon. 2002. Responses of coastal wetlands to rising sea level. Ecology 83:2869–2877.

Morton, R. A., and J. A. Barras. 2011. Hurricane Impacts on Coastal Wetlands: A Half-Century Record of Storm-Generated Features from Southern Louisiana. Journal of Coastal Research 275:27–43.

Mutanga, O., and A. K. Skidmore. 2004. Narrow band vegetation indices overcome the saturation problem in biomass estimation. International Journal of Remote Sensing 25:3999–4014.

Myneni, R. B., F. G. Hall, P. J. Sellers, and A. L. Marshak. 1995. Interpretation of spectral vegetation indexes. IEEE Transactions on Geoscience and Remote Sensing 33:481–486.

National Digital Elevation Program (NDEP). 2004. Guidelines for Digital Elevation Data, Version 1.0. 10 May 2004, 93 p. http://www.ndep.gov/NDEP_Elevation_Guidelines_Ver1_10_May2004.pdf

National Oceanic and Atmospheric Administration (NOAA). 2010. Technical considerations or the use of geospatial data in sea level change mapping and assessment. Silver Spring, Maryland: U.S. Department of Commerce, NOAA NOA Technical Report, NOAA National Ocean Service, 141 p. http://www.csc.noaa.gov/digitalcoast/_/pdf/SLC_Technicial_Considerations_Document.pdp.

National Research Council. 2012. Sea-Level Rise for the Coasts of California, Oregon, and Washington: Past, Present, and Future.

Nisqually Restoration. http://nisquallydeltarestoration.org/science_geomorphology_sedimentation.php, accessed 27 September 2016.

Nixon, A. S. W., J. W. Ammerman, L. P. Atkinson, V. M. Berounsky, G. Billen, C. Boicourt, W. R. Boynton, T. M. Church, D. M. Ditoro, R. Elmgren, J. H. Garber, R. A. Jahnke, N. J. P. Owens, M. E. Q. Pilson, and S. P. Seitzinger. 1996. The Fate of Nitrogen and Phosphorus at the Land-Sea Margin of the North Atlantic Ocean. Biogeochemistry 35:141–180.

Noe, G. B., and J. B. Zedler. 2000. Differential effects of four abiotic factors on the

germination of salt marsh annuals. American Journal of Botany 87:1679–1692.

Nyman, J. A., R. D. Delaune, H. H. Roberts, and W. H. Patrick. 1993. Relationship between vegetation and soil formation in a rapidly submerging coastal marsh. Marine Ecology Progress Series 96:269–279.

O'Donnell, J. P. R., and J. F. Schalles. 2016. Examination of abiotic drivers and their influence on Spartina alterniflora biomass over a twenty-eight year period using Landsat 5 TM satellite imagery of the Central Georgia Coast. Remote Sensing 8:477–499.

Osland, M. J., N. M. Enwright, R. H. Day, C. A. Gabler, C. L. Stagg, and J. B. Grace. 2016. Beyond just sea-level rise: Considering macroclimatic drivers within coastal wetland vulnerability assessments to climate change. Global Change Biology 22:1–11.

Ovaskainen, O., S. Skorokhodova, M. Yakovleva, A. Sukhov, and A. Kutenkov. 2013. Community level phenological response to climate change. Proceedings of the National Academy of Sciences 110:13434–13439.

Parson, E. A., P. W. Mote, A. F. Hamlet, W. S. Keeton, D. Lettenmaier, N. Mantua, E. L. Miles, D. W. Peterson, D. L. Peterson, R. Slaughter, and A. K. Snover. 2003. Forests for climatic change: The water, salmon and forests of the Pacific Northwest. Climate Change 61:45–88.

Pennings, S. C., R. M. Callaway, N. Apr, and M. C. Way. 1992. Salt Marsh Plant Zonation: The Relative Importance of Competition and Physical Factors. Ecology 73:681–690.

Pérez-Peña, J. V., J. M. Azañón, and A. Azor. 2009. CalHypso: An ArcGIS extension to calculate hypsometric curves and their statistical moments. Applications to drainage basin analysis in SE Spain. Computers and Geosciences 35:1214–1223.

Pettorelli, N., J. O. Vik, A. Mysterud, J. M. Gaillard, C. J. Tucker, and N. C. Stenseth. 2005. Using the satellite-derived NDVI to assess ecological responses to environmental change. Trends in Ecology and Evolution 20:503–510.

PRISM Climate Group, Oregon State University, http://prism.oregonstate.edu

van Proosdij, D., R. G. D. Davidson-Arnott, and J. Ollerhead. 2006. Controls on spatial patterns of sediment deposition across a macro-tidal salt marsh surface over single tidal cycles. Estuarine, Coastal and Shelf Science 69:64–86.

Rahmstorf, S. 2007. Projecting Future Sea-Level Rise. Science 315:368–370.

Ritchie, J., and J. R. Mchenry. 1990. Application of Radioactive Fallout Cesium-137 for Measuring Soil Erosion and Sediment Accumulation Rates and Patterns : A Review. Journal of Environmental Quality 19:215–233.

Rosencranz, J. A., N. K. Ganju, R. F. Ambrose, S. M. Brosnahan, P. J. Dickhudt, G. R. Guntenspergen, G. M. MacDonald, J. Y. Takekawa, and K. M. Thorne. 2016.

Balanced Sediment Fluxes in Southern California's Mediterranean-Climate Zone Salt Marshes. Estuaries and Coasts 39:1035–1049.

Rosso, P. H., S. L. Ustin, and A. Hastings. 2005. Mapping marshland vegetation of San Francisco Bay, California, using hyperspectral data. International Journal of Remote Sensing 26:5169–5191.

Roy, D. P., V. Kovalskyy, H. K. Zhang, E. F. Vermote, L. Yan, S. S. Kumar, and A. Egorov. 2016. Characterization of Landsat-7 to Landsat-8 reflective wavelength and normalized difference vegetation index continuity. Remote Sensing of Environment 185:57–70.

Sadro, S., M. Gastil-Buhl, and J. Melack. 2007. Characterizing patterns of plant distribution in a southern California salt marsh using remotely sensed topographic and hyperspectral data and local tidal fluctuations. Remote Sensing of Environment 110:226–239.

Scavia, D., J. C. Field, D. F. Boesch, R. W. Buddemeier, V. Burkett, D. R. Cayan, M. Fogarity, M. A. Harwell, R. W. Howarth, C. Mason, D. J. Reed, T. C. Royer, A. H. Sallenger, and J. G. Titus. 2002. Climate Change Impacts on U. S. Coastal and Marine Ecosystems. Estuaries 25:149–164.

Schile, L. M., J. C. Callaway, J. T. Morris, D. Stralberg, V. Thomas Parker, and M. Kelly. 2014. Modeling tidal marsh distribution with sea-level rise: Evaluating the role of vegetation, sediment, and upland habitat in marsh resiliency. PLoS ONE 9.

Schmid, K. A., B. C. Hadley, and N. Wijekoon. 2011. Vertical Accuracy and Use of Topographic LIDAR Data in Coastal Marshes. Journal of Coastal Research 275:116–132.

Schwartzberg, E. G., M. A. Jamieson, K. F. Raffa, P. B. Reich, R. A. Montgomery, and R. L. Lindroth. 2014. Simulated climate warming alters phenological synchrony between an outbreak insect herbivore and host trees. Oecologia 175:1041–1049.

Shaughnessy, F. J., W. Gilkerson, J. M. Black, D. H. Ward, and M. Petrie. 2012. Predicted eelgrass response to sea level rise and its availability to foraging Black Brant in Pacific coast estuaries. Ecological Applications 22:1743–1761.

Silvestri, S., A. Defina, and M. Marani. 2005. Tidal regime, salinity and salt marsh plant zonation. Estuarine, Coastal and Shelf Science 62:119–130.

Stenseth, N. C., A. Mysterud, and G. Ottersen. 2002. Ecological effects of climate fluctuations. Science 297:1292–1296.

Sutton-Grier, A. E., and A. Moore. 2016. Leveraging Carbon Services of Coastal Ecosystems for Habitat Protection and Restoration. Coastal Management 753:259–277.

Swanson, K. M., J. Z. Drexler, C. Fuller, and D. H. Schoellhamer. 2015. Modeling tidal freshwater marsh sustainability in the Sacramento-San Juaquin Delta under a broad

suite of potential future scenarios. San Francisco Estuary and Watershed Science 13:217–220.

Swanson, K. M., J. Z. Drexler, D. H. Schoellhamer, K. M. Thorne, M. L. Casazza, C. T. Overton, J. C. Callaway, and J. Y. Takekawa. 2013. Wetland Accretion Rate Model of Ecosystem Resilience (WARMER) and Its Application to Habitat Sustainability for Endangered Species in the San Francisco Estuary. Estuaries and Coasts 37:476–492.

SWAT 2016. Skokomish Watershed Action Team, Skokomish Watershed Action Plan Update 2016. Available: http://hccc.wa.gov/content/salmon-recovery-planning

Takekawa, J. Y., I. Woo, K. M. Thorne, K. J. Buffington, N. Nur, M. L. Casazza, and J. T. Ackerman. 2012. Chapter 12: Bird communities: effects of fragmentation, disturbance, and sea level rise on population viability. Pages 175–194Ecology, Conservation, and Restoration of Tidal Marshes: The San Francisco Estuary.

Temmerman, S., G. Govers, S. Wartel, and P. Meire. 2004. Modelling estuarine variations in tidal marsh sedimentation: response to changing sea level and suspended sediment concentrations. Marine Geology 212:1–19.

Thorne, K. M., K. J. Buffington, K. M. Swanson, and J. Y. Takekawa. 2013. Storm Surges and Climate Change Implications for Tidal Marshes: Insight from the San Francisco Bay Estuary, California, USA. The International Journal of Climate Change: Impacts and Responses 4:169–190.

Thorne, K. M., J. Y. Takekawa, and D. L. Elliott-Fisk. 2012. Ecological Effects of Climate Change on Salt Marsh Wildlife: A Case Study from a Highly Urbanized Estuary. Journal of Coastal Research 285:1477–1487.

Thorne, K. M., Dugger, B. D., Buffington, K. J., Freeman, C. M., Janousek, C. N., Powelson, K. W., Gutenspergen, G. R., and Takekawa, J. Y., 2015. Marshes to mudflats—Effects of sea-level rise on tidal marshes along a latitudinal gradient in the Pacific Northwest: U.S. Geological Survey Open-File Report 2015-1204, 54 p. plus appendixes, http://dx.doi.org/10.3133/ofr20151204.

Thorne, K.M., MacDonald, G.M., Ambrose, R. F., Buffington, K.J., Freeman, C.M., Janousek, C.N., Brown, L.N., Holmquist, J.R., Gutenspergen, G.R., Powelson, K.W., Barnard, P.L., and Takekawa, J.Y. 2016. Effects of climate change on tidal marshes along a latitudinal gradient in California: U.S. Geological Survey Open-File Report 2016-1125, 75 p., http://dx.doi.org/10.3133/ofr20161125.

TIGER/Line Shapefiles (machine readable data files), prepared by the U.S. Census Bureau, 2015.

Torio, D. D., and G. L. Chmura. 2013. Assessing Coastal Squeeze of Tidal Wetlands. Journal of Coastal Research 29:1049–1061.

Tsao, D. C., J. Y. Takekawa, I. Woo, J. L. Yee, and J. G. Evens. 2009. Home Range,

Habitat Selection, and Movements of California Black Rails at Tidal Marshes at San Francisco Bay, California. The Condor 111:599–610.

U.S. Fish and Wildlife Service. 2012a. Bandon Marsh National Wildlife Refuge draft Comprehensive Conservation Plan and Environmental Assessment. U.S. Department of the Interior, Fish and Wildlife Service, Region 1, Portland, OR. 431 pp.

U.S. Fish and Wildlife Service. 2012b. Siletz Bay National Wildlife Refuge draft Comprehensive Conservation Plan and Environmental Assessment. U.S. Department of the Interior, Fish and Wildlife Service, Region 1, Portland, OR. 418 pp.

Ustin, S. L., R. W. Pearcy, and D. E. Bayer. 1982. Plant Water Relations in a San Francisco Bay Salt Marsh. Botanical Gazette 143:368–373.

Vermeer, M., and S. Rahmstorf. 2009. Global sea level linked to global temperature. Proceedings of the National Academy of Sciences of the United States of America 106:21527–21532.

Verstraete, M. M., B. Pinty, R. B. Myneni, and M. M. Verstraete. 1996. Potential and limitations of information extraction on the terrestrial biosphere from satellite remote sensing. Remote Sensing of Environment 58:201–214.

Vicente-Serrano, S. M., S. Beguería, and J. I. López-Moreno. 2010. A multiscalar drought index sensitive to global warming: The standardized precipitation evapotranspiration index. Journal of Climate 23:1696–1718.

Visser, M. E., and C. Both. 2005. Shifts in phenology due to global climate change : the need for a yardstick Shifts in phenology due to global climate change: the need for a yardstick. Proceedings of the Royal Society B 272:2561–2569.

van der Wal, D., and K. Pye. 2004. Patterns, rates and possible causes of saltmarsh erosion in the Greater Thames area (UK). Geomorphology 61:373–391.

Walther, G.-R. 2010. Community and ecosystem responses to recent climate change. Philosophical Transactions of the Royal Society B: Biological Sciences 365:2019–24.

Walther, G.-R., E. Post, P. Convey, A. Menzel, C. Parmesan, T. J. C. Beebee, J.-M. Fromentin, O. Hoegh-Guldberg, and F. Bairlein. 2002. Ecological responses to recent climate change. Nature 416:389–395.

Ward, K. M., J. C. Callaway, and J. B. Zedler. 2003. Episodic colonization of an intertidal mudflat by native cordgrass (Spartina foliosa) at Tijuana Estuary. Estuaries 26:116–130.

Ward, R. D., N. G. Burnside, C. B. Joyce, K. Sepp, and P. A. Teasdale. 2016. Improved modelling of the impacts of sea level rise on coastal wetland plant communities. Hydrobiologia 774:203–216.

Watson, E. B., and R. Byrne. 2013. Late Holocene Marsh Expansion in Southern San Francisco Bay, California. Estuaries and Coasts 36:643–653.

Wells, N., S. Goddard, and M. J. Hayes. 2004. A self-calibrating Palmer Drought Severity Index. Journal of Climate 17:2335–2351.

Weston, N. B. 2014. Declining Sediments and Rising Seas: An Unfortunate Convergence for Tidal Wetlands. Estuaries and Coasts 37:1–23.

Wetson, A. M., C. Zorb, E. A. John, and T. J. Flowers. 2012. High phenotypic plasticity of Suaeda maritima observed under hypoxic conditions in relation to its physiological basis. Annals of Botany 109:1027–1036.

Williams, S. J. 2013. Sea-Level Rise Implications for Coastal Regions. Journal of Coastal Research 29:184–196.

Wright, S. A., and D. H. Schoellhamer. 2004. Trends in the sediment yield of the Sacramento River, California, 1957 – 2001. San Francisco Estuary and Watershed Science 2:1–14.

Yang, Z., K. L. Sobocinski, D. Heatwole, T. Khangaonkar, R. Thom, and R. Fuller. 2010. Hydrodynamic and ecological assessment of nearshore restoration: A modeling study. Ecological Modelling 221:1043–1053.

Zedler, J. B. 1993. Canopy Architecture of Natural and Planted Cordgrass Marshes: Selecting Habitat Evaluation Criteria. Ecological Applications 3:123–138.

Zhang, H., and S. M. Gorelick. 2014. Coupled impacts of sea-level rise and tidal marsh restoration on endangered California clapper rail. Biological Conservation 172:89–100.

Zhu, Z., and C. E. Woodcock. 2012. Object-based cloud and cloud shadow detection in Landsat imagery. Remote Sensing of Environment 118:83–94.

APPENDIX A. Supplemental material for Chapter 2.

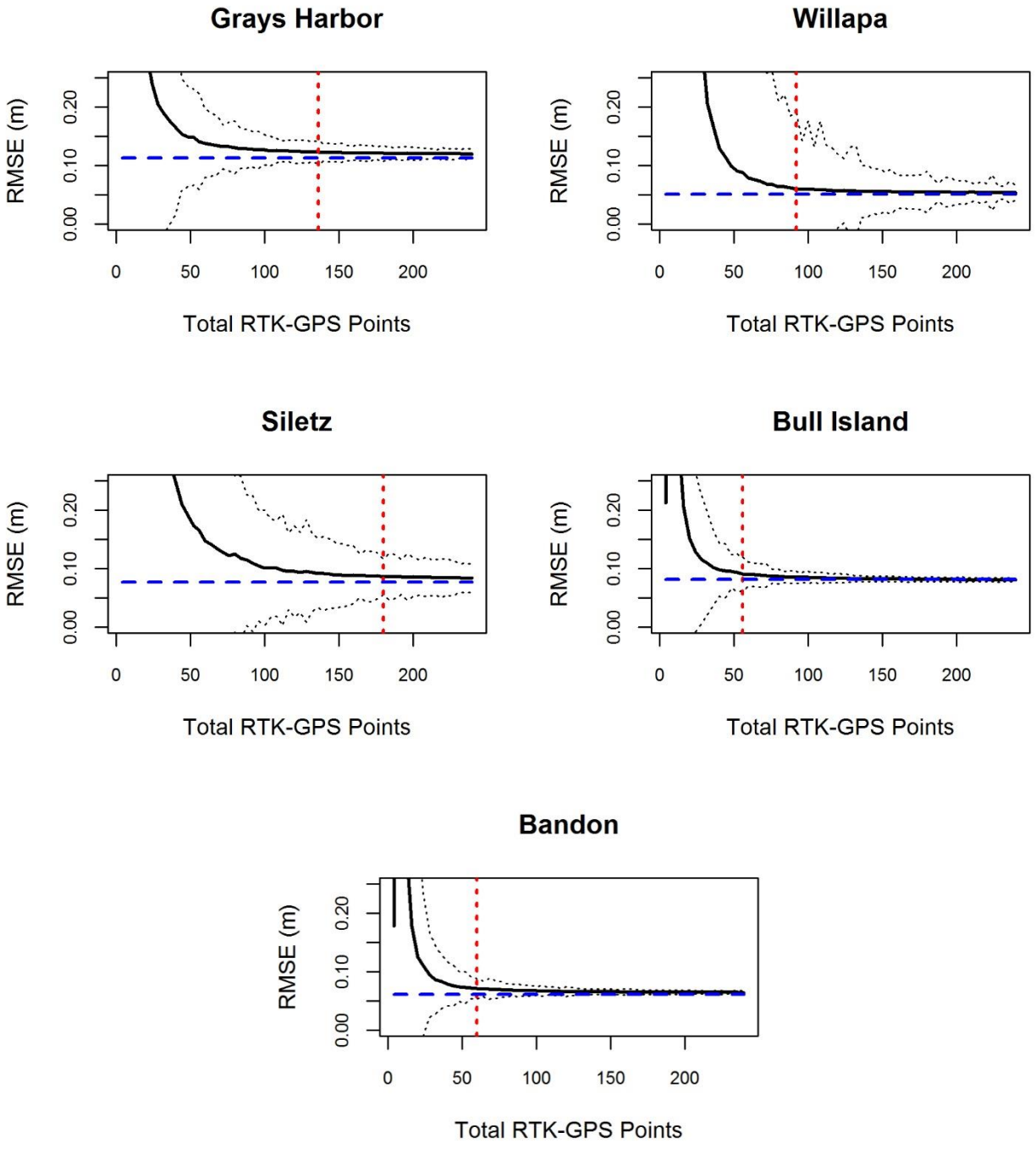

S1. Power analysis results by study site for the Pacific Northwest sites. The solid black lines are the mean root mean squared error (RMSE) across the range of input RTK-GPS points, the dotted black lines represent one standard deviation, the blue line represents the mean cross-validated RMSE and the red vertical line denotes the number of RTK-GPS points that bring the RMSE within 1 cm of the cross-validated RMSE.

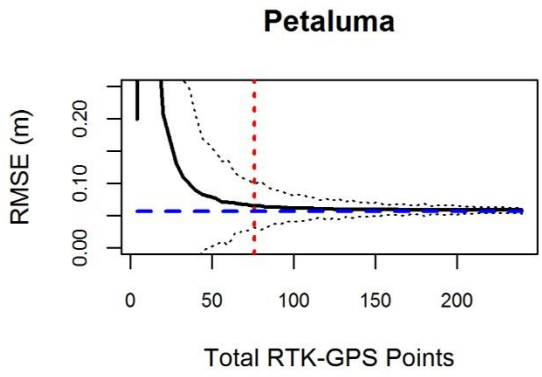
Petaluma
RMSE (m)
0.00
0.10
0.20
0
50
100
150
200
Total RTK-GPS Points

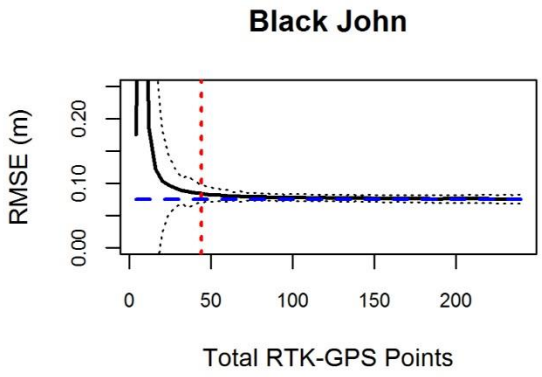
Black John
RMSE (m)
0.00
0.10
0.20
0
50
100
150
200
Total RTK-GPS Points

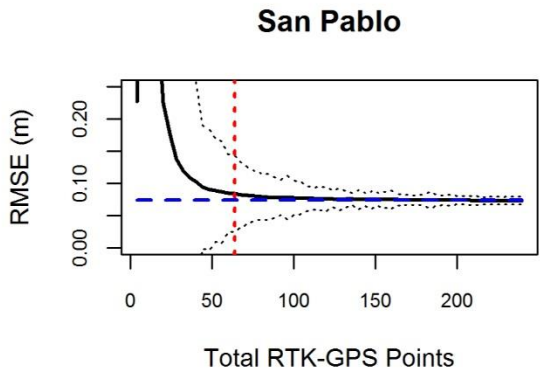
San Pablo
RMSE (m)
0.00
0.10
0.20
0
50
100
150
200
Total RTK-GPS Points

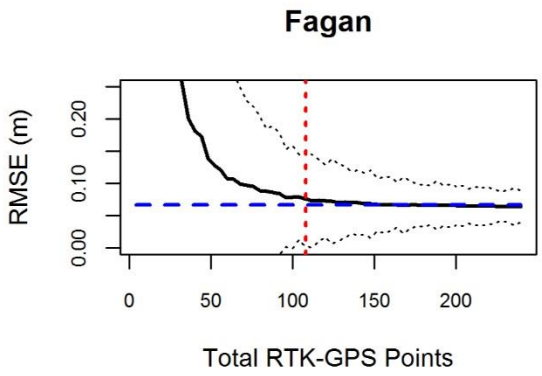
Fagan
RMSE (m)
0.00
0.10
0.20
0
50
100
150
200
Total RTK-GPS Points

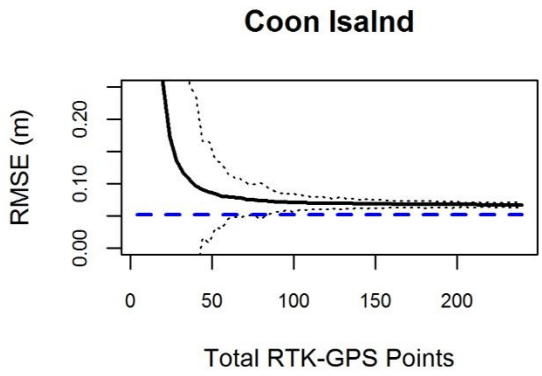
Coon Isalnd
RMSE (m)
0.00
0.10
0.20
0
50
100
150
200
Total RTK-GPS Points

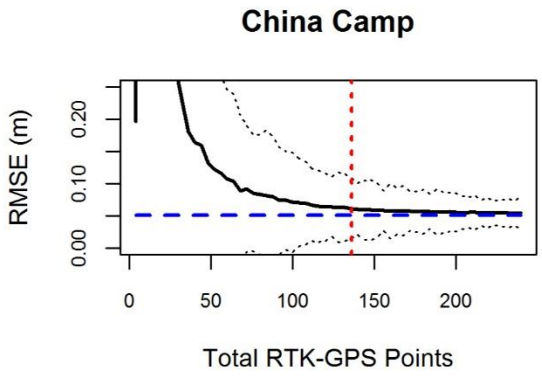
China Camp
RMSE (m)
0.00
0.10
0.20
0
50
100
150
200
Total RTK-GPS Points

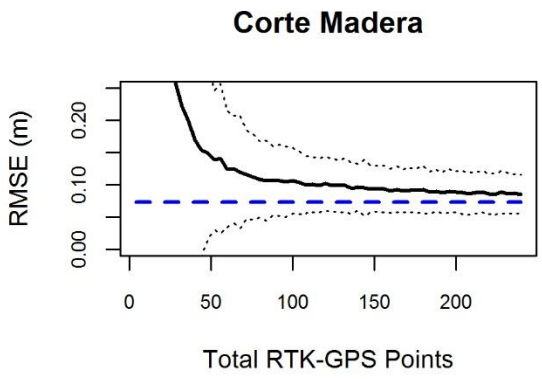
Corte Madera
RMSE (m)
0.00
0.10
0.20
0
50
100
150
200
Total RTK-GPS Points

S2. Power analysis results by study site for the San Francisco Bay sites. The solid black lines are the mean root mean squared error (RMSE) across the range of input RTK-GPS points, the dotted black lines represent one standard deviation, the blue line represents the mean cross-validated RMSE and the red vertical line denotes the number of RTK-GPS points that bring the RMSE within 1 cm of the cross-validated RMSE.

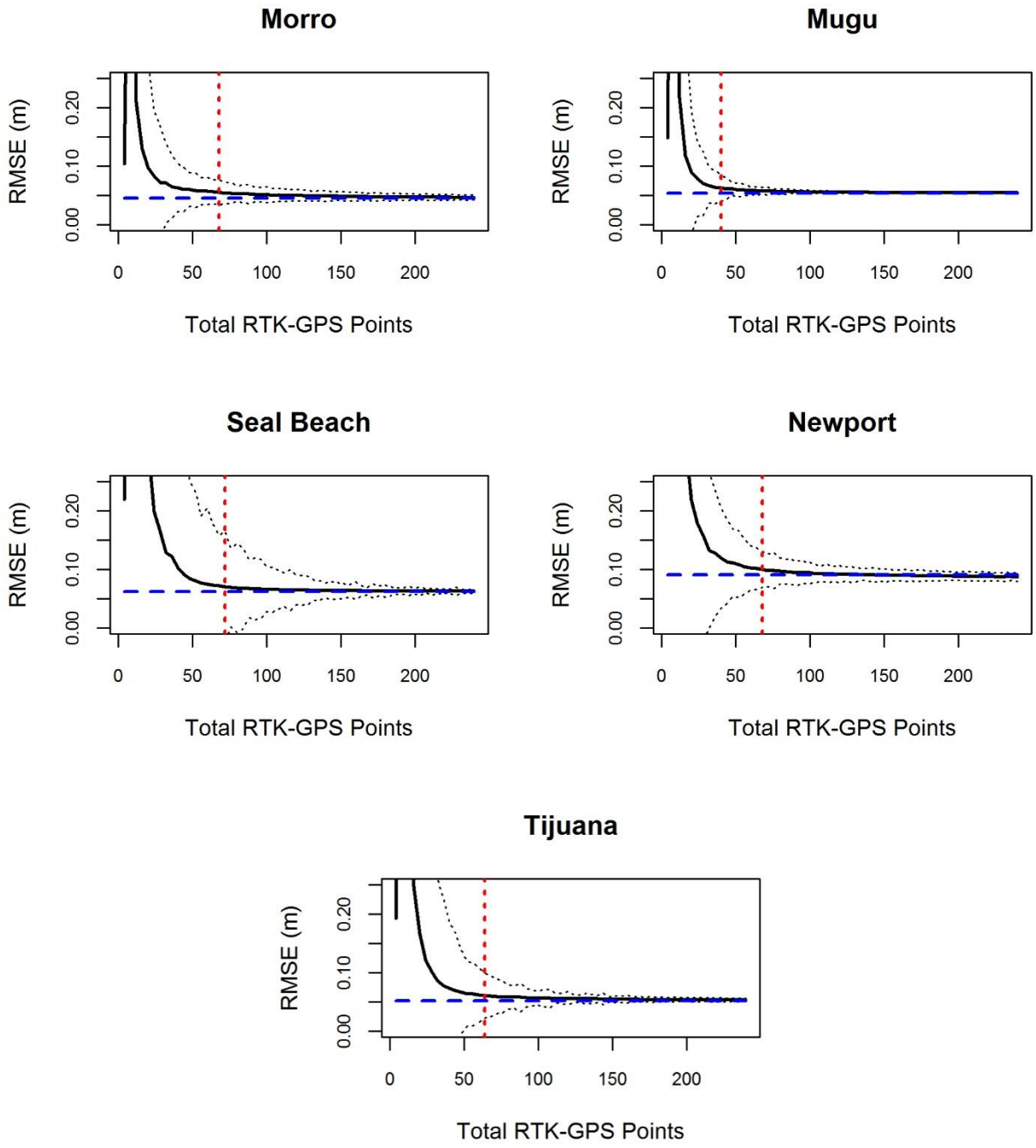

S3. Power analysis results by study site for the Southern California sites. The solid black lines are the mean root mean squared error (RMSE) across the range of input RTK-GPS points, the dotted black lines represent one standard deviation, the blue line represents the mean cross-validated RMSE and the red vertical line denotes the number of RTK-GPS points that bring the RMSE within 1 cm of the cross-validated RMSE.

APPENDIX B. Supplemental material for Chapter 4.

S1. Area weighted accumulation rates and other watershed characteristics for eight estuaries across the Pacific Northwest.

	Bandon	Coos	Siletz	Willapa	Grays Harbor	Nisqually	Skokomish	Port Susan	Source
Vertical Accretion (mm yr^{-1})	2.3	3.3	2.7	6.4	7.3	3.3	2.5	6.7	Cores
Organic Matter Accumulation (g m^{-2} yr^{-1})	52.4	59.9	151.1	225.6	150.0	144.3	109.0	307.7	Cores
Mineral Accumulation (g m^{-2} yr^{-1})	289.9	314.7	654.2	2330.7	2764.8	719.9	314.7	3690.3	Cores
Watershed Area (km^2)	2736	1590	955	2760	6996.4	1243	394	2173	HUD10
Hypsometric Integral	0.29	0.30	0.28	0.18	0.13	0.18	0.27	0.23	This Study
Tide Range (cm)	103	118	111	168	142	150	147	167	NOAA
Total Precipitation (cm)	151.9	163.2	203.5	194.2	181.3	106.8	196.9	78.9	PRISM
Growing Season Precip (cm)	4.0	4.2	6.5	2.9	3.8	3.2	1.9	2.8	PRISM
Mean Annual Temp (C)	11.3	11.1	10.9	10.6	10.6	10.9	10.6	9.7	PRISM
Max Annual Temp (C)	14.8	15.0	13.9	14.2	14.6	15.8	15.3	13.4	PRISM
Mean Growing Season Temp (C)	13.2	13.6	13.3	14.3	15.1	16.1	18.2	17.6	PRISM
Road Density	1.91	2.58	2.03	1.48	1.83	2.70	2.04	1.71	TigerLines
Stream Density	4.09	3.75	4.26	5.44	3.91	2.01	2.98	3.72	TigerLines
Urban (%)	0.01	0.02	0.00	0.01	0.02	0.04	0.01	0.02	NDLC2011
Development (%)	0.05	0.06	0.06	0.06	0.06	0.11	0.05	0.08	NDLC2011
Disturbed (%)	0.18	0.31	0.30	0.43	0.19	0.24	0.21	0.16	NDLC2011
Fluvial Discharge (cfs)	3419	1986	1669	5411	8204	1227	1321	6254	USGS
Watershed Precip Volume (km^3)	4.68	2.96	2.48	5.73	14.76	1.51	2.04	5.20	PRISM

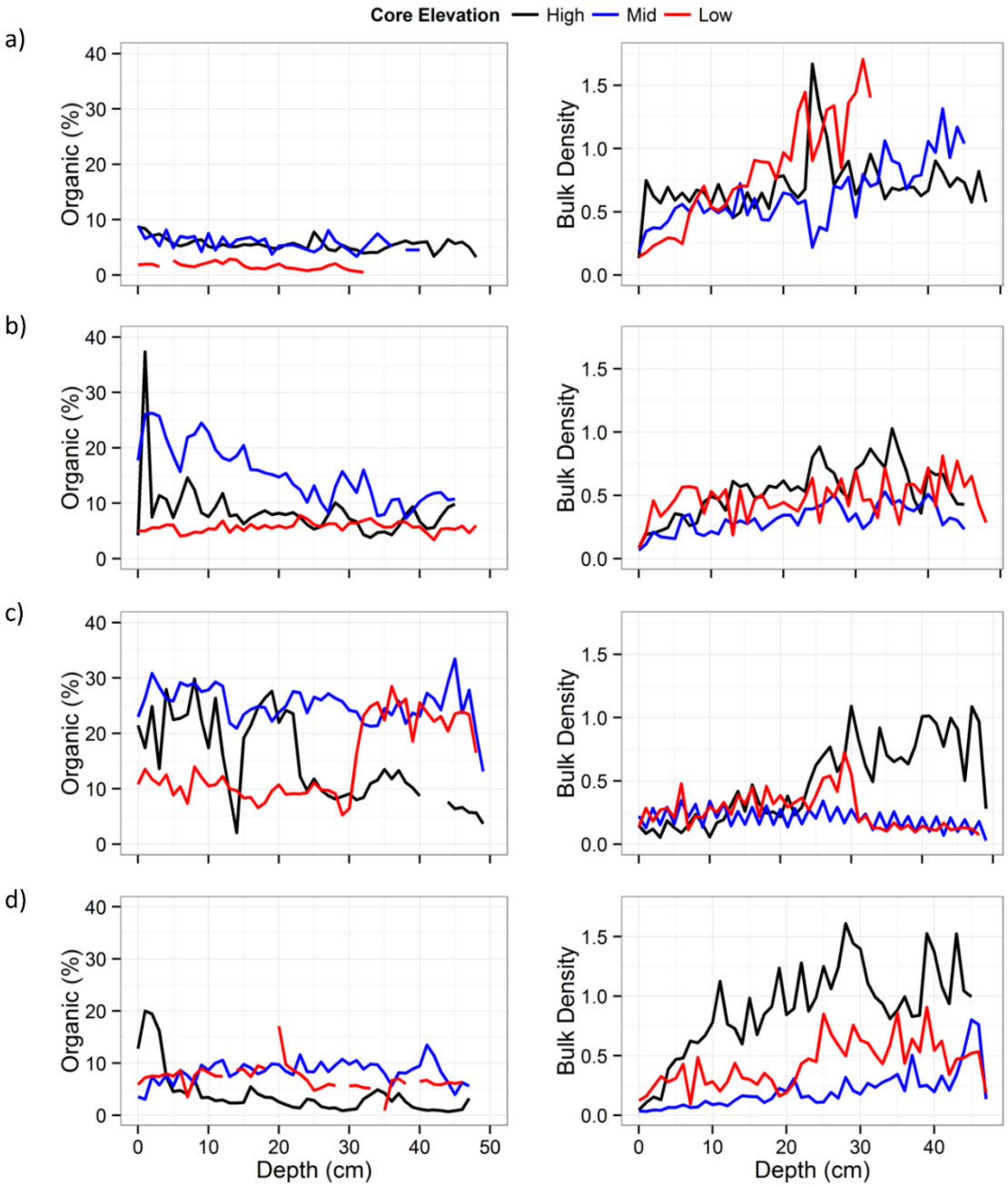
Core Elevation High Mid Low
a)
b)
c)
d)
Organic (%)
Bulk Density
Depth (cm)

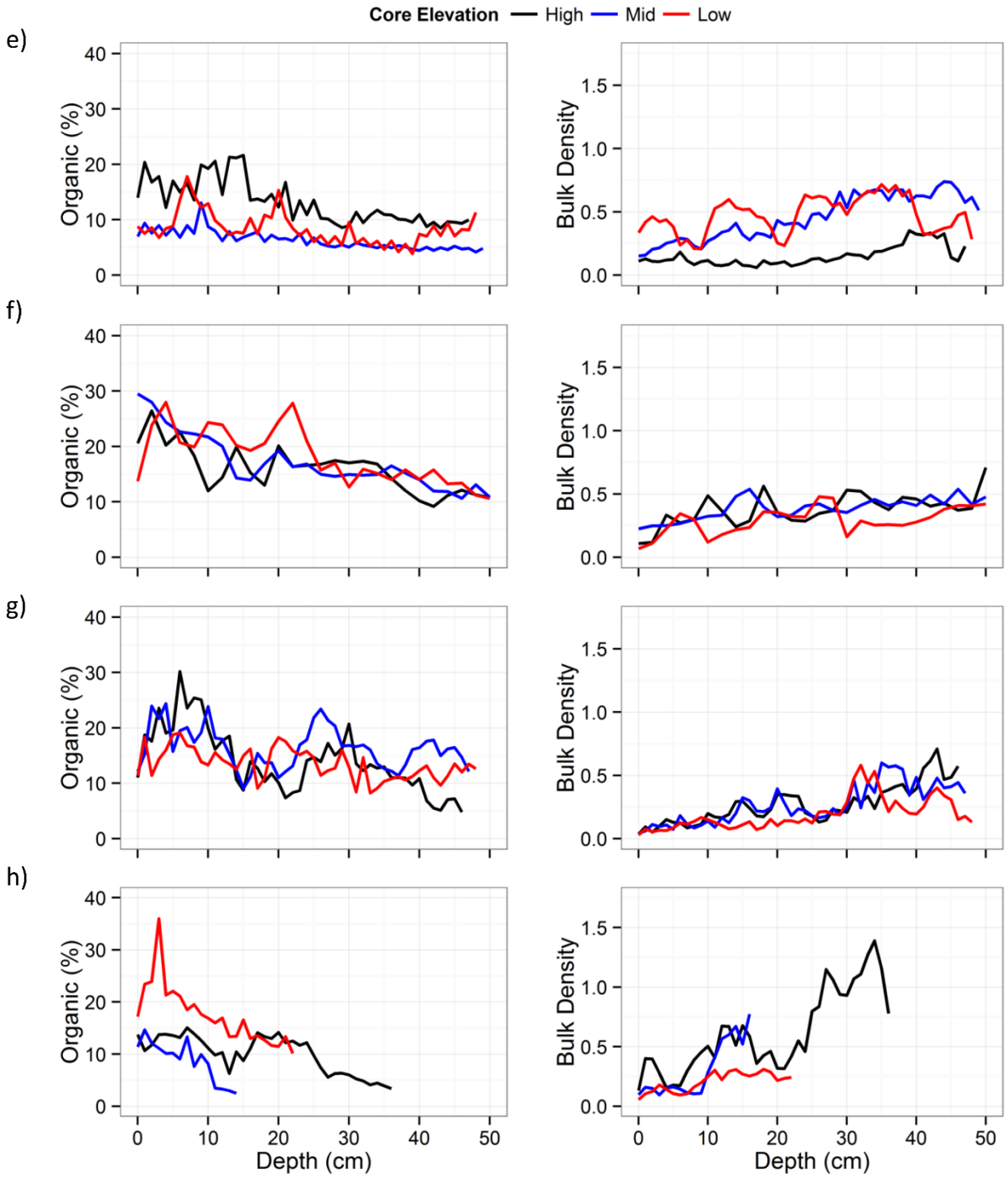

S2. Organic matter (%) and bulk density depth profiles from soil cores collected at low, mid, and high elevations. (a- Port Susan, b-Nisqually, c-Skokomish, d-Grays Harbor, e-Willapa, f-Siletz, g-Coos, h-Bandon).

S3. AIC ranking of vertical accretion (area weighted mean), mineral accumulation, and organic accumulation across eight Pacific Northwest Estuaries from single-variable generalized linear models and sorted by ΔAIC. Raw values used for these models are in Table S1.

	Predictors	Resid. Df	Log-likelihood	AICc	ΔAICc	weight
Vertical Accretion	Discharge	6	8.57	-5.15	0	0.89
	Hypsometric Integral	6	5.03	1.95	7.1	0.03
	Watershed Precip Vol	6	4.95	2.09	7.24	0.02
	Intercept-Only	7	1.69	3.02	8.17	0.01
	Watershed Area	6	4.36	3.29	8.43	0.01
	Conifers 10-50 y.o.	6	4.2	3.61	8.75	0.01
	Tide Range	6	4.16	3.67	8.82	0.01
	Road Density	6	2.97	6.07	11.22	0
	Max Annual Temp	6	2.54	6.91	12.06	0
	Stream Density	6	2.05	7.9	13.05	0
	Urban (%)	6	1.99	8.02	13.17	0
	GS Precip	6	1.98	8.04	13.19	0
	GS Mean Temp	6	1.87	8.26	13.4	0
	Annual Precip	6	1.83	8.34	13.49	0
	Sea-Level Rise Rate	6	1.82	8.35	13.5	0
	Development (%)	6	1.73	8.55	13.7	0
	Disturbed (%)	6	1.69	8.61	13.76	0
Mineral Accumulation	Discharge	6	-62.9	137.8	0	0.77
	Intercept-Only	7	-68.42	143.25	5.45	0.05
	Tide Range	6	-65.77	143.54	5.74	0.04
	Max Annual Temp	6	-66.07	144.13	6.33	0.03
	Hypsometric Integral	6	-66.43	144.85	7.05	0.02
	Watershed Precip Vol	6	-66.55	145.1	7.3	0.02
	Watershed Size	6	-67	146.01	8.21	0.01
	Conifers 10 - 50 y.o.	6	-67.07	146.13	8.33	0.01
	Stream Density	6	-67.81	147.61	9.81	0.01
	Annual Precip	6	-67.85	147.7	9.9	0.01
	Road Density	6	-67.91	147.81	10.01	0.01
	GS Mean Temp	6	-67.95	147.91	10.11	0
	Sea Level Rise Rate	6	-68.04	148.07	10.27	0
	Urban (%)	6	-68.09	148.17	10.37	0
	GS Precip	6	-68.13	148.25	10.45	0
	Development (%)	6	-68.35	148.69	10.89	0
	Disturbed (%)	6	-68.36	148.71	10.91	0

Organic Accumulation	Tide Range	6	-42.43	96.86	0	0.46
	Intercept-Only	7	-46.31	99.02	2.16	0.16
	Max Annual Temp	6	-43.81	99.61	2.75	0.12
	Sea Level Rise Rate	6	-44.52	101.04	4.18	0.06
	Discharge	6	-44.98	101.96	5.1	0.04
	Hypsometric Integral	6	-45.38	102.75	5.89	0.02
	Growing Season Mean Temp	6	-45.4	102.8	5.94	0.02
	Annual Precip	6	-45.59	103.18	6.32	0.02
	Road Density	6	-45.79	103.58	6.72	0.02
	Development (%)	6	-45.94	103.88	7.02	0.01
	Urban (%)	6	-45.96	103.91	7.05	0.01
	Stream Density	6	-46.04	104.08	7.22	0.01
	Growing Season Precip	6	-46.05	104.11	7.25	0.01
	Watershed Precip Vol	6	-46.19	104.37	7.51	0.01
	Conifers 10-50 y.o	6	-46.27	104.54	7.68	0.01
	Watershed Area	6	-46.28	104.55	7.69	0.01
	Disturbed (%)	6	-46.3	104.61	7.75	0.01

GS is growing season